AD-A055 835 FLORIDA UNIV GAINESVILLE DEPT OF ELECTRICAL ENGINEERING F/G 20/3
LIGHT SCATTERING FROM IRREGULAR DIELECTRIC PARTICLES.(U)
MAR 78 G WARD DAHC04-75-G-0100
UNCLASSIFIED ARO-12178.1-GS NL

1 OF 2
AD
A055 835

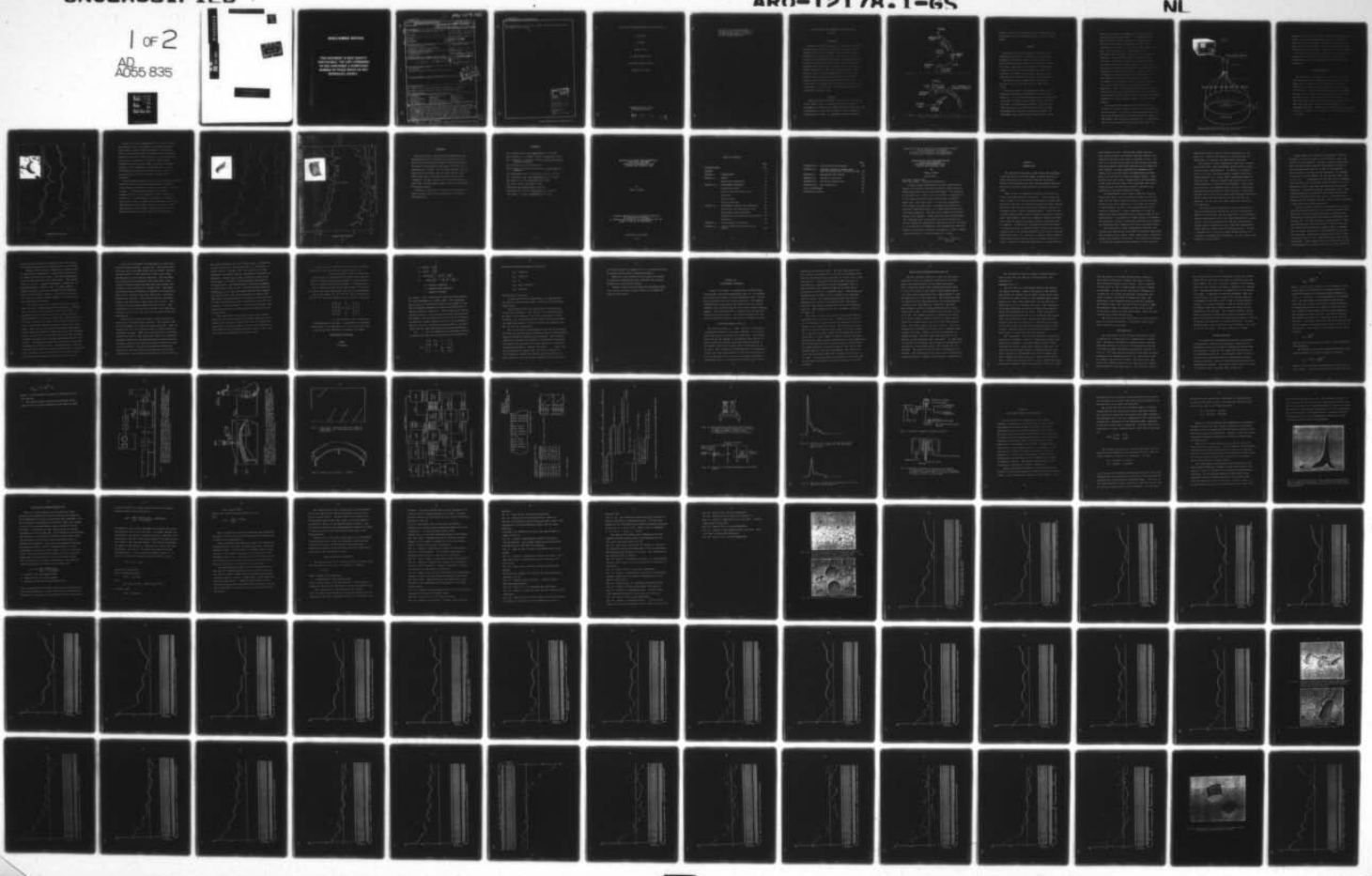

DISCLAIMER NOTICE

THIS DOCUMENT IS BEST QUALITY PRACTICABLE. THE COPY FURNISHED TO DDC CONTAINED A SIGNIFICANT NUMBER OF PAGES WHICH DO NOT REPRODUCE LEGIBLY.

ARO 12178.1-GS

UNCLASSIFIED

SECURITY CLASSIFICATION OF THIS PAGE (When Data Entered)

REPORT DOCUMENTATION PAGE

READ INSTRUCTIONS BEFORE COMPLETING FORM

1. REPORT NUMBER

2. GOVT ACCESSION NO.

3. RECIPIENT'S CATALOG NUMBER

Final rept. 1 Mar 75-28 Feb 78

4. TITLE (and Subtitle)

LIGHT SCATTERING FROM IRREGULAR DIELECTRIC PARTICLES.

5. TYPE OF REPORT & PERIOD COVERED

FINAL REPORT, 3/1/75-2/28/78

6. PERFORMING ORG. REPORT NUMBER

7. AUTHOR(s)

Gray Ward

8. CONTRACT OR GRANT NUMBER(s)

DAHC04-75-G-0100

9. PERFORMING ORGANIZATION NAME AND ADDRESS

University of Florida
Department of Electrical Engineering
Gainesville, Florida 32611

10. PROGRAM ELEMENT, PROJECT, TASK AREA & WORK UNIT NUMBERS

11. CONTROLLING OFFICE NAME AND ADDRESS

U.S.Army Research Office
P.O.Box 12211
Research Triangle Park, North Carolina 27709

12. REPORT DATE

March 28, 1978

13. NUMBER OF PAGES

177 p.

14. MONITORING AGENCY NAME & ADDRESS (if different from Controlling Office)

ARO 12178.1-GS

15. SECURITY CLASS. (of this report)

Unclassified

15a. DECLASSIFICATION/DOWNGRADING SCHEDULE

16. DISTRIBUTION STATEMENT (of this Report)

Unrestricted
Approved for public release; distribution unlimited.

DDC
RECEIVED
JUN 28 1978
F

17. DISTRIBUTION STATEMENT (of the abstract entered in Block 20, if different from Report)

18. SUPPLEMENTARY NOTES

The findings in this report are not to be construed as an official Department of the Army position, unless so designated by other authorized documents.

19. KEY WORDS (Continue on reverse side if necessary and identify by block number)

Scattering	Bistatic Scattering	Monodispersion
Light Scattering	Spheroidal	Backscatter
Irregular Particles	Cladosporium	Tumbled particles
Nephalometer	Non-spherical particles	Mie Theory
Polar Nephalometer	Dielectric particles	Electromagnetic Scattering

20. ABSTRACT (Continue on reverse side if necessary and identify by block number)

A digital polar nephalometer has been constructed to measure the intensity and polarization of light pulses scattered into 94 angles from 9° to 176° deg. from monodisperse aerosol particles of controlled shape. The light source was a tuneable dye laser giving 10 kW 4 ns pulses, operated at 627 nm. Calibration data from polystyrene latex spheres agrees with Mie theory within about 10%. Data for spheroidal 2 (μm) cladosporium and quasi-cubical 4 (μm) NaCl particles are shown. It is found that the backscatter from non-spherical particles (of size parameter about 10) differs significantly → next page JCB

micrometers micrometers

DD FORM 1 JAN 73 1473 EDITION OF 1 NOV 65 IS OBSOLETE

404 825

SECURITY CLASSIFICATION OF THIS PAGE (When Data Entered)

from that for the best fit sphere, so that a tumbled irregular particle is not equivalent to a sphere.

LIGHT SCATTERING FROM IRREGULAR DIELECTRIC PARTICLES

FINAL REPORT

GRAY WARD

MARCH 28, 1978

U.S. ARMY RESEARCH OFFICE

Grant Number DAHC04-75-G-0100

UNIVERSITY OF FLORIDA

THE FINDINGS IN THIS REPORT ARE NOT TO BE CONSTRUED AS AN OFFICIAL DEPARTMENT OF THE ARMY POSITION, UNLESS SO DESIGNATED BY OTHER AUTHORIZED DOCUMENTS.

LIGHT SCATTERING FROM IRREGULAR DIELECTRIC PARTICLES

Gray Ward

Introduction

Accurate experimental measurements of scattering from irregular dielectric particles of known size and shape are needed to verify theoretical calculations of scattering from these objects when the wavelength of the incident radiation is comparable to the particle dimension. Holland and Gagne [1] have made careful measurements from irregular silica particles from 18° to 166°, and find significant deviations from spherical models. Parmenter [2-4] has measured the angular distribution of scattering from randomly oriented single particles of quasi-ellipsoidal $BaSO_4$, and also finds significant deviations from spherical particle scattering near backscatter. Pinnick, Carroll and Hofmann [5] measured the scattering from clumps of NaCl and KSO_4 particles, and found that for particles with size parameters larger than about 5, Mie theory overestimates the scattering at backscatter angles.

Objectives

LIDAR measurements of atmospheric aerosols utilize the spherical particle model and look at backscatter. We wished to extend the measurements of scattering from irregular particles to angles very close to backscatter to see how serious an error is being introduced by neglecting particle shape. We also wanted to determine whether an

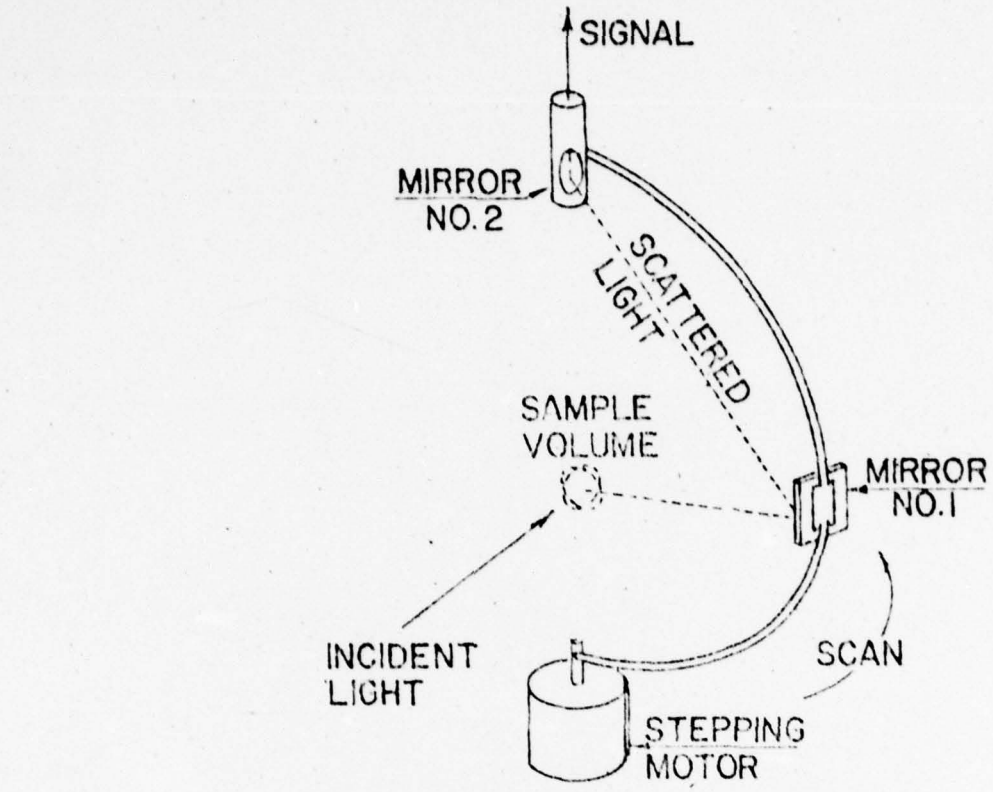

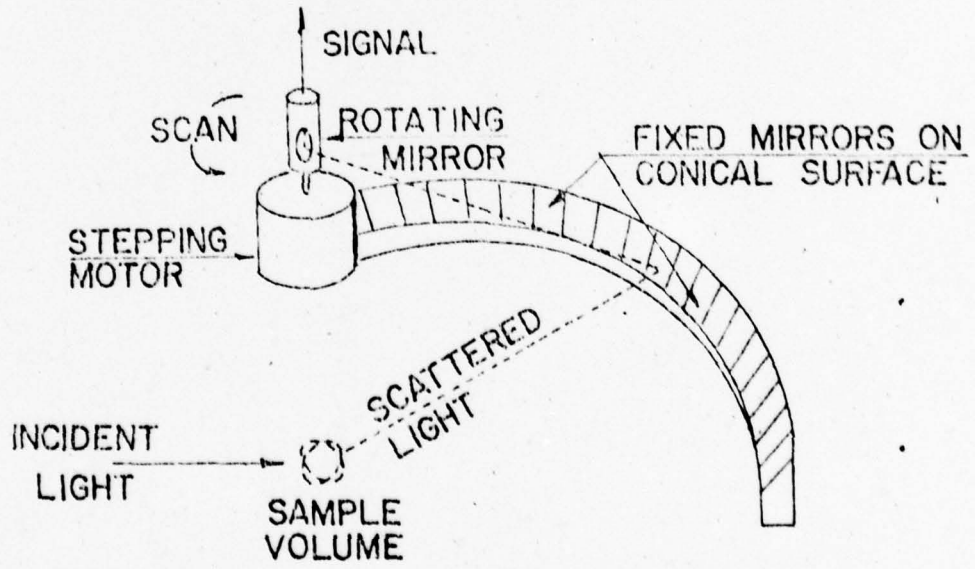

Figure 1. Top, scanning mirror is on a rotating arm.
Bottom, the scanning mirror is on a small rotating tube.

ensemble of tumbled irregular particles could be represented by an equivalent sphere in the backscatter range as it can be in forward scatter.

Approach

Mie scattering from low-loss spheres of one size has very pronounced structure, which is washed out by size dispersion or by departure from spherical shape. We elected to work with optical scattering in the laboratory with aerosols of controlled size, shape, composition, and size dispersion. Monodispersions of particles of known size and shape were generated with a Berglund-Liu [6] vibrating-orifice aerosol generator. Particle shape and size distribution was monitored by SEM photographs.

The light source was a pulsed nitrogen laser pumping a dye laser. Pulses were typically 10 kW 4 ns FWHM at 627 nm, 10 pps.

The polar nephalometer went through three models. The first model used a scanning mirror mounted on an arm to sample and reflect a 1° x 1° portion of the scattered light to a small mirror on the axis of rotation, and out through the tube on which the arm pivoted. The scanning was controlled by a stepping motor. Light was analyzed by a fixed quartz analysis prism, detected by photomultipliers. Mechanical overshoot was a problem. The second model, used to obtain the data reported herein, used 96

fixed mirrors in place of the scanning arm (Figure 1). Scanning was accomplished by rotating a small 1.2 cm diameter mirror on the axis of rotation; though controlled by a stepping motor, the system had no problems with mechanical overshoot. The scanning was accomplished in 23 sec, limited by paper tape punch rate. The third model, which is being tested at present, eliminates scanning altogether. It uses fiber optics at angles selected by a Backus-Gilbert[7] routine, of various lengths so as to delay each scattered pulse by a different amount, forming an optical parallel-to-serial pulse converter. The longer fibers not only have more delay, they have higher loss, and they are placed strategically at angles where scattering is stronger, so there is compression of the dynamic range of the detector output. The fiber bundle goes to a photomultiplier detector (Figure 2). The chamber in the third model contains provisions for suspension of a single oriented particle, and is vacuum-tight. We are attempting to capture single particles after scattering on a glass slide and to prepare them for SEM photography in the same apparatus. The third model provides a pulse train with the scattering information obtained from a single laser pulse incident on a single oriented particle.

The data acquisition system was designed and built at the University of Florida, which was a mistake. It delayed the program at least two years. It consists of a fast sample-and-hold unit for each of two photomultipliers, one for each polarization channel, an A/D converter, paper tape punch, and control logic. It could capture the 4 ns pulse and perform a 12-bit digitization reliably. (The

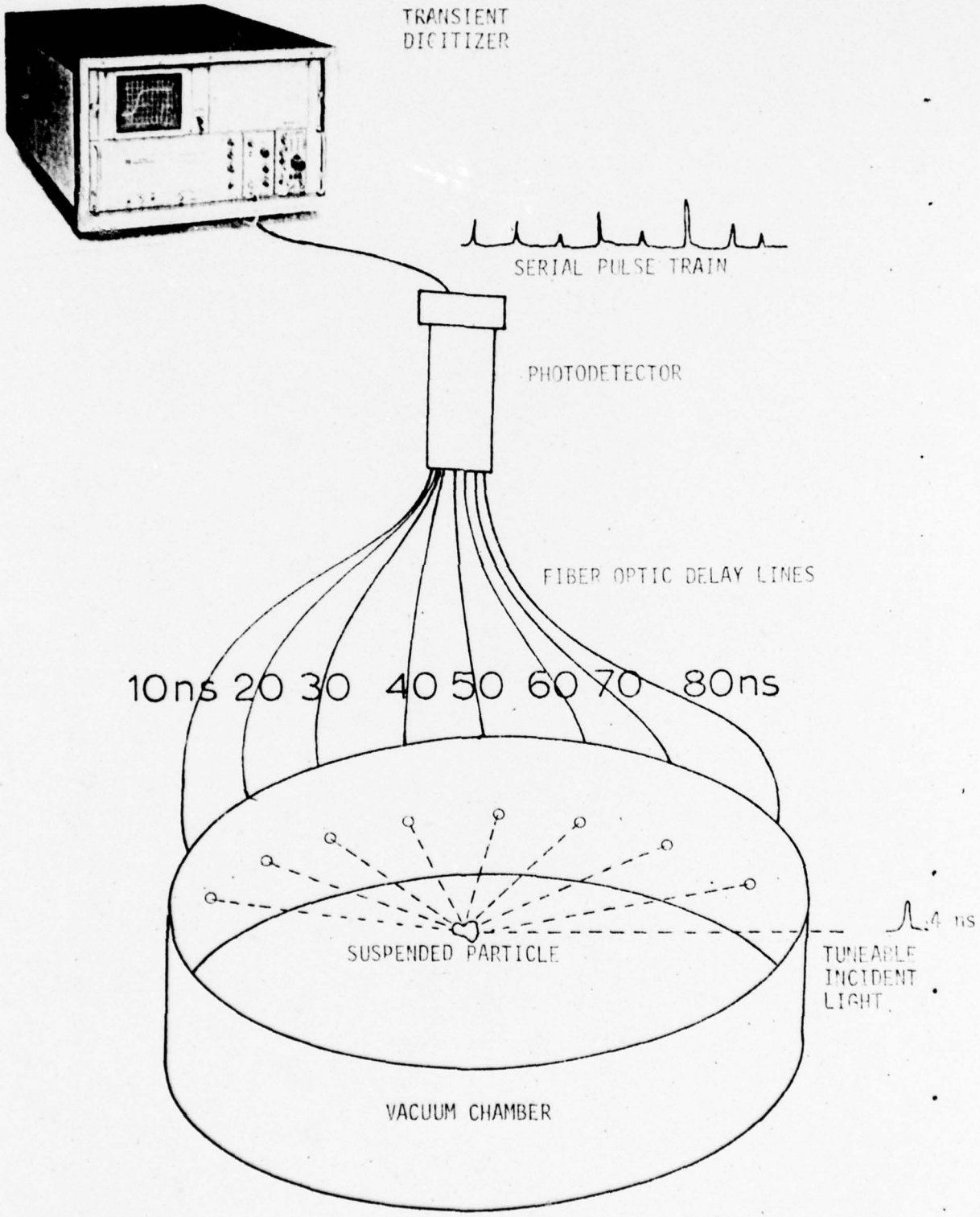

Figure 2. Fiber optic delay lines are used for a parallel to serial pulse converter, and for dynamic range compression.

development problems were due to noise pickup from the thyratron in the nitrogen laser, combined with personnel changes in the Electronics Shop.) At the time it was built, it exceeded the capabilities of any commercially available equipment. For the third model nephalometer, a different data acquisition system is required, such as Tek R7912/Wp 2010.

The procedure was to build the apparatus, test with spheres and compare with Mie theory, test with ellipsoids and compare with published results of others, then proceed to cubes and other shapes we manufacture.

Experimental Results

The calibration of the apparatus is shown in Figure 3. The upper curve shows the experimental data points with individual error bars together with the theoretical curve calculated from Mie theory, using the index of refraction and size dispersion data provided by the manufacturer. There are only two adjustable constants altogether: the gain of each photomultiplier. Calibration runs are taken before and after each experimental run with non-spherical particles. In this case we would expect the data to agree with the theoretical curve, and to the extent that it does not, further improvement in our experimental procedures is indicated. A SEM photograph of the calibration particles is included. The fit in Channel 2 is very good, and in Channel 1 it is fair.

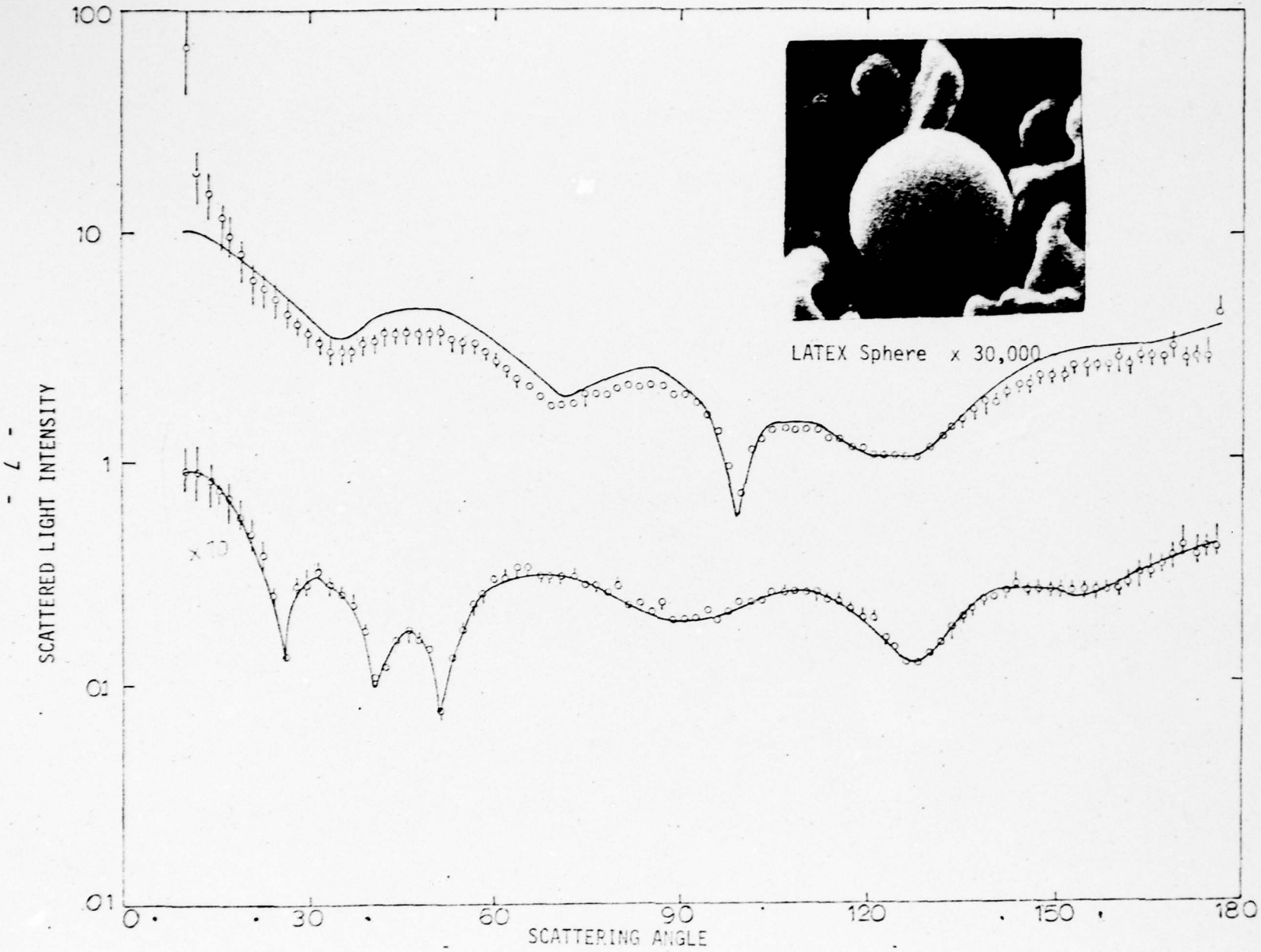

Figure 3. Calibration of light scattering instrument with spheres.

The data taken from Cladosporium particles is shown in Figure 4. The theoretical curves are the best fit that could be obtained by using a spherical particle model and varying the size parameter. The fit is qualitatively correct in the middle range of scattering angles, but does not fit the data as well as in the calibration runs. This difference in goodness of fit indicates that the tumbled Cladosporium particles are only crudely represented by a spherical scatterer. An SEM photograph of a cladosporium spore is shown. (The SEM preparation process has dried out the spore so that it has partially collapsed, but its original spheroidal shape is discernable.)

The data from NaCl crystals is shown in Figure 5.Again the theoretical curves are the best fit that could be obtained using a spherical particle model and varying the size parameter (the index of refraction is known). The SEM photograph shows that we have avoided clumping of the salt crystals through beta-particle irradiation of the aerosol. (It is questionable if the particles are rounded on only one side as shown; the shape has been influenced by the collection and/or sample preparation process. The volume is correct.) We see that the spherical particle model is qualitatively correct, but it does not fit the data as well as it did in the calibration runs.

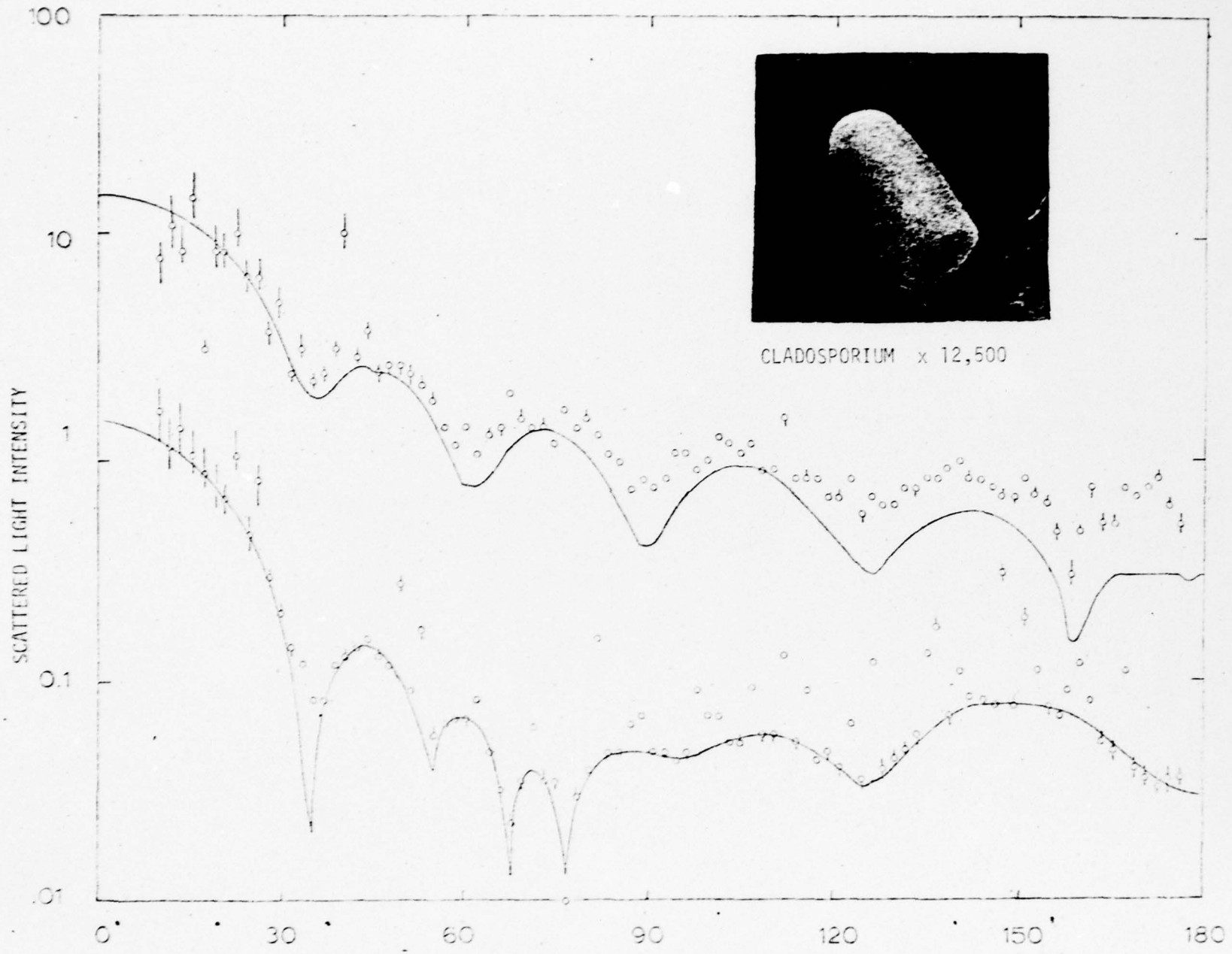

Figure 4. Cladosporiums (2μm) data with best fit spherical model (k=7.2)

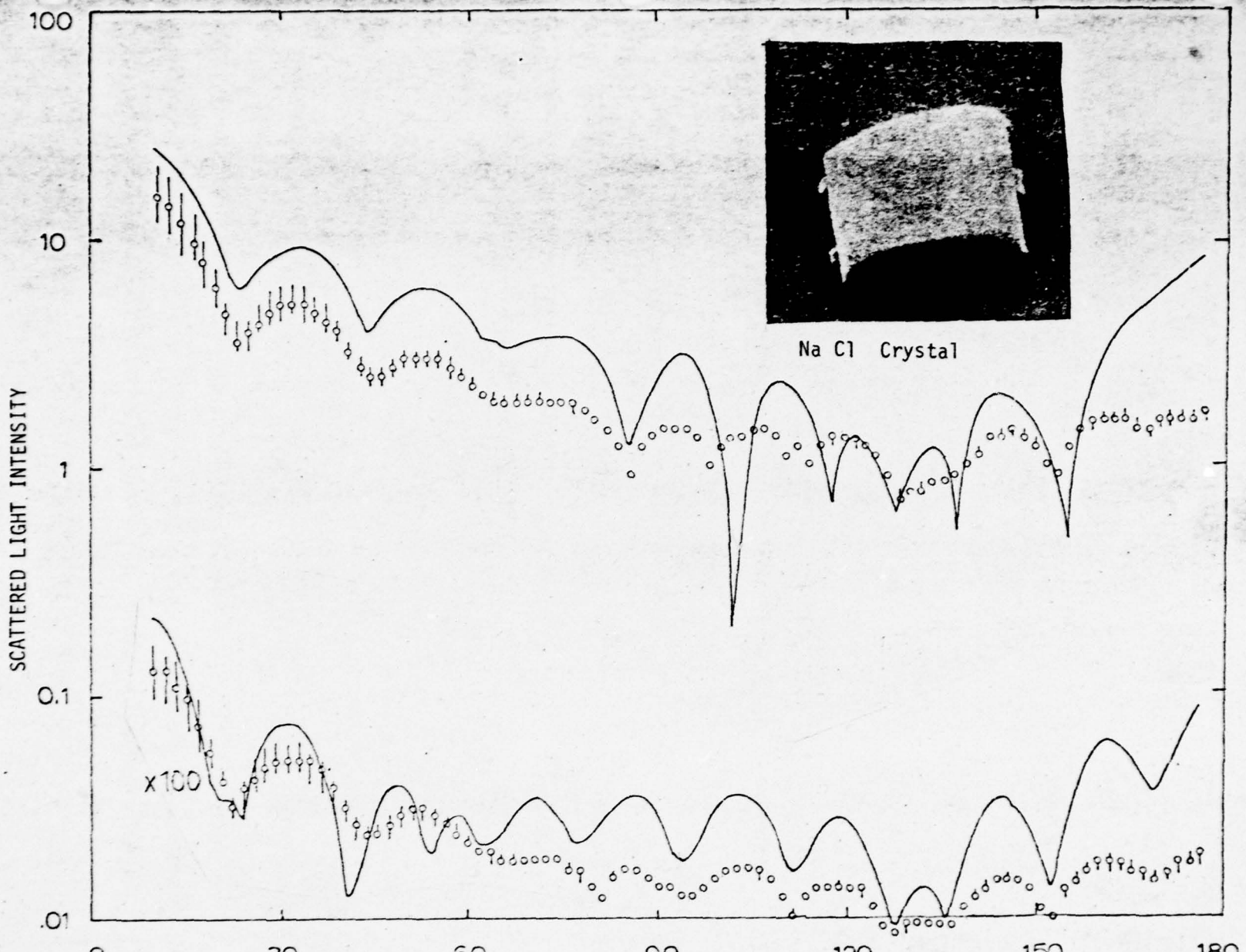

Figure 5. Quasi-cubical NaCl Crystals (4μm) with best fit spherical model(k=10.2)

Conclusions

We have constructed a digital polar nephalometer which takes accurate detailed scattering patterns from irregular dielectric particles of known and irregular shape in tumbled monodispersions. The accuracy of the apparatus at this point is indicated by the calibration runs in Figure 3. We have taken subsequent scattering patterns from two different types of irregular particles about which we have index of refraction information and some shape information. The data is not well fit by any sort of equivalent sphere model; therefore tumbled irregular particles do not scatter like eqivalent spheres.

Further work is warranted. The data is of sufficiently high quality to lend itself to fitting with theories for irregular particles[8]-[12].

Bibliography

[1] A.C.Holland and G. Gagne, Applied Optics 9, 1113(1970)

[2] T.R.Marshall, C.S.Parmenter, M.Seaver, Science 190,375(1975)

[3] T.R.Marshall, C.S.Parmenter, M.Seaver,J.Colloid and Interface Science 55, 624(1976)

[4] C.S.Parmenter, private communication.

[5] R.G.Pinnick, D.E.Carroll and D.J.Hofmann, Applied Optics 15, 384(1976)

[6] R.N.Berglund and B.Y. Liu, Env. Sci. & Tech. 7, 147(1973)

[7] E.R.Westwater and A.Cohen, Applied Optics 12, 1340(1973)

[8] G.Ward, Proc. IEEE, Southeastcon 74,160(1974)

[9] C.Yeh, P.Barber, UCLA-ENG-7431 (1974)

[10] Reiner Eiden, Applied Optics 5, 569(1966)

[11] Herschel Weil, C.M.Chu. Applied Optics 15, 1832(1976)

[12] S.Asano, G. Yamamoto, Applied Optics 14, 29(1975)

SCATTERING OF LIGHT FROM NONSPHERICAL DIELECTRIC PARTICLES: SPHEROIDAL CLADOSPORIUMS (2μm) CUBICAL NaCl CRYSTALS (4μm)

By

ISMAIL KIRMACI

A THESIS PRESENTED TO THE GRADUATE COUNCIL OF
THE UNIVERSITY OF FLORIDA
IN PARTIAL FULFILLMENT OF THE REQUIREMENTS FOR THE
DEGREE OF MASTER OF ENGINEERING

UNIVERSITY OF FLORIDA

1978

TABLE OF CONTENTS

Abstract of Thesis Presented to the Graduate Council
of the University of Florida
in Partial Fulfillment of the Requirements
for the Degree of Master of Engineering

SCATTERING OF LIGHT FROM NONSPHERICAL DIELECTRIC PARTICLES: SPHEROIDAL CLADOSPORIUMS (2μm) CUBICAL NaCl CRYSTALS (4μm)

By

Ismail Kirmaci

March 1978

Chairman: Markus Zahn
Major Department: Electrical Engineering

A digital polar nephalometer has been constructed to measure the intensity and polarization of light scattered from aerosol particles of controlled shape. The scattering at 94 angles (0° to 180° in 1.8° intervals) is digitized by a fast sample-and-hold circuit and recorded on punched paper tape. The light source is a dye laser pumped by a 120 kilowatts nitrogen laser, providing approximately 10 kilowatt 2 nanosecond pulses at a chosen wavelength across the visible spectrum. The device was calibrated with polystyrene latex spheres. Sample data for spheroidal particles (2μm cladosporiums), and cubical particles (4μm NaCl particles) formed by a Berglund-Liu aerosol generator, are shown. It is found that the backscatter from nonspherical particles differs significantly from that for spheres so that a tumbled irregular particle is not equivalent to a sphere.

Markus Zahn
Chairman

CHAPTER I

INTRODUCTION

The experiment described in this thesis was performed to provide data to test and compare existing theories of light scattering from irregular dielectric particles. Several theories giving both exact and approximate solutions have been put forth independently in this area in recent years.

Ward [1] has an approximate solution for convex particles using the Rayleigh hypothesis. Yeh and Barber [2] have a nearly exact solution using Waterman's extended boundary value approach [3], properly treating the region outside the surface but using an approximate extension between the irregular surface and the inscribed sphere. Eiden [4] gave an exact solution which treats irregular particles as spheres with a wave number k which is an arbitrary function of position, which he applied to objects with one rotational axis of symmetry. Herschel Wiel extended his integral-differential representation of induced surface currents and their reradiated field from conducting objects to dielectric objects, namely thin disks [5]. Ward gave a solution using a generalized boundary value approach [6], but without numerical results. Acquista [7] has developed Shifrin's integrodifferen-

tial equation [8] into a potentially useful approach. These theories need to be further expanded, applied, and compared to determine the range of validity of each. Our role is to provide further data of high accuracy and high resolution against which these theories may be checked by other workers. We have calibrated our apparatus with spheres, for which the theory is unquestioned, and have gone on to take data for some very simple shapes. Close attention has been given to measurements near backscatter in the range 160-178° where little published data exists (Pinnick et al. [9] have data to 170°), and where the scattering is strongly affected by shape.

The experimental work is done to obtain a relation between the shape, size and refractive index of the scatterer and the angular distribution of the scattered light. Accuracy is of great importance to elucidate the effects of the variables involved. The instrumentation must be carefully calibrated. A polar nephalometer is used to measure the angular distribution of scattered light in two polarizations. It consists of a light source to illuminate the particles, a means of collecting information by scanning the scattered light, detectors and a data recording system.

Many varieties of polar nephalometers have been constructed and used and are being used for aerosol measurements. Ours is unique in its angular range, digital data acquisition system, and tuneable laser source. The information obtained is in form of intensity and polarization of the scattered

light which later is used to find the properties of the scatterer. Accuracy and economy were the principal considerations in designing the experimental apparatus.

The history of polar nephalometers goes back to Elterman's work (1952) with searchlights which could be termed an early "polar nephalometer." In 1960 B. S. Pritchard and W. G. Elliott [10] used tungsten filament lamp with a calcite polarizer as a source with a synchronous motor to take the scan. Angular resolution was said to be 2° to 7° chosen according to sensitivity measurements. Angle range was not given. One photomultiplier was used for detection. Information was recorded on a chart recorder. Calibration was done with a then new procedure which employed a diffusing plastic screen of known reflectance and admittance as a standard. In this case the sample volume was outside in the atmosphere.

The formulation and modeling of light scattering properties obtained from experimental data was tried by Kurt Bullrich [11] in 1964. He was interested in the scattering function and polarization of the light scattered by a volume of air. His light sources were a 500 watt high-pressure mercury lamp for short waves and a 1000 watt high-pressure xenon lamp for visible and near infrared regions. He used a "Waldram iris" to keep the sample volume constant and eliminate the background illumination. He also used a photomultiplier for detection.

Reiner Eiden [12] studied the polarization (1966) to determine the imaginary part of the refractive index and aerosol size distribution. He used a polarized xenon pressure lamp with uniform spectral emittance as a source to scan an angle range from 50° to 160° in 10° intervals. A photomultiplier tube was used for detection. He measured the aerosol size distribution for the particle radii from .1 to 3 μm, and pointed out that 70% relative humidity was a dividing line for aerosol growth because of the condensation of water vapor upon the surface of the aerosol particles. Using three different wavelengths (.443, .548, .639 micrometers) he stated that the accuracy of the magnitude of the refractive index was 1%. His results were affected by the turbulence of dust in the air since he worked in the actual atmospheric conditions.

The first careful laboratory experiments on irregular particles were carried out by A. C. Holland and Gagne [13]. They used a tungsten halogen lamp and a recording polar nephalometer consisting of two identical telescopes, one fixed at 11°, the other scanning a range from 18° to 166°. The particles were carried by a jet of dry nitrogen gas. The calibration procedure was based on using a standard sheet of known reflectivity. Photomultipliers were used for detection. The particles used were 5μm silica with a refractive index of 1.55. Measurements were made at two wavelengths. They concluded that the light scattering for a polydispersion of randomly oriented irregular particles

was very similar to that for spherical particles except near back-scattering where the differences were striking.

Studies collecting more information on complex index of refraction of atmospheric aerosols have been made by G. Grams [14] from 1973 to date. His polar nephalometer moves the chopped He-Ne laser light source. The angular range is 15°-165°. Angular resolution is limited to .5°, by photomultiplier field of view. In these airborne studies, particles are also collected with am impaction device for microscopic analysis. Mie theory is used to fit curves for various complex indices of refraction and size distribution functions.

H. H. Blau et al. [15] constructed a polar nephalometer in 1970 to study spherical Mie scattering. A He-Ne laser was used to scan an angular range of 10°-170°. A photomultiplier was used for detection. The scatterers were suspended in an electric field; size ranged from 7.5μm to 11μm in diameter and indices of refraction from 1.55 to 1.63. Calibration procedures were not mentioned in this paper. Blau et al. [16] constructed another nephalometer to determine water droplet concentrations and size distributions. In this case a Ga-As diode laser with .6W Cw output at 8500A° was used, the scattering was measured at 30°, 45° and 60°. Calibration was made by a known size droplet from a hypodermic injection needle. A photomultiplier tube was used; the pulse height was taken as proportional to projected area, and pulse rate as proportional to particle density. In both cases the angular resolution was less than 1°.

A very fast instrument for measurement of light scattering was made by Gucker et al. [17]. The system used a He-Ne gas laser with 50MW output power at 6328Å. Scanning was made from 7° to 173° and 187° to 353° in 14.5 msec. Photomultipliers were used for detection. The instrument was calibrated with polystyrene latex particles. More complex instruments have also been made, for example that of Arlon J. Hunt and Donald R. Huffman [18]. They used a piezo-birefringence modulator to modulate the polarization state of the incident light beam, which was a collimated high pressure Hg lamp. Detection was done by a photomultiplier tube covering an angle range of 0° to 168°. Their results for latex spheres agreed with Mie theory. They concluded that the fluctuations were due to the additional particles in the latex sols that were not specified by the manufacturer.

Many different forms of aerosol sizing and counting instruments are commercially available. The problems with these instruments are calibration and maintenance. With the utmost care still the accuracy of 10% in sizing becomes an optimistic estimate. While this continues to be a practical problem that has not been solved yet, there is a reasonable agreement between the integrated scattering coefficient for irregular particles and equivalent spheres fitting the same size distribution. So-called integrating nephalometers measure all the light scattered ray between 60° and 120°. Irregularity of the scattering particle has little effect on

the total scattering into this angular range. A comparison of this is given in a recent paper by R. G. Pinnick, D. E. Carroll and D. J. Hofmann [19]. The objectives of this experiment are similar, but the experimental techniques are different. Pinnick et al. used an argon ion laser of 2W output power at 514.5nm. All measurements were made at this wavelength. The scattering was collected throughout an angle range of 10° to 170°. Several monodispersions of polystyrene latex, salt, and sodium chloride were sampled. They concluded that the scattering might be modeled with some success using Mie theory for spherical solid particles of equal cross-sectional area, providing the particle size parameter is less than about 5. For larger particles, they found that Mie theory overestimated the scattering in non-forward angles.

This particular research aims to help find a better model for light scattering from irregular shapes by experimenting with a variety of shapes and sizes of aerosols and wavelengths of incident light. At this point of progress we were only able to experiment with three shapes of one size each using one wavelength of incident light.

CHAPTER II

THEORY

Theoretical Background

Solutions to Maxwell's equations lead to the fact that scattering event can be described as a linear transformation (see Appendix I). The matrix multiplication representing this transformation is,

$$\begin{bmatrix} I_s \\ Q_s \\ U_s \\ V_s \end{bmatrix} = \frac{1}{k^2} \begin{bmatrix} \\ S_{ij} \\ \\ \end{bmatrix} \begin{bmatrix} I_o \\ Q_o \\ U_o \\ V_o \end{bmatrix}$$

The Stokes vectors of both incident light (I_o, Q_o, U_o, V_o) and scattered light (I_s, Q_s, U_s, V_s) depend only on the characteristic of the two light beams, while the scattering matrix (S_{ij}) depends only on the characteristics of the scattering media. Light plane polarized parallel to the reference plane of scattering has Stokes vector (1,0,0,0) and light plane polarized perpendicular to the plane of scattering has Stokes vector (0,1,0,0).

I, Q, V, and U involve the parallel and perpendicular components of time averaged complex electric field,

$$I = \langle E_{//} E_{//}^{*} + E_{\perp} E_{\perp}^{*} \rangle$$

$$Q = \langle E_{//} E_{//}^{*} - E_{\perp} E_{\perp}^{*} \rangle$$

$$U = \langle 2\mathrm{Re}(E_{//} E_{\perp}^{*}) \rangle = \langle E_{//} E_{\perp}^{*} + E_{\perp} E_{//}^{*} \rangle$$

$$V = \langle 2\mathrm{Im}(E_{//} E_{\perp}^{*}) \rangle = \langle i(E_{//} E_{\perp}^{*} + E_{\perp} E_{//}^{*}) \rangle$$

// - parallel component

$\perp$ - perpendicular component

* - complex conjugate

$E_{//}$ and $E_{\perp}$, U and V characterize elliptical polarization, k is the wavenumber of incident light. The scattering matrix (S_{ij}) is a 4x4 matrix which can be reduced to less than 16 elements depending on symmetry considerations in various scattering situations. These elements can then be related directly to the intensity functions obtained from Mie theory. The intensity functions are given in terms of the particle complex refractive index m, size parameter x, which is the ratio of particle circumference to the wavelength and the angle from forward scattering direction, θ.

For scattering in a medium that is isotropic and free of optical activity the scattering matrix is found to be

$$S_{ij} = \begin{bmatrix} S_{11} & S_{12} & 0 & 0 \\ S_{12} & S_{22} & 0 & 0 \\ 0 & 0 & S_{33} & S_{34} \\ 0 & 0 & -S_{34} & S_{44} \end{bmatrix}$$

For single homogeneous spherical particles,

$$S_{11} = I_2(m,x,\theta)$$

$$S_{22} = I_1(m,x,\theta)$$

$$S_{12} = 0$$

$$S_{33} = S_{44} = L(m,x,\theta)$$

$$S_{34} = D(m,x,\theta)$$

The intensity functions:

I_1 characterizes the perpendicular, I_2 characterizes the parallel polarizations where L and D are for elliptical polarization.

This theory for the characterization of polarization is not shape dependent. The values of the elements depend on shape. Measurements of the average intensity of light scattered from uniform polystyrene latex particles were made for comparison with Mie scattering theory (see Appendix II). This is used for calibration.

The scattering of electromagnetic waves by an ellipsoid of arbitrary size and optical properties may be solved exactly, using the method of separation of variables. The procedure would be to formulate the problem in ellipsoidal coordinates and express the solution of the wave equation in a series of ellipsoidal harmonics. However, Stevenson used a different approach by showing that the general solution of electromagnetic scattering problems can be expressed as a power series in the ratio of the dimension of the scatterer

to the wavelength (see Appendix III). We used this theory to analyze scattering by cladosporium spores.

While the exact solutions give a means of standard to check the experimental work, solutions for irregular particles are not yet well known.

Further studies have been made on the subject which will not be explained in detail since it is beyond the scope of this thesis.

CHAPTER III

EXPERIMENTAL APPARATUS

A polar nephalometer is constructed to digitize and record light scattering measurements (Fig. 1). It consists of a scattering chamber, nitrogen pumped dye laser, digital data recording system and aerosol generator. The tumbled monodispersions generated by the vibrating orifice aerosol generator are illuminated by the laser beam in the scattering chamber. The scattered light is collected by the photomultipliers at several angles. The detected signals are sampled and recorded through a digital data acquisition system.

Scattering Chamber (Fig. 2)

The scattering chamber is a light tight box of dimensions (34x48x78 cm) made of .5 cm thick aluminum. It is lined with black velvet to prevent any reflections. The aerosols flow into the box through a 7 cm diameter hole and are removed through two outlets which have negative pressure to the chamber located 10 cm above and 10 cm beneath the inlet hole. The aerosols are illuminated by the incoming 0.5 cm dia. f/12 laser beam about 8 cm from the injection port. A 1.5 cm portion of the 7 cm x 0.5 cm roughly cylindrical illuminated volume is viewed by the detector optics and is

called the interaction region. The laser beam enters the box through a rectangular slit of .5x2.2 cm focussed (f/12) into the interaction region and then it is sent into a light trap (Fig. 3). The light scattered by the particles is collected by a semicircular mirror arrangement (Fig. 4) which redirects the scattered light to an axial mirror mounted on the shaft of a stepping motor. Light passes out though the hollow shaft, and is analyzed in a stationary Glan air prism. The light passing through the prism is decomposed into parallel and perpendicular components, which the intensities are separately detected by photomultipliers. The secondary mirror has an angular resolution of about 1.3°.

The volume of the interaction region is individually calculated for each laser beam. A spherical lens with 12 in. focal length is used to focus the nitrogen lasers' UV output at the interaction region. Different lens arrangements are used for the dye lasers either to focus the beam or to prevent divergence because of the dimensions of the light trap. A light stopper is used to prevent the direct scattering of light from the entrance slit at the backscatter. The mirrors used are front surface mirrors, silver coated by vacuum deposition on glass slides of 1 mm. thick. The stepping motor is the Sigma Instruments, Inc. 29A-21 Bipolar R/1 Drive motor which has a torque of 115 oz-in. at 2.4 amps. Two microswitches are provided at the 0° and 180° of the motor revolution to stop the operation in case of overshoot.

Digital Data Recording System (Fig. 5)

The data recording system is a very fast digitized electronics which is capable of synchronizing the laser pulse, the stepping motor and the paper tape punch. Laser triggering starts with a manual push button while the mirror connected to the shaft of the stepping motor is at the forward scattering angle, approximately 2° from the optical axis of the laser beam. The scattering light is collected by the photomultipliers and is multiplied to a voltage level detectable by a sensitive instrument. This voltage is fed to a sample-and-hold circuit with a delay time of 10ns. The threshold level for this circuit is 2.5 mV. The samples voltages are digitized by means of a 12-bit analog to digital converter in 40μs, and recorded on a punched paper tape with a BCD coded sequence count. The 12-bit coding is shown in Fig. 6. After the information is punched on the paper tape a command signal triggers the laser, advances the motor and proceeds to sample-and-hold. The main time-limiting factor of the process is the mechanical paper tape punch. It takes about .24 seconds for the paper tape to punch an information set consisting of the sequence count, and voltages for two channels. The whole scan of 94 steps is completed in 23 seconds. The information on the paper tape is decoded and analyzed by using a computer program given in Appendix IV.

The A/D converter and the sample and hold amplifier used are ADC-12QZ and SHA1-2A of Analog Devices, Inc. respectively.

Operation (Fig. 7)

The start box is a push button control with forward and reverse switches. Closing the switch in the forward mode causes the control unit to send a signal to the relay to release the short circuit on the photomultiplier inputs and puts the S/H in the sample mode. At the same time a short pulse of 1.7 μs triggers the laser. The information on the photomultipliers A and B are integrated, partially using the capacitance of the lines. After a very short sampling the mode on the S/H is set to hold by the control unit. The FET control then chooses the input with the fastest hold rate to be digitized. The hold in one input is 10 times longer than the other by manufacturers specifications. Upon the convert command from the control unit this signal is converted by the A/D converter.

The information from the A/D converter is stored in either A or B latches. After it is stored the control unit sets the FET control to the other signal, which is then converted and stored in the other latch the same way. By this time the five-state counter is cleared and the first motor position is put through gate 1 to the output gate and is punched on paper tape upon a signal by the control unit. During the punching there is a busy signal that keeps the counter blocked. With the completion of the first punch

the busy signal is released and punch again command is given which through gate 2 punches the first 6 lines of the information stored in the A latch. This is repeated 4 times until all four 6 lines stored in A and B latches are recorded. As soon as the last bit of information is recorded and the restart is activated, the control unit sends a signal to the motor to proceed one step. The operation up until punching takes 10.4 ms but including the limiting punch time, one set of data is taken in 240ms. The operation, then, is repeated 94 times which is part of the logic circuitry in the control unit. After the 94th step the logic stops the operation.

The reverse mode on the start box is to take the motor back to its original position. During this, none of the other circuitry is activated.

Nitrogen Laser

The construction of the nitrogen laser which is used to pump the dye is from a paper by P. Schenck and H. Metcalf [20]. The design incorporates a bandsaw blade as multiple electrode structure to ensure an even transverse discharge in flowing nitrogen and produces superradiant emission at 337.1 nm. The laser channel consists of two plates of glass supported on an aluminum base (Fig. 7a), which serves both for support and electrical ground. The high voltage edge of the laser channel consists of a copper bus bar, bandsaw blade electrode, and copper spacer. The electrode geometry

has been altered to keep the discharge off the glass walls. Twenty 590 pF capacitors are mounted in parallel, along the laser channel (Fig. 7b). The laser channels is continuously pumped and the nitrogen gas input is leaked in at a constant rate. The storage capacitor is charged to 10-15 kV through a resistor. A Thyratron is used for switching. When the switch closes, the positive side of the storage capacitor is grounded and the other side is kept at a high negative voltage. Its charge, therefore, flows on the bus bar to the dumping capacitors, which provide the energy for the discharge in the nitrogen. This results in direct electron impact excitation of the triplet stages of molecular nitrogen's second positive band and superradiant lasing at 337.1 nm. An Amperex 5C22 Thyratron is used for switching. The best measured power outlet of the N_2 laser of 40 mm Hg. and 12 kV is 120 kW (Fig. 8a,b). The pulse width is 2 ns FWHM.

Aerosol Generator

The generation of monodisperse aerosols is achieved by a Berglund-Liu vibrating orifice aerosol generator [21] machined by University of Florida Engineering Machine Shop. The generator is based on the instability and break-up of a cylindrical liquid jet. A cylindrical liquid jet that is unstable for controlled mechanical disturbances produces equalized droplets, which are dispersed and diluted to form monodisperse aerosols. The minimum liquid velocity to form a liquid jet from a capillary tube is given by,

$$V_{j_{min}} = \left(\frac{8\sigma}{\rho D_j}\right)^{1/2}$$

where σ is the surface tension, ρ is the density of the liquid and D_j is the diameter of liquid cylinder jet. A practical formula for producing uniform droplets is, $3.5D_j < \lambda < 7D_j$ where λ is the wavelength of the disturbance. The disturbance in the system is created by a piezo electric ceramic connected to a signal generator. A syringe pump delivers the liquid at a constant rate. This liquid jet then breaks up into uniform droplets at the frequency of the ac voltage. The uniform droplets then disperse by means of a turbulent air jet for the particles. A schematic diagram of the entire flow system and the dispersion system is given in Fig. 9 and Fig. 10 respectively. The diameter of the droplet can be calculated by,

$$D_d = \left(\frac{6Q}{\pi f}\right)^{1/3}$$

where Q is the liquid flow rate and f is the frequency of the disturbance.

The diameter of an aerosol made by dissolving a non-volatile solute in a volatile solvent is given by,

$$D_p = C^{1/3} D_d = \left(\frac{6QC}{\pi f}\right)^{1/3}$$

where C is the volumetric concentration of the solute in this solvent. Correcting this value for impurities gives

$$D_{p_{corr}} = \left(1 + \frac{I}{C}\right)^{1/3} D_p$$

where I is the volumetric fraction of the impurities in the solution.

The output aerosol concentration is equal to the ratio of the ac voltage frequency to the total air flow.

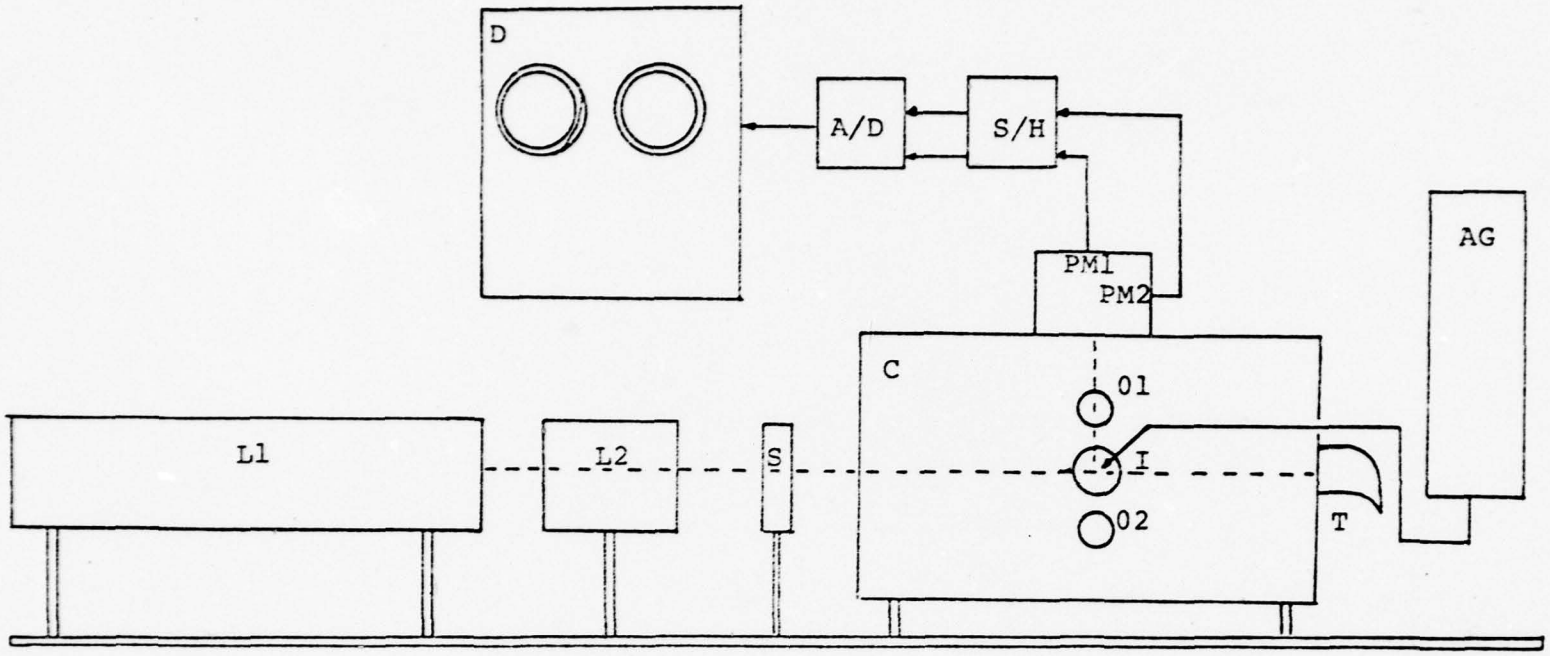

Fig. 1 Schematic diagram of experimental apparatus. L1: Nitrogen laser; L2: Dye cell complex; S: Variable entrance slit; C: Scattering chamber; AG: Aerosol generator; I: Aerosol inlet to the chamber; 01,02: Aerosol outlets; PM1,PM2: Photomultipliers for vertical and horizontal polarizations; S/H: Sample and hold; A/D: Analog to digital converter; D: Digital data recording system with paper tape punch.

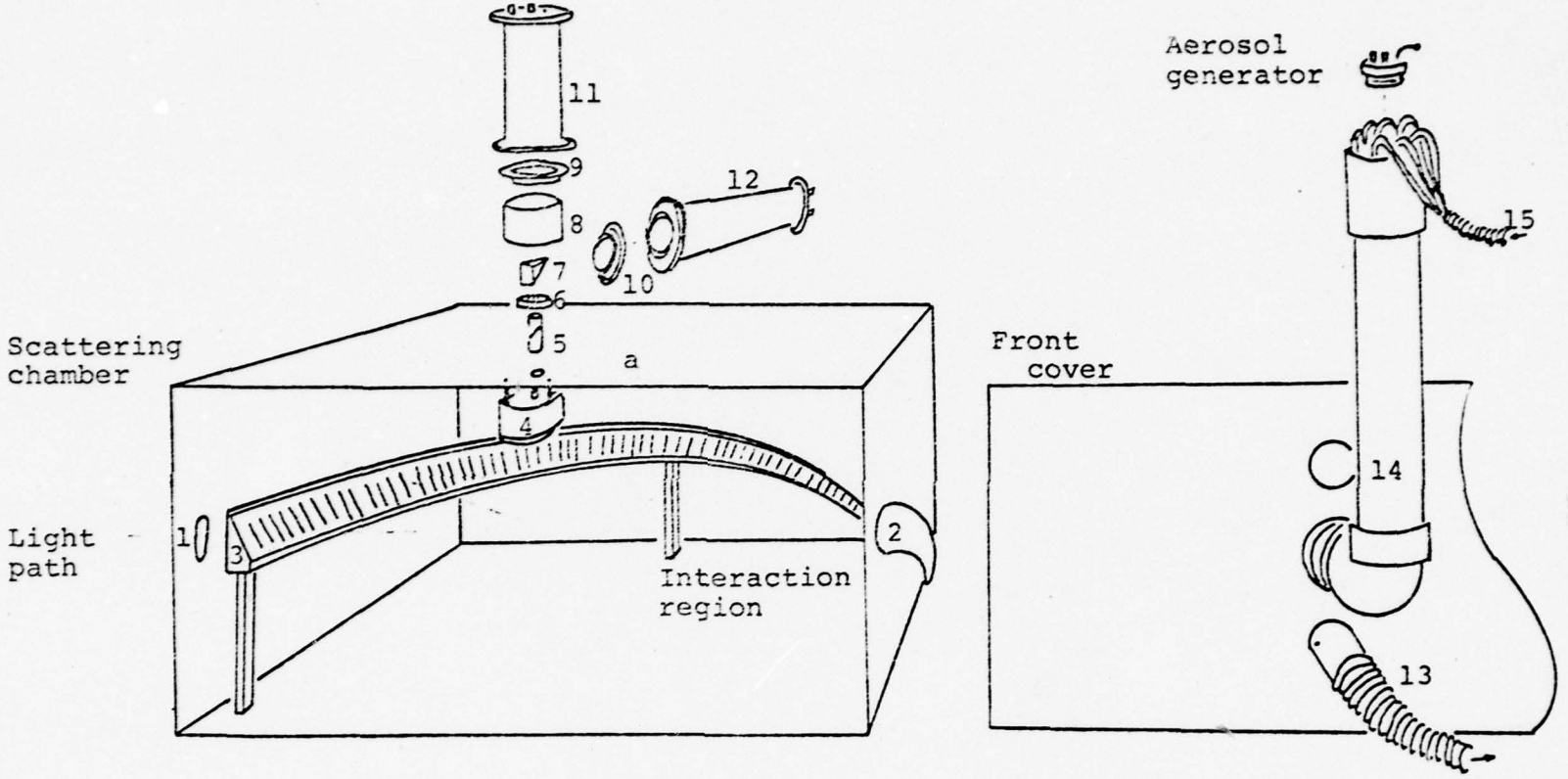

Fig. 2 Scattering chamber:
1: Entrance slit; 2: Light trap; 3: Circular mirror arrangement for first order scattering; 4: Stepping motor; 5: Secondary mirror attached to motor shaft; 6: Ball bearing; 7: Glan air prism for different polarizations; 8: Housing for prism; 9,10: Photomultiplier mounts; 11,12: Photomultipliers; 13: Aerosol outlet; 14: Aerosol inlet; 15: Particle free dilution air, a: Microswitches to avoid motor overshoot.

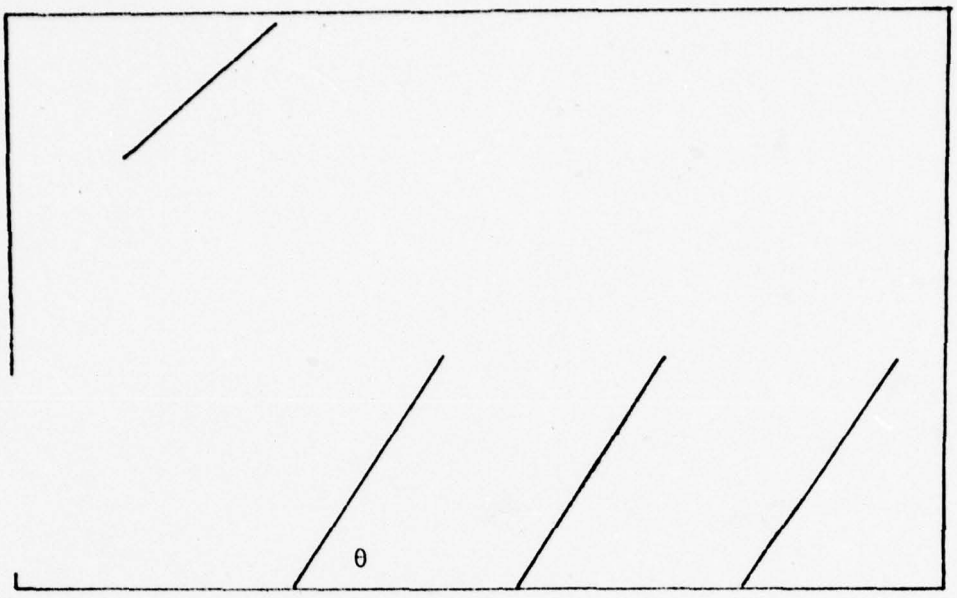

Fig. 3 Light trap: Brewster angle 57°, index of refraction: 1.55 3mm black glass (Actual dimensions).

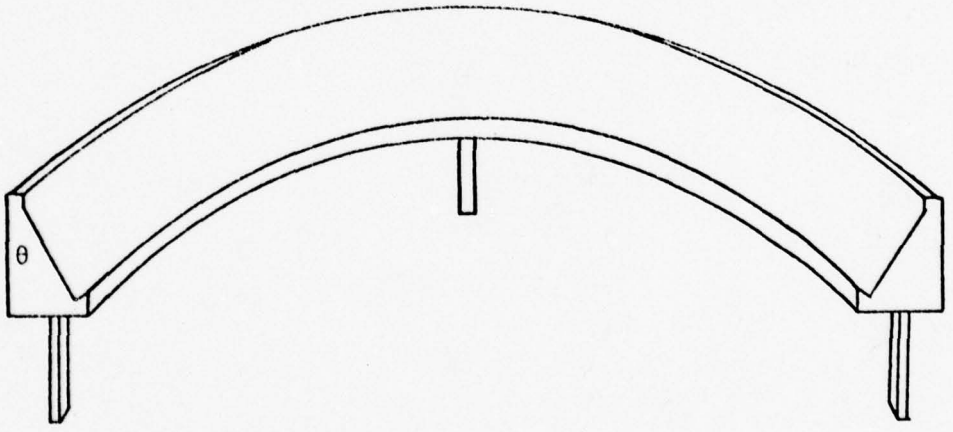

Fig. 4 Primary mirror mount θ = 12.095°.

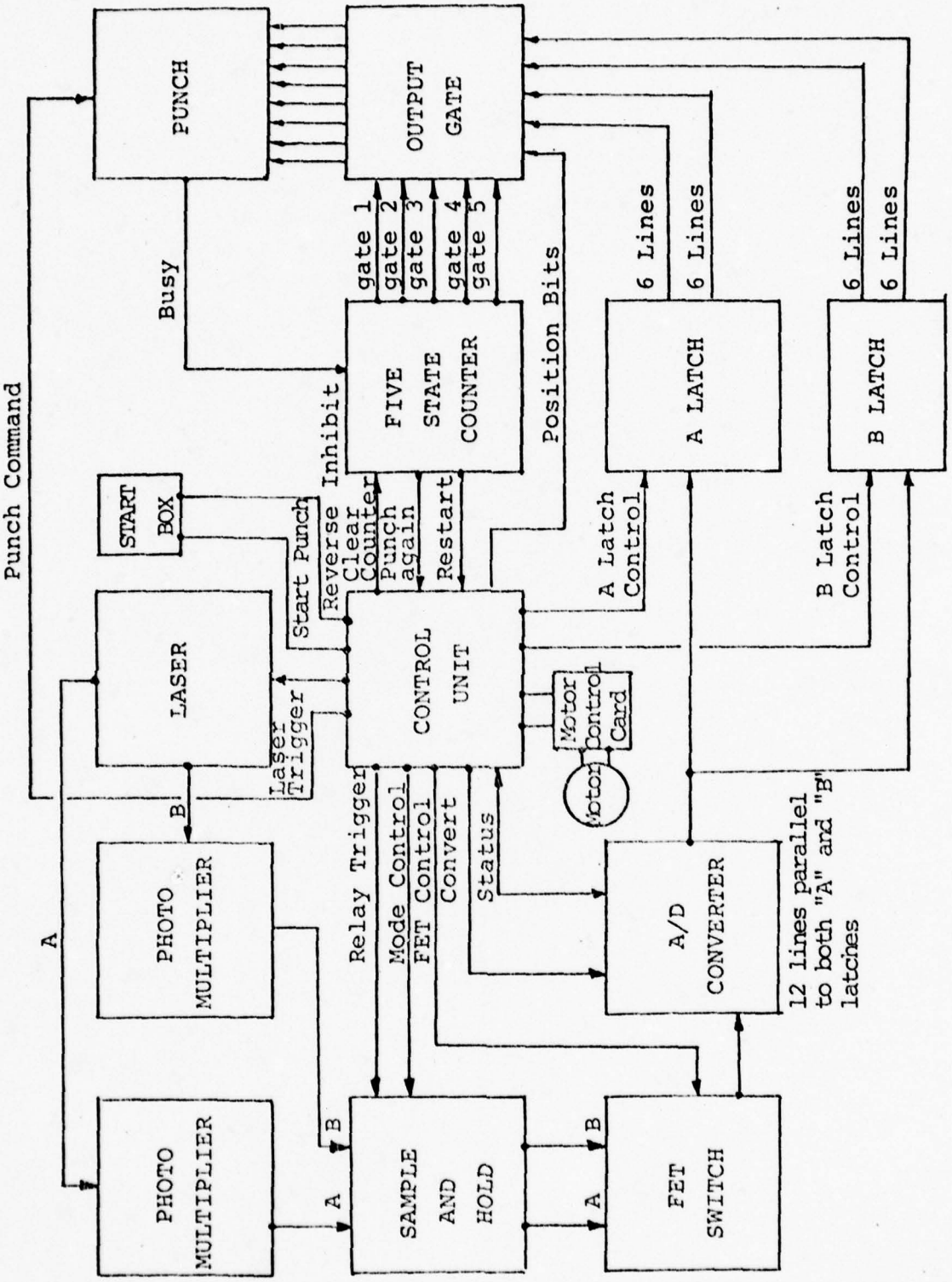

Fig. 5 Block diagram digital control system.

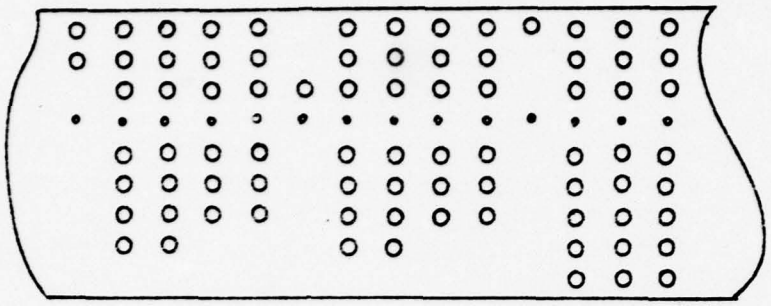

Identifies channel #2

Channels one and two are binary coded as follows:

Binary#	Bit#		Bit#	Binary#
2^5	7		1	2^{11}
2^4	8		2	2^{10}
2^3	9		3	2^9
2^2	1Ø		4	2^8
2^1	11		5	2^7
2^0	12		6	2^6

(Full scale = 10V = 12^{12}-1)

Binary#	Digit
2^0	U
2^1	N
2^2	I
	T
2^3	S
2^0	T
2^1	E
2^2	N
2^3	S

Fig. 6 BCD coding.

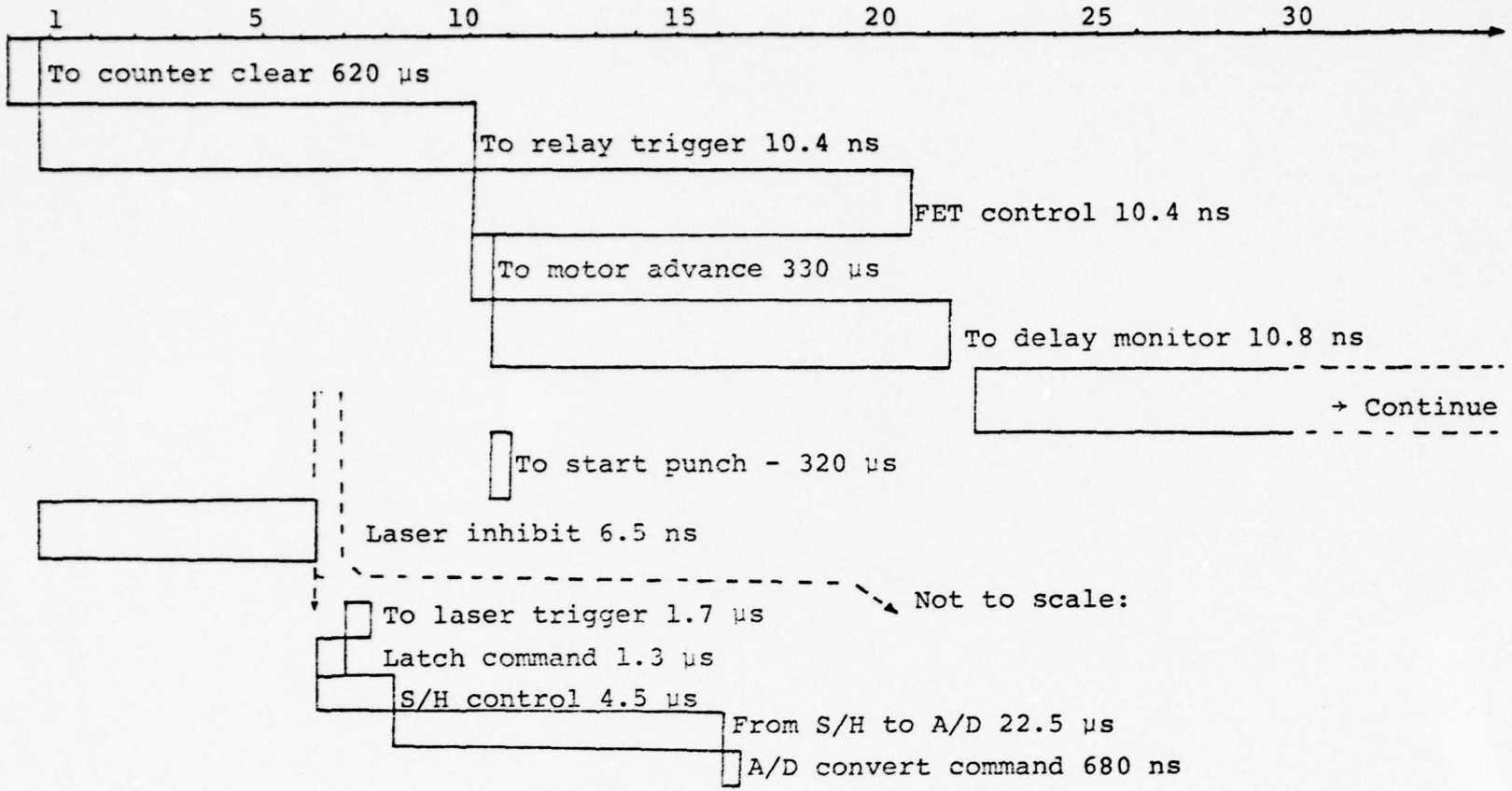

Fig. 7 Timing diagram for the operation of the digital data recording system.

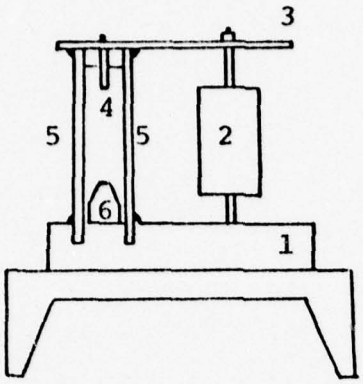

Fig. 7a Cross sectional diagram of laser channel.
1: Base; 2: Dumping capacitor; 3: Bus bar;
4: Band saw blade; 5: Plate glass;
6: Aluminum bar to centralize discharge.

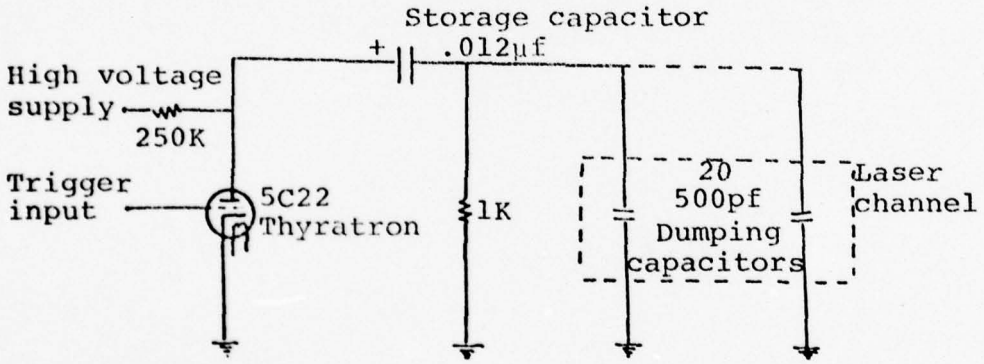

Fig. 7b Diagram of discharge electronics in nitrogen laser.

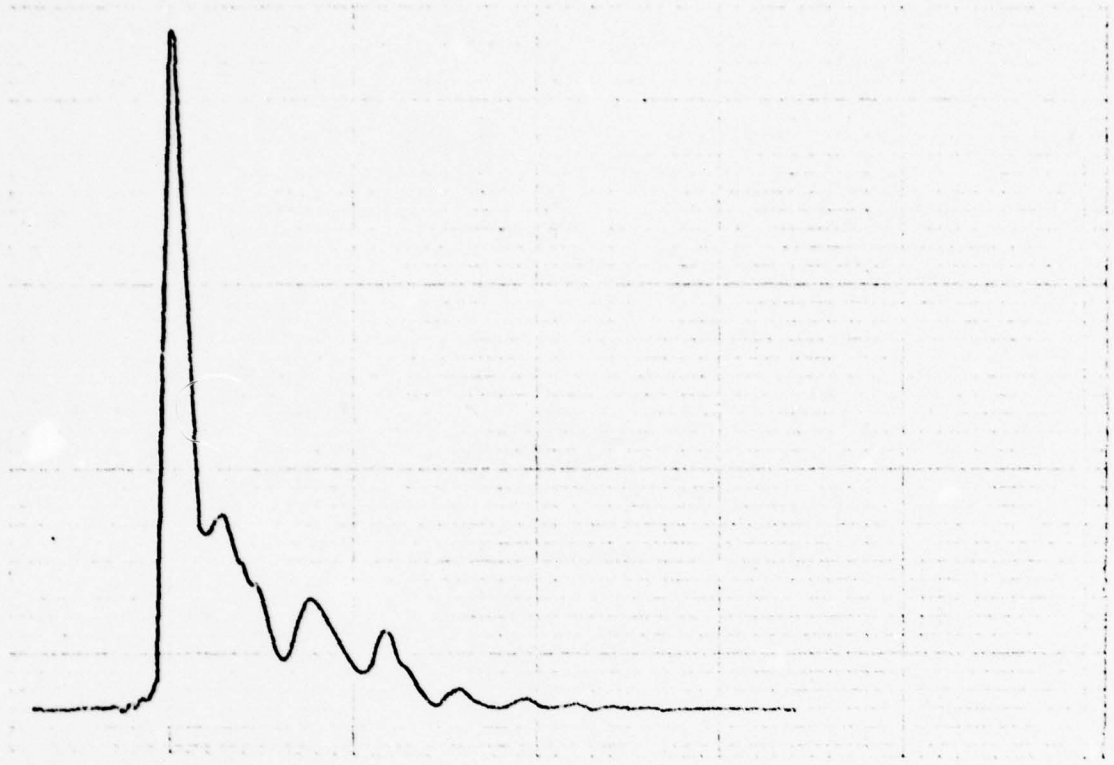

Fig. 8a Nitrogen laser output through photo diode oscilloscope at 40 ns/div and 40 nV/div. FWHM = 6 ns.

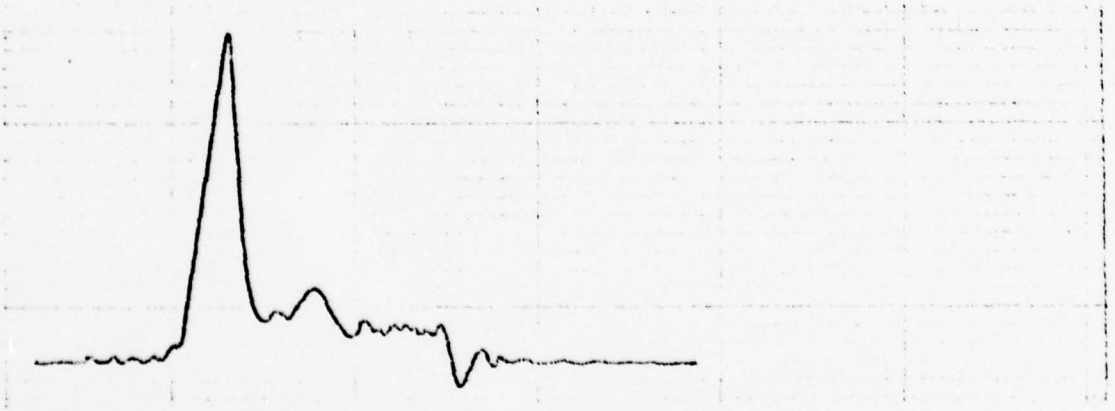

Fig. 8b Dye laser output using Rhodamine B at 627 nm. 20 ns/div and 40 nV/div.

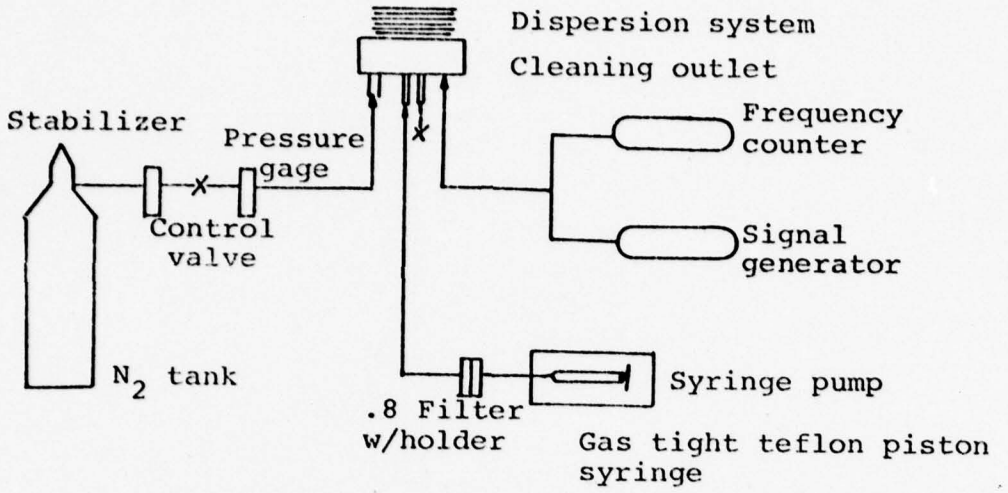

Fig. 9 Schematic diagram of Aerosol generator.

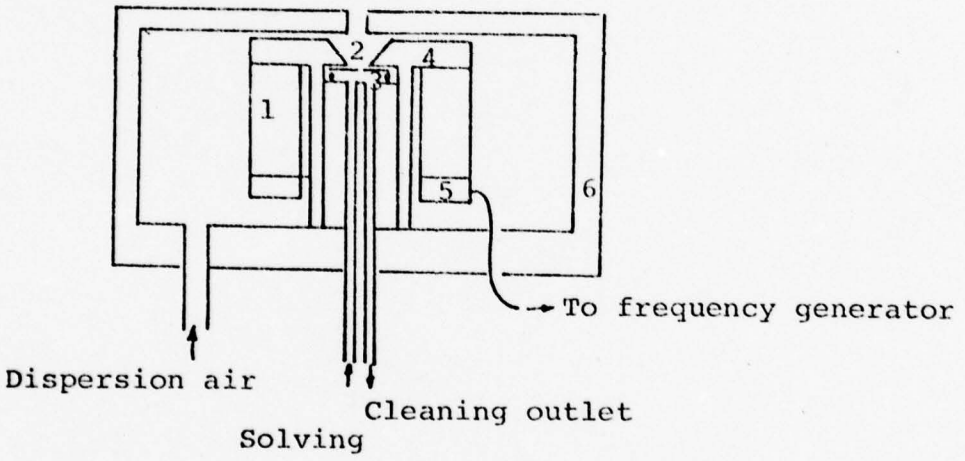

Fig. 10 Schematic diagram of the dispersion system. 1: Transducer (piezoelectric); 2: 25μm Platinum orifice; 3: Teflon O ring; 4: Housing 1 grounded; 5: Housing 2 live; 6: Slip cover.

CHAPTER IV

EXPERIMENTAL RESULTS AND CONCLUSION

The data that will be presented in this chapter consists of experimental and theoretical results obtained from spherical polystyrene latex particles, elliptical cladosporium spores and cubical sodium chloride crystals. The experimental apparatus is calibrated by the comparison of theoretical Mie calculations for spheres and experimental scattering measurements from 1.091μm polystyrene latex particles of Dow Chemicals run LS 1028 E (standard deviation .0082). A discussion of this is in Appendices VI and VIII and the statistical program developed is given in Appendix IV. Evaluation of experimental results and comparisons with the theories are fully automated by a series of computer programs. The computer program used for theoretical Mie calculations is given in Appendix V.

Several corrections are made on the experimental data because of scattering geometry and statistical error calculations. In the comparison of theory and experiment, a set of

two different, log intensity versus scattering angle, graphs are presented for incident light plane polarized parallel and perpendicular to the plane of scattering.

Due to the fact that the scattered light is collected through 180° by the rotation of a mirror and then analysed by a stationary prism, the intensity of the light received at each photomultiplier tube is a combination of the parallel and perpendicular components of the polarized light, regardless of how the incident beam is polarized. This phenomena can be explained by a simple rotation matrix, which can be expressed as:

$$M(\theta) = \begin{bmatrix} \cos\theta & \sin\theta \\ -\sin\theta & \cos\theta \end{bmatrix}$$

The analyser prism divides the scattered light into its parallel and perpendicular polarizations; therefore when the light incident to the prism is rotated by θ we get:

$$I_1 = (I_{//}\cos\theta + I_{\perp} \sin\theta)^2$$
$$I_2 = (I_{\perp}\cos\theta - I_{//} \sin\theta)^2$$

I_1 and I_2 are the intensities observed by the first and second photomultipliers respectively; $I_{//}$ and $I_{\perp}$ are the parallel and perpendicular polarizations of scattered light. The terms on the right hand side of the equations are amplitude squares that are directly proportional to the intensities. So, to recover

the parallel and perpendicular components of scattered light we have to take square roots of the observed intensities and solve for $I_{//}$ and $I_{\perp}$. By doing so we get:

$$I_{\perp} = \sqrt{I_1}\ \sin\theta + I_2\ \cos\theta$$
$$I_{//} = \sqrt{I_1}\ \cos\theta - \sqrt{I_2}\ \sin\theta$$

Because of the involvement and complexity of the computer program that processes the raw data, instead of rotating the obtained results we applied the inverse rotation matrix to the theoretical curves for comparison. Appendix V shows the computer program developed to perform this rotation on theoretical Mie calculations.

The results are then analyzed as I_1 and I_2, first and second channels respectively. Several computer plotted graphs of experimental results and theoretical curves are given for each run of parallel and perpendicular polarized incident beam. (an analyser prism is used in the entrance slit to achieve linear polarization of incident light)

The light source used throughout this experiment is N_2 laser pumped Rhodamine B (Eastman # 4453) which lases in the range of 685nm to 616 nm due to its tuning and superradiant character. An oscilloscope picture of this output versus wavelenght, using a monochrometer and a slow sweep of the scope by modulated z axis on time base, is given in Fig. 11. It was impossible to detect the wavelength of the laser light

each time the experiment was run. The variables involved in the tuning of the dye laser and the operation of N_2 laser caused the wavelengths to be slightly different at each set of runs. Therefore, we took the best theoretical fit to the experimental data as the theory to be compared with. A scanning electron microscope picture of the scatterers in each case are also included in the data set to be presented.

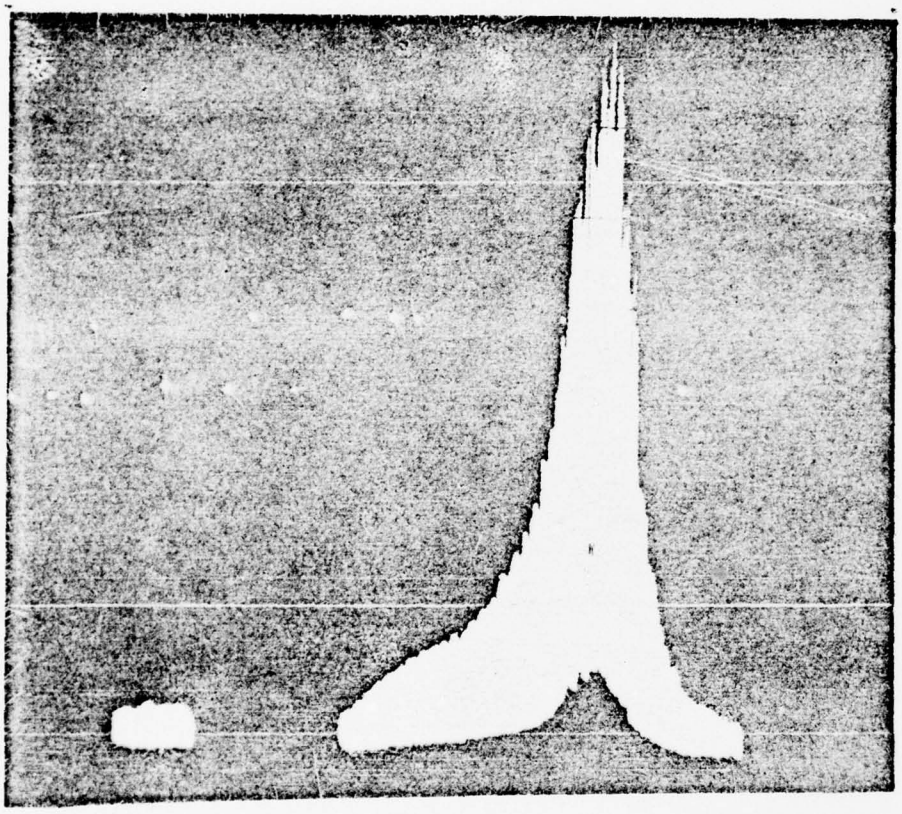

Fig. 11 A picture of the dye laser output versus wavelength taken through an oscilloscope. The tail ends at 641.0nm and starts at 640.0nm. The first peak is due to the superradiance of Rhodamine B.

Corrections For Experimental Data

There are several factors in the experimental data gathering that effected the results directly and indirectly. It is impossible to separate and isolate these problems. The major correction performed on the raw data takes into account the fact that, the scattering is from a volume of several particles. In addition to this, the particles are moving perpendicular to the light path. The velocity of the particles are controlled to be kept at relatively insignificant levels and the number of particles in the interaction region is assumed to be constant. There are also coagulated particles and tumbling effects. Most of these problems are easily eliminated by averaging a large number of runs for each data point. The raw data had to be corrected for the volumetric scattering from the particles in the interaction region. This is treated as an angular gain problem. The effective cross sectional area is found to be (Appendix VI)

$$A_\theta = 2rL \frac{\cos\theta}{\sin\theta} \frac{R\cos\theta + L/2}{R + (L/2)\cos\theta}$$

L - length of the interaction region

r - radius of the interaction region

R - distance of particles from primary mirror

This is divided by the maximum cross sectional area which is 2rL and multiplied by a factor N (0) which is inversely proportional to the square of the distance and the fourth power

of sin $\theta/2$.[26] As a result we get an arbitrary weighing function which can be expressed as:

$$G(\theta) = \frac{\cos\theta}{\sin\theta} \frac{R\cos\theta + L/2}{R + (L/2)\cos\theta} \div (R^2 \sin^4 \theta/2)$$

The observed values can be expressed as a convolution of one particle with $G(\theta)$ in the real time. To recover the data for one particle, an inverse filtration process is applied to the data points since the intensities we need are already multiplied by $G(\theta)$ in the frequency domain. Fast fourier techniques are used for this purpose. A study of this can be explained as follows: Let $a(\theta)$ be the intensities observed by the photomultipliers. This is already a digital quantity. If $i(\theta)$ is the scattered intensity of one particle, we have

$$a(\theta) = i(\theta) * g(\theta)$$

in the real time domain

Then in frequency domain:

$$A(\theta) = I(\theta)\ G(\theta)$$

Since

$$\int_{-\infty}^{\infty} i(\theta)\ g(t-\theta)d\theta = \int_{-\infty}^{\infty} I(\theta)\ G(\theta)e^{-i\theta t}d\theta$$

to recover $i(\theta)$:

$$I(\theta) = A(\theta)/G(\theta)$$

$$i(\theta) = \int I(\theta) e^{-i\theta t} d\theta$$

which is the inverse Fourier transform of $I(\theta)$.

Then,

$$i(\theta) = \int \frac{A(\theta)}{G(\theta)} e^{-i(\theta)t} d\theta$$

This is found to be the best correction (by statistical analysis) in order to fit the calibration data to theory and is used for all the outputs.

Other corrections that had to be taken into account are the threshold of the analog to digital converter, and photomultiplier noise. The threshold for channel 1 and 2 of the electronic data acquisition system is measured to be 73mV and 68mV respectively. An average of 0.1 volt deviation was also found; and the relative calibration of the electronic system is entered as a correction to the raw data.

The photomultiplier tubes used in this experiment are RCA type 7265. Photomultiplier noise is measured to be in the range of 120mV to 240mV into 10 Megaohms, which yields a current range of .017μA to .024μA which is well below the specified dark current. Comparing these values with the scattering expectations (Appendix VII) we made sure that the lowest detectable intensity is greater than the background intensities.

The calibration for the relative gain of the photomultipliers are done by dark current measurements and by using several optical fibers. Actually this is not needed in our calculations since we give the results in form of channel 1 and channel 2 which are the photomultipliers outputs. The operational voltages of the photomultipliers chosen are based on this criteria and the linearity of their gain in the desired region.

Fluctuations in the laser output power are not included in these calculations since the negligible variations were corrected by a large sum averaging at each data point. A statistical analysis of the averaging and error calculations are given in the proceeding sections.

Experimental Data And Graphs

The experimental data is given by computer plotted graphs. The variables used are; the size parameter x, which is

$$x = 2\pi r/\lambda$$

where r=Radius of the scatterer,

λ=wavelength of the incident light,

and refractive index R, of the scatterer. The theoretical graphs are chosen to be the best fit to the experimental data.

The explanations of the figures are as follows:

Fig. 12 a,b-The scanning electron microscope pictures of the calibration particle, polystyrene latex, of Dow Chemicals run

LS 1028 E. Particle diameter given by the manufacturer is 1.091 μm and the standard deviation is 0.0082. The mean particle diameter we determined from the electron microscope pictures is 1.04 μm.

Fig. 13 - Theoretical Mie calculations for Channel 1, relative log intensity versus scattering angle with a size parameter of 5.01 and refractive index, 1.592.

Figures 14 to 17 are with scattering volume of 5cm length and .3cm radius. Concentration of the particles yield a number of 15 for number of particles in the interaction region. Corrections are done accordingly.

Fig. 14 - Channel 1 experimental results for polystyrene latex of 1.04 μm diameter. The incident light plane is polarized perpendicular to the plane of scattering.

Fig. 15 - Same as Fig. 14 before subtracting the background.

Fig. 16 - Channel 1 experimental results for polystyrene latex of 1.04 μm diameter. Incident light plane is polarized parallel to the plane of scattering.

Fig. 17 - Same as Fig. 16 before subtracting the background.

Figures 18 to 21 are with scattering volume of 2cm length and .5cm radius. Concentration of the particles are increased to have approximately 35 particles in the interaction region.

Fig. 18 - Channel 1 experimental results for latex particles. Perpendicular polarized incident light.

Fig. 19 - Same as Fig. 7 with the background.

Fig. 20 - Channel 1 latex data. Incident light polarized

parallel.

Fig. 21 - Same as Fig. 20 with the background.

Fig. 22 - Theoretical Mie calculations for channel 2, relative log intensity versus scattering angle, with a size parameter of 5.01 and refractive index 1.592 for latex particles.

Conditions for figures 23 to 26 are the same as those of figures 14 to 17.

Fig. 23 - Channel 2 experimental results for latex of 1.04 μm diameter. The incident light plane is polarized perpendicular to the plane of scattering.

Fig. 24 - Same as Fig. 23 before the subtraction of background.

Fig. 25 - Channel 2 experimental results for latex. Incident light plane is polarized parallel to the plane of scatterine.

Fig. 26 - Same as Fig. 25 without subtracting the background.

Conditions for figures 27 to 30 are the same as those for figures 18 to 21.

Fig. 27 - Channel 2 data for latex. Incident light is polarized perpendicular.

Fig. 28 - Same as Fig 27 including the background.

Fig. 29 - Channel 2 latex data with incident light parallel polarized.

Fig. 30 - Same as Fig. 29 before subtracting the background.

An example of how these data are tabulated is given in

Appendix VIII.

Fig. 31 a,b - The scanning electron microscope pictures of prolate spheroidal, cladosporium spores. Mean particle dimensions are determined from electron microscope pictures, to be 3 μm x 1.5 μm x 1.5 μm. That is for the ellipsoid a = 1.5 μm, b = .75 μm, c = .75 μm.

The experimental results for cladosporium are best compared with Mie theory using a size parameter of 12.1 and a real refractive index of 1.12.

Fig. 32 - Theoretical Mie result for Channel 1, relative log intensity versus scattering angle, using an equivalent spherical particle diameter of 2.47 μm. The wavelength of the incident light is 640 nm.

Fig. 33 - Channel 1 experimental results, for cladosporium. Incident light plane is polarized parallel to the plane of scattering.

Fig. 34 - Same as Fig. 33 with the backgrounds.

Fig. 35 - Channel 1 experimental results for cladosporium. Incident light plane is polarized perpendicular to the plane of scattering.

Fig. 36 - Same as Fig. 35, including background values.

Fig. 37 - Theoretical Mie calculations for Channel 2.

Fig. 38 - Channel 2 cladosporium data. Incident light plane polarized parallel to the plane of scattering.

Fig. 39 - Same as Fig. 38 plus background.

Fig. 40 - Channel 2 cladosporium data. Incident light plane is polarized perpendicular to the plane of scattering.

Fig. 49 - Same as Fig. 48 with backgrounds.

Fig. 50 - Theoretical Mie results for Channel 2.

Fig. 51 - Channel 2 experimental data for NaCl. Incident light parallel polarized.

Fig. 52 - Same as Fig. 51 with backgrounds.

Fig. 53 - Channel 2 experimental results for NaCl. Incident light perpendicular polarized.

Fig. 54 - Same as Fig. 53 with backgrounds.

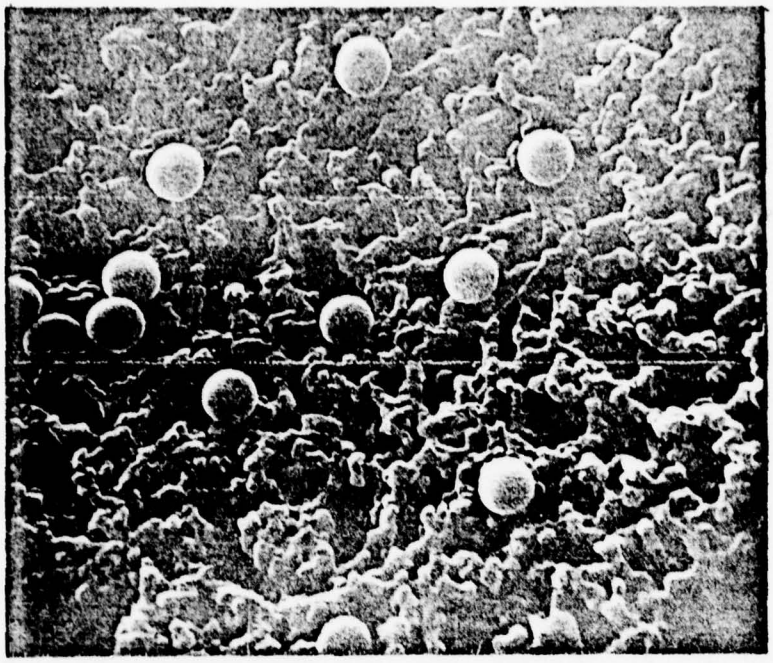

Fig. 12a Spherical polystyrene latex particles collected on millipore filter paper. Measured mean diameter = 1.04 μm. Real Refractive index = 1.592 Magnification in this picture is 7500.

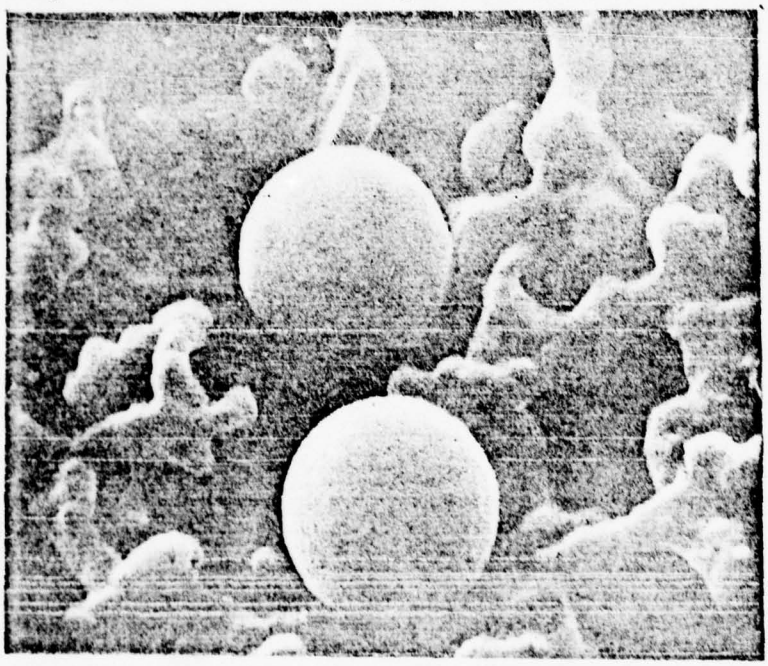

Fig. 12b Same as Fig. 12a with the magnification of 30000.

Fig. 13 Theoretical Mie results for channel 1, x=5.01, R=1.592. Relative Log intensity versus scattering angle.

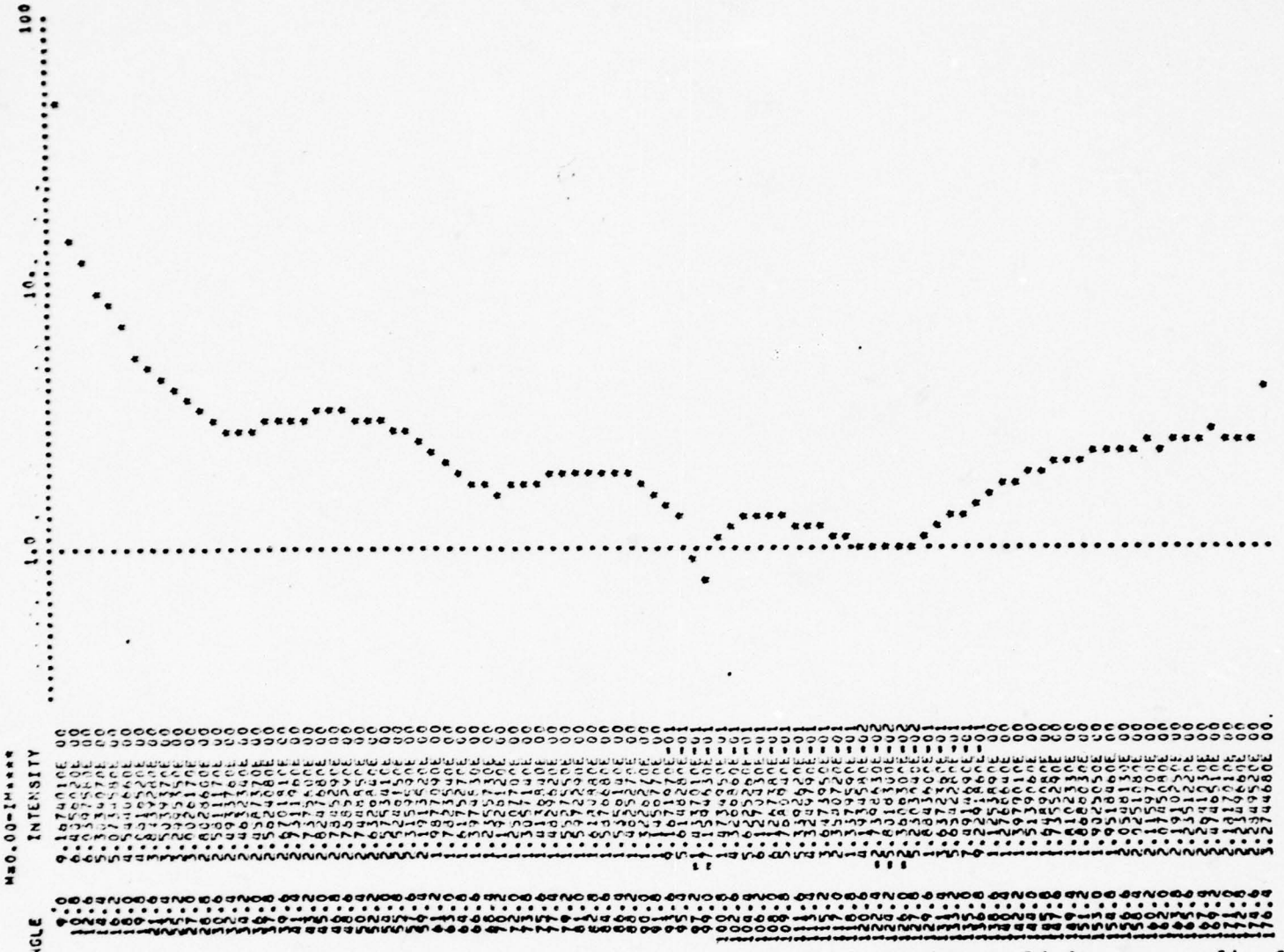

Fig. 14 Experimental polystyrene latex scattering; incident light perpendicular polarized. Channel 1.

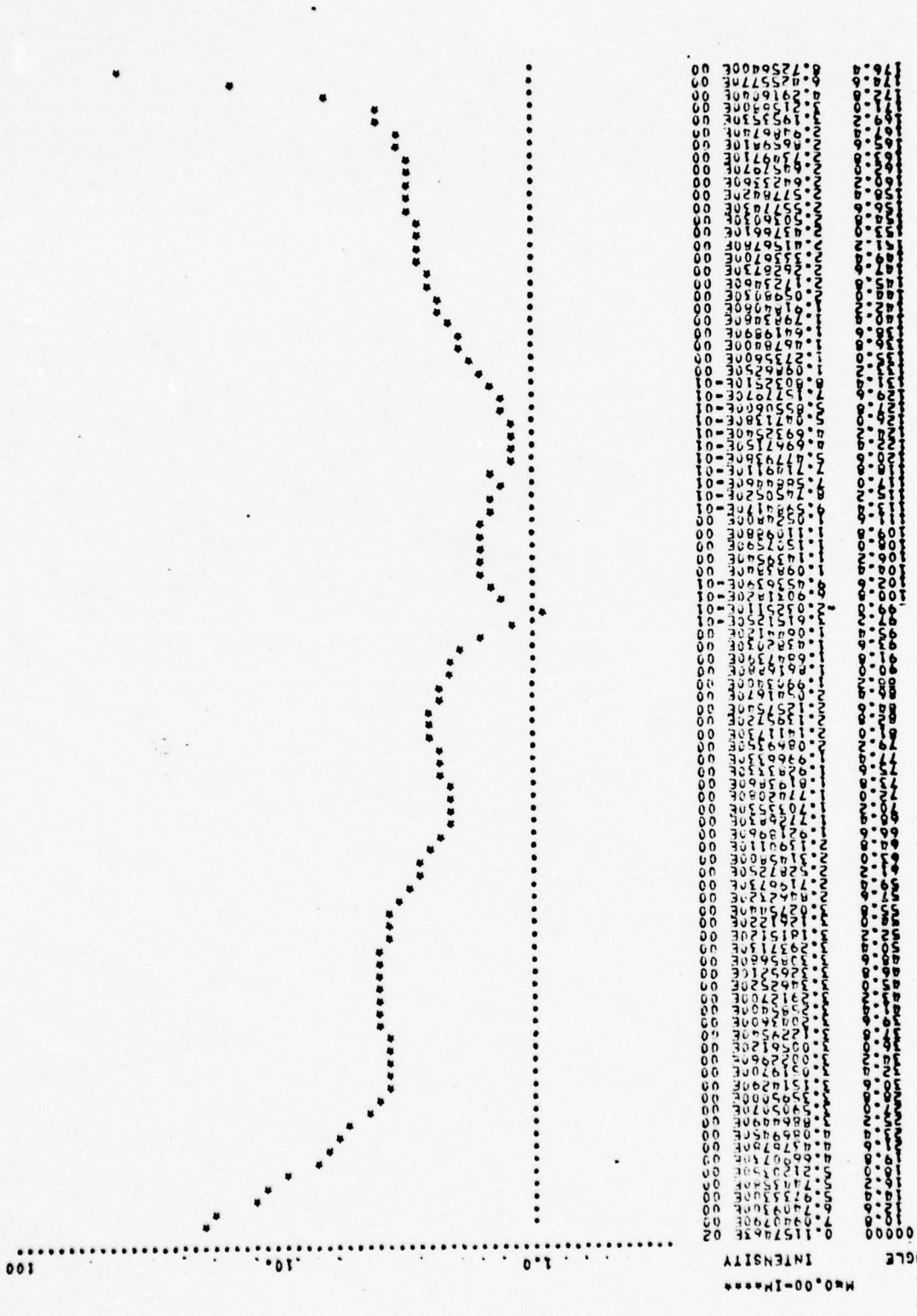

Fig. 15 Data of Fig. 14 before subtracting the background.

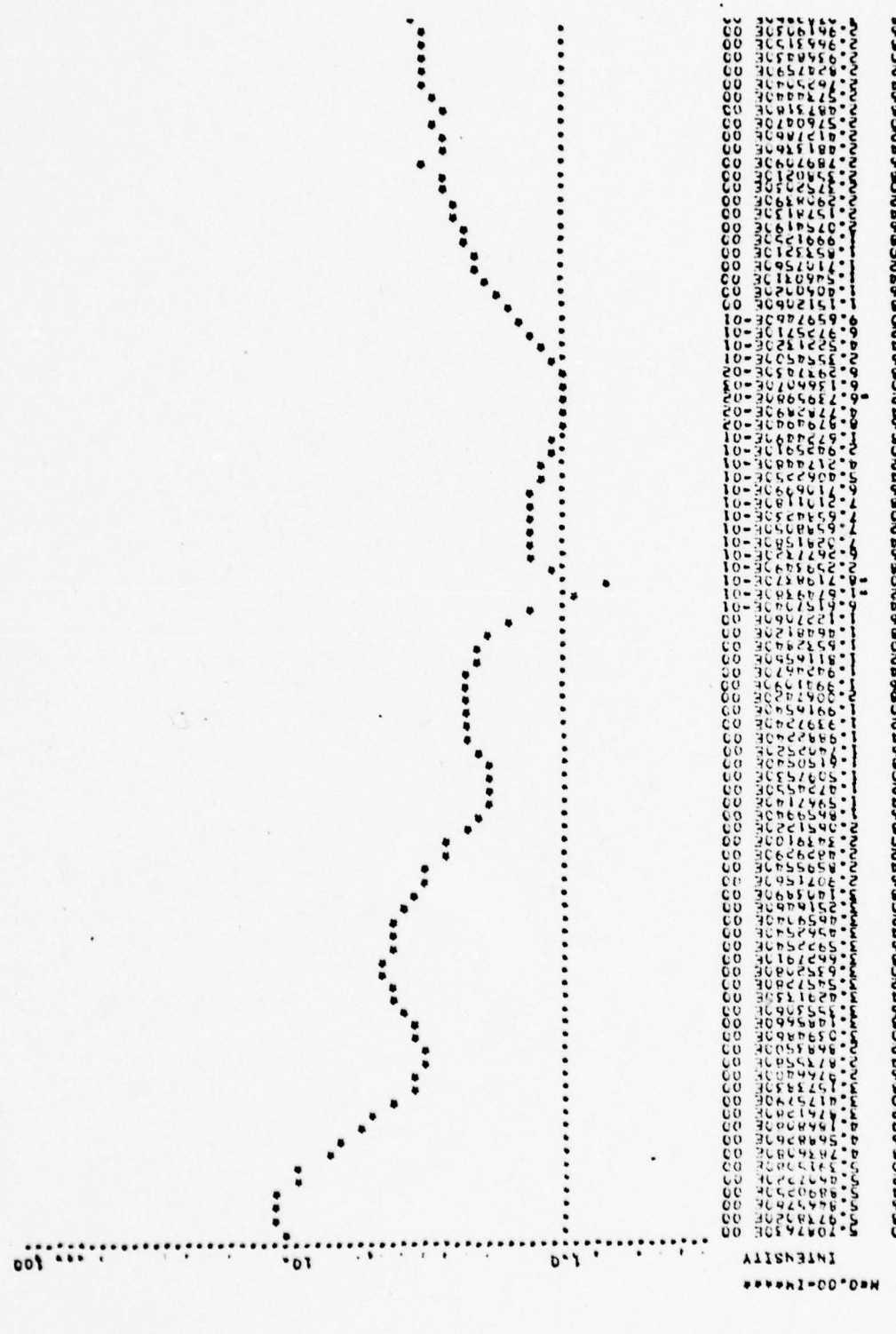

Fig. 16 Experimental data of channel 1 for polysyrene latex of 1.04μm diameter. Incident light parallel polarized.

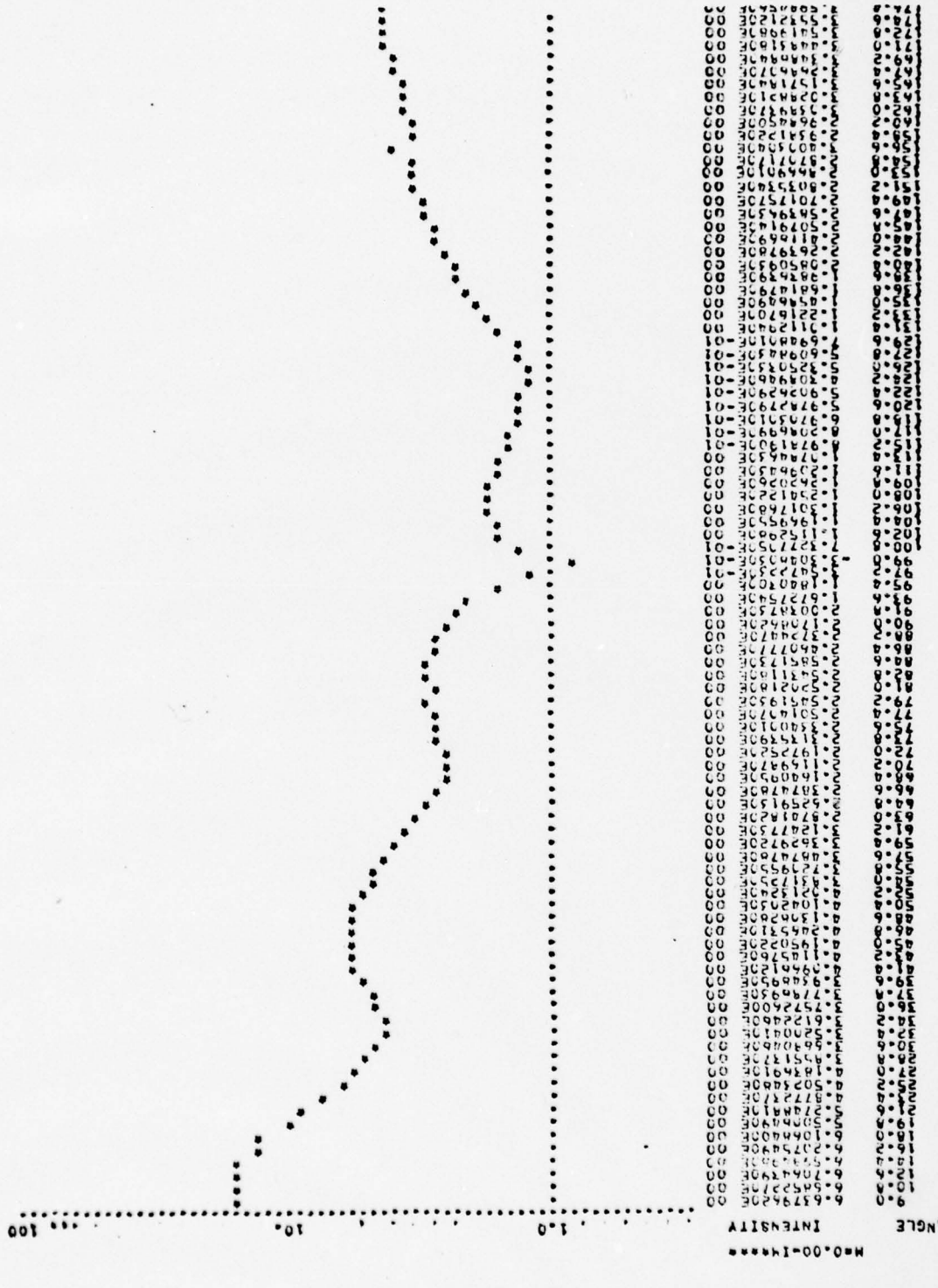

Fig. 17 Data of Fig. 16 before subtracting the background.

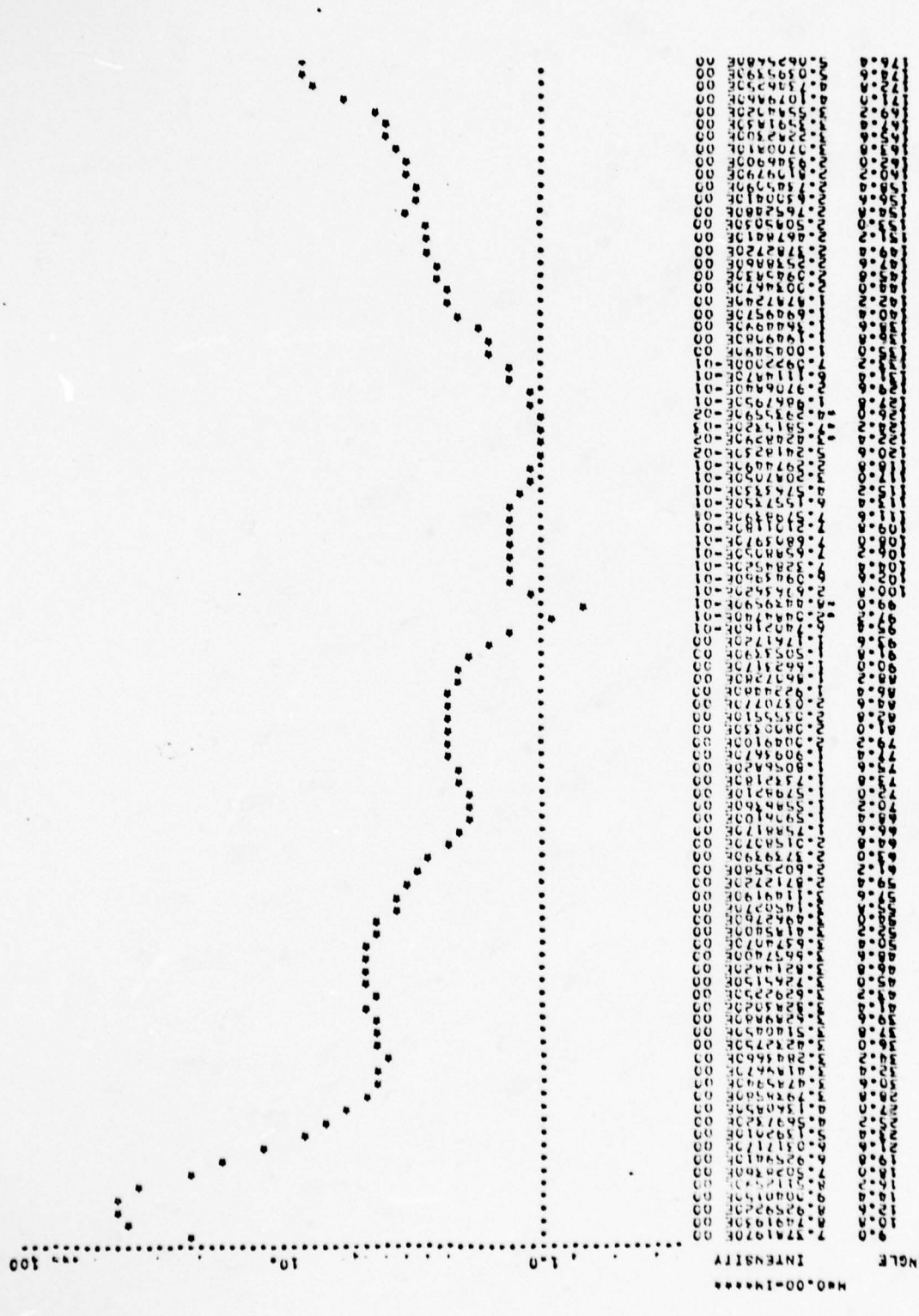

Fig. 18 Latex data with incident light perpendicular polarized.

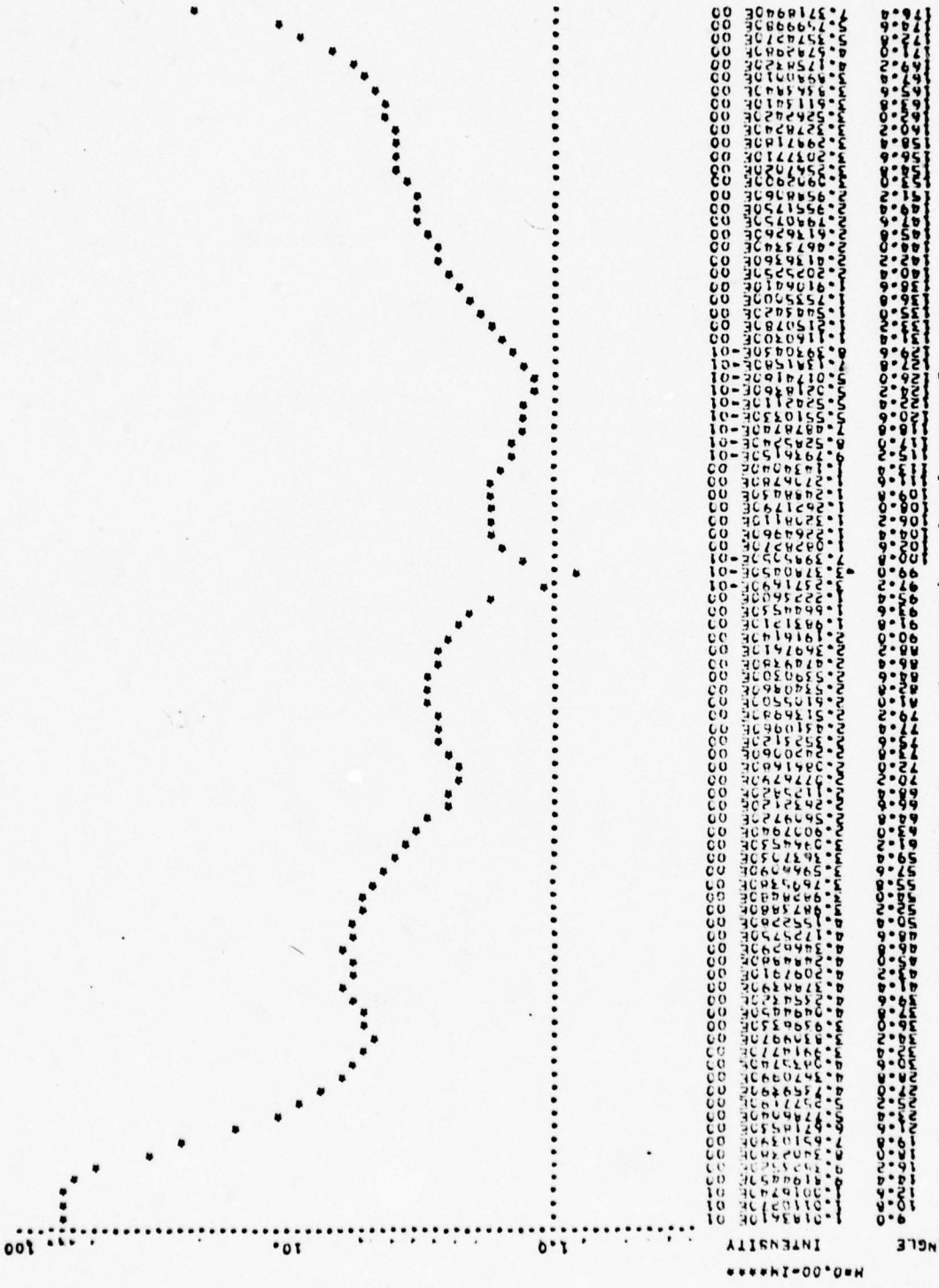

Fig. 19 Data of Fig. 18 before subtracting background.

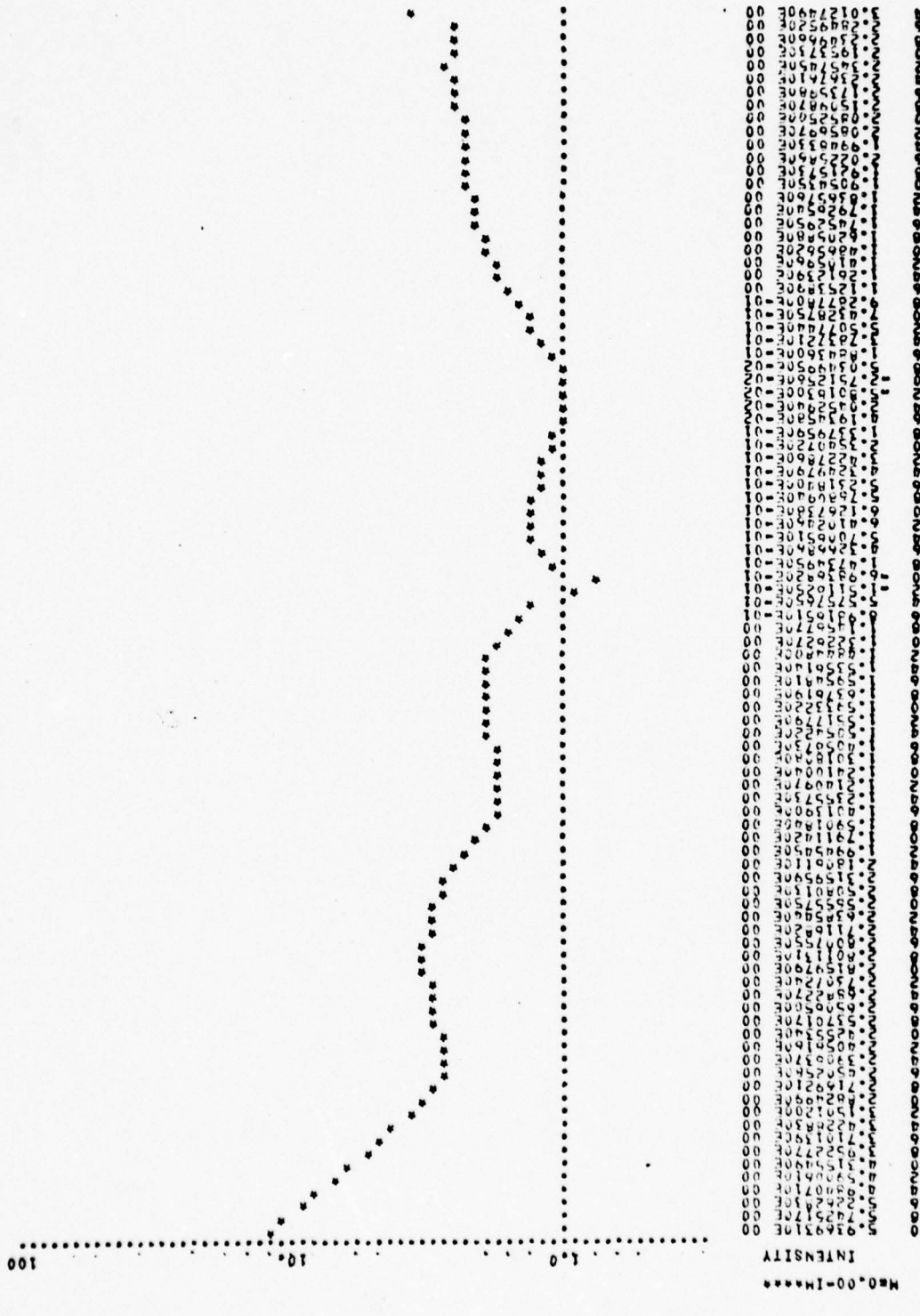

Fig. 20 Latex data. Incident light parallel polarized.

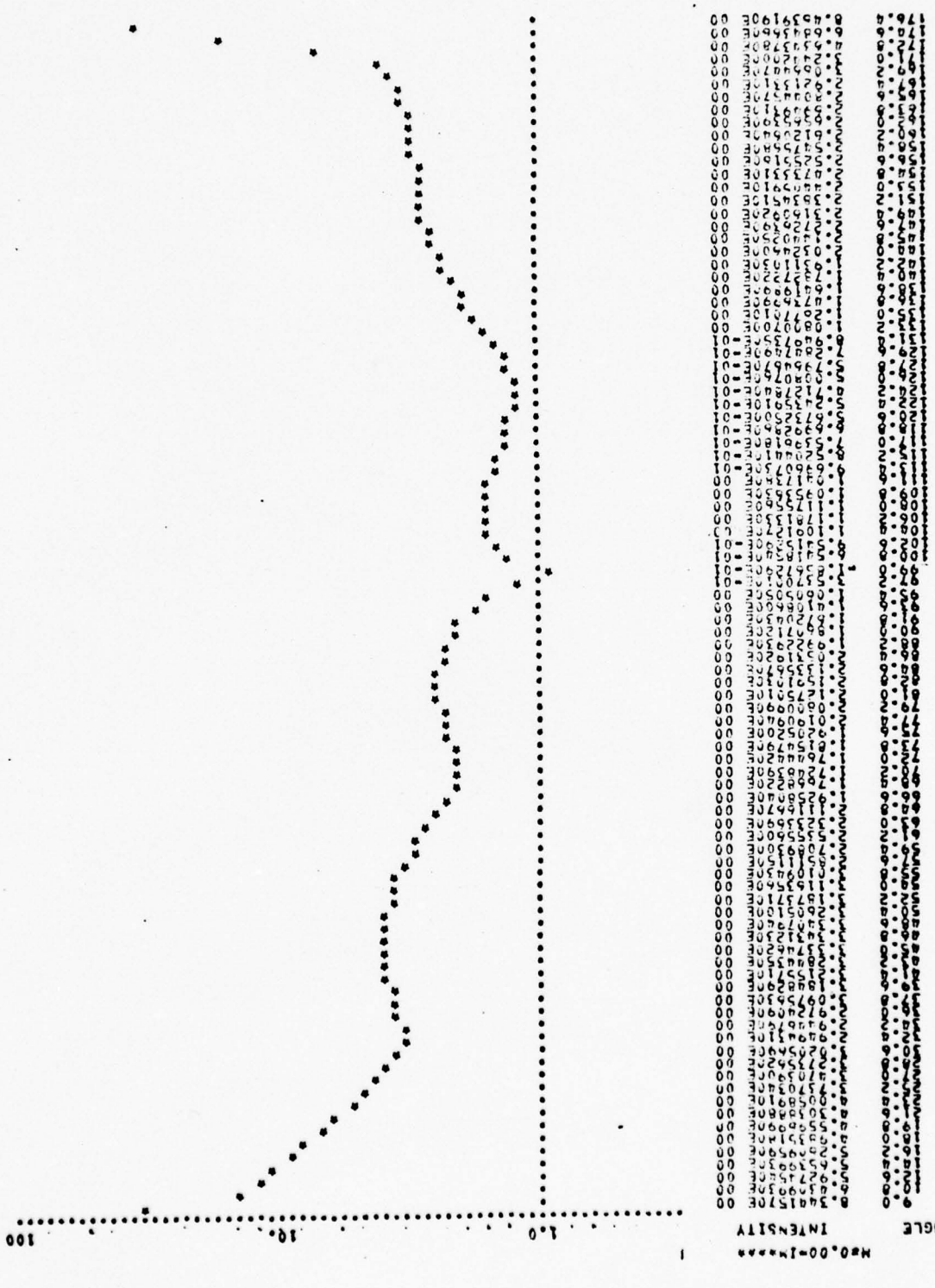

Fig. 21 Data of Fig. 20 before subtracting the background.

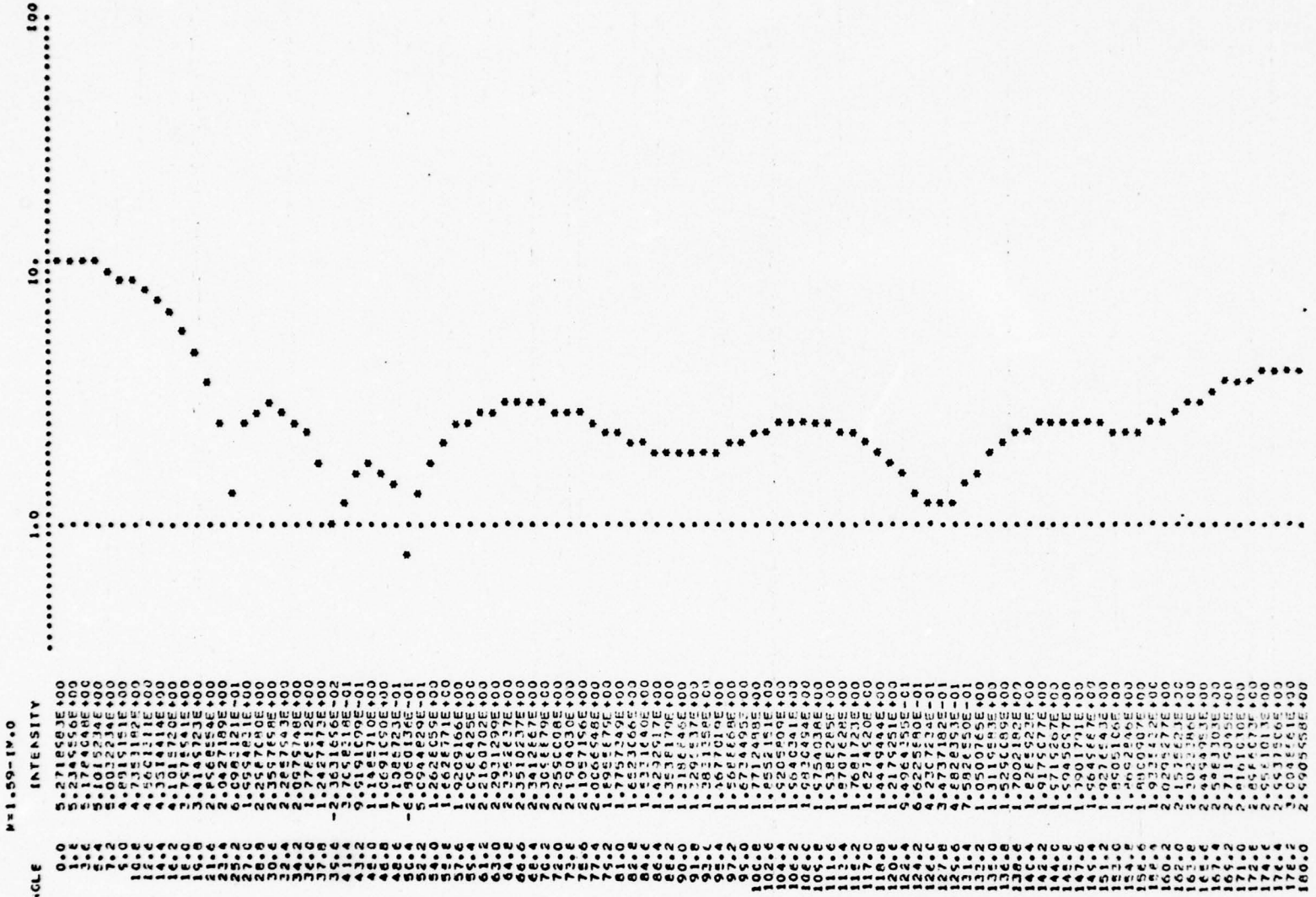

Fig. 22 Theoretical Mie results for channel 2, x=5.01, R=1.592. Relative Log intensity versus scattering angle.

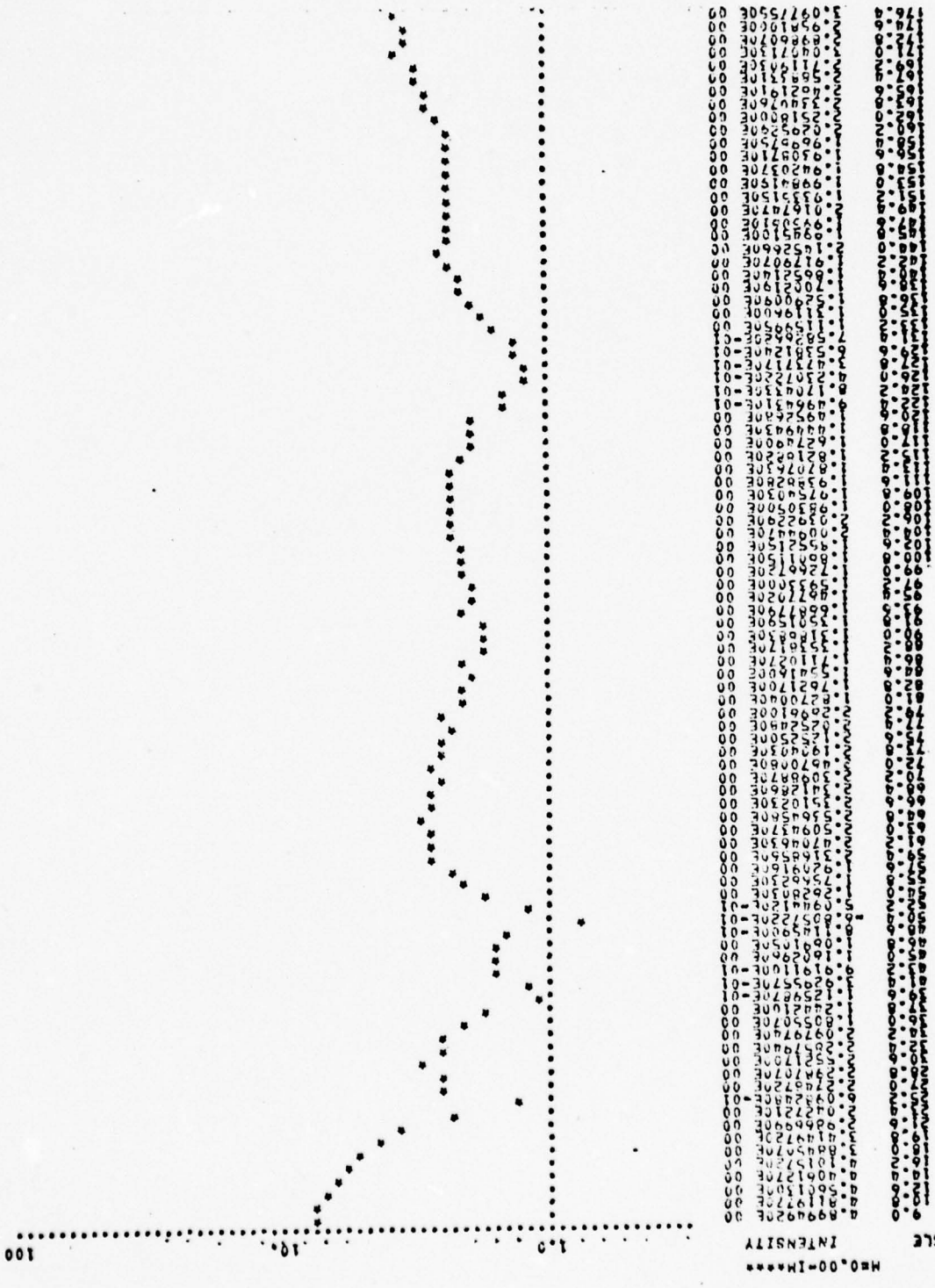

Fig. 23 Experimental latex scattering data; incident light perpendicular polarized. Channel 2.

Fig. 24 Data of Fig. 23 before subtracting the background.

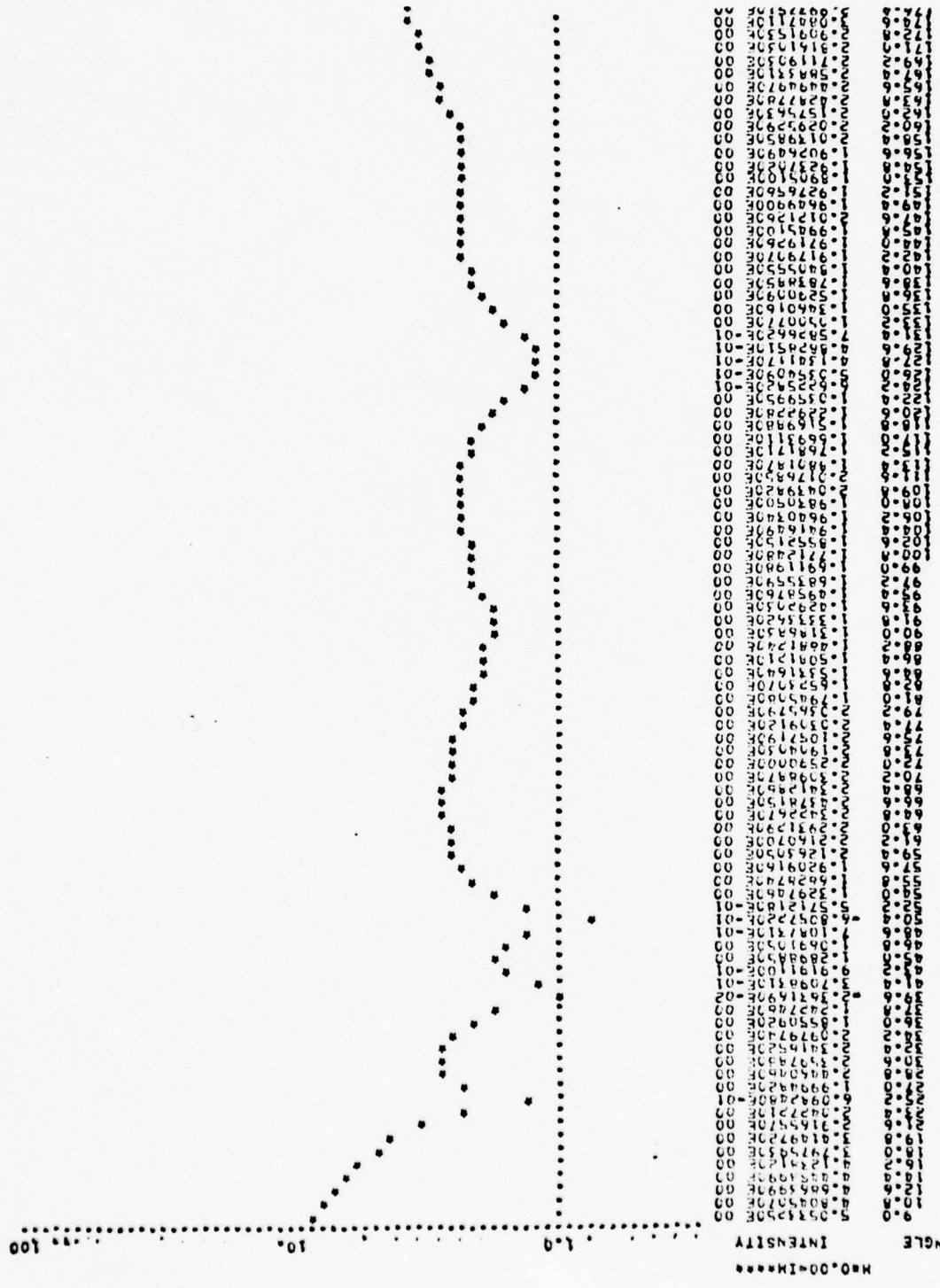

Fig. 25 Channel 2 data for latex. Incident light parallel polarized.

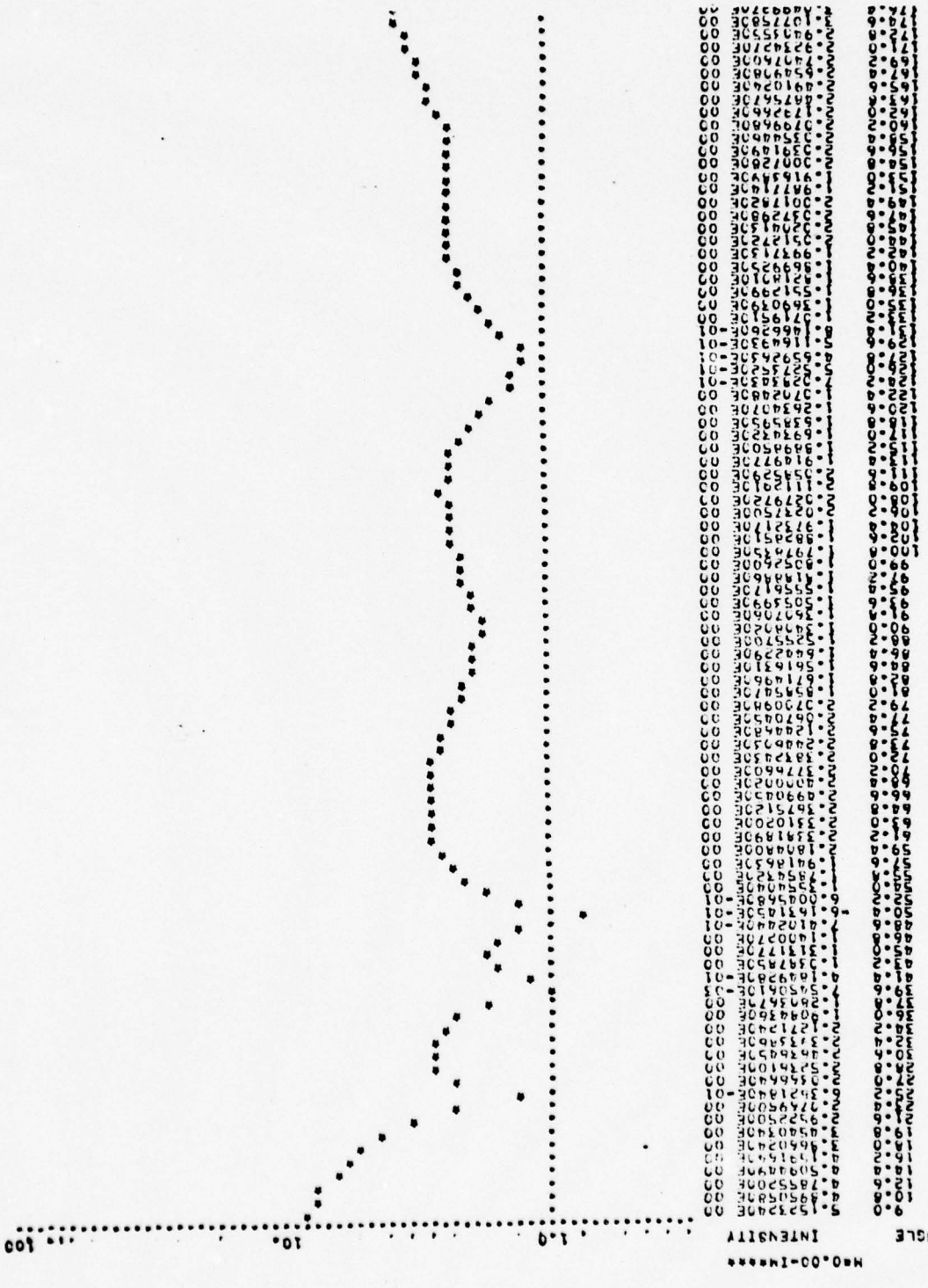

Fig. 26 Data of Fig. 25 with the background.

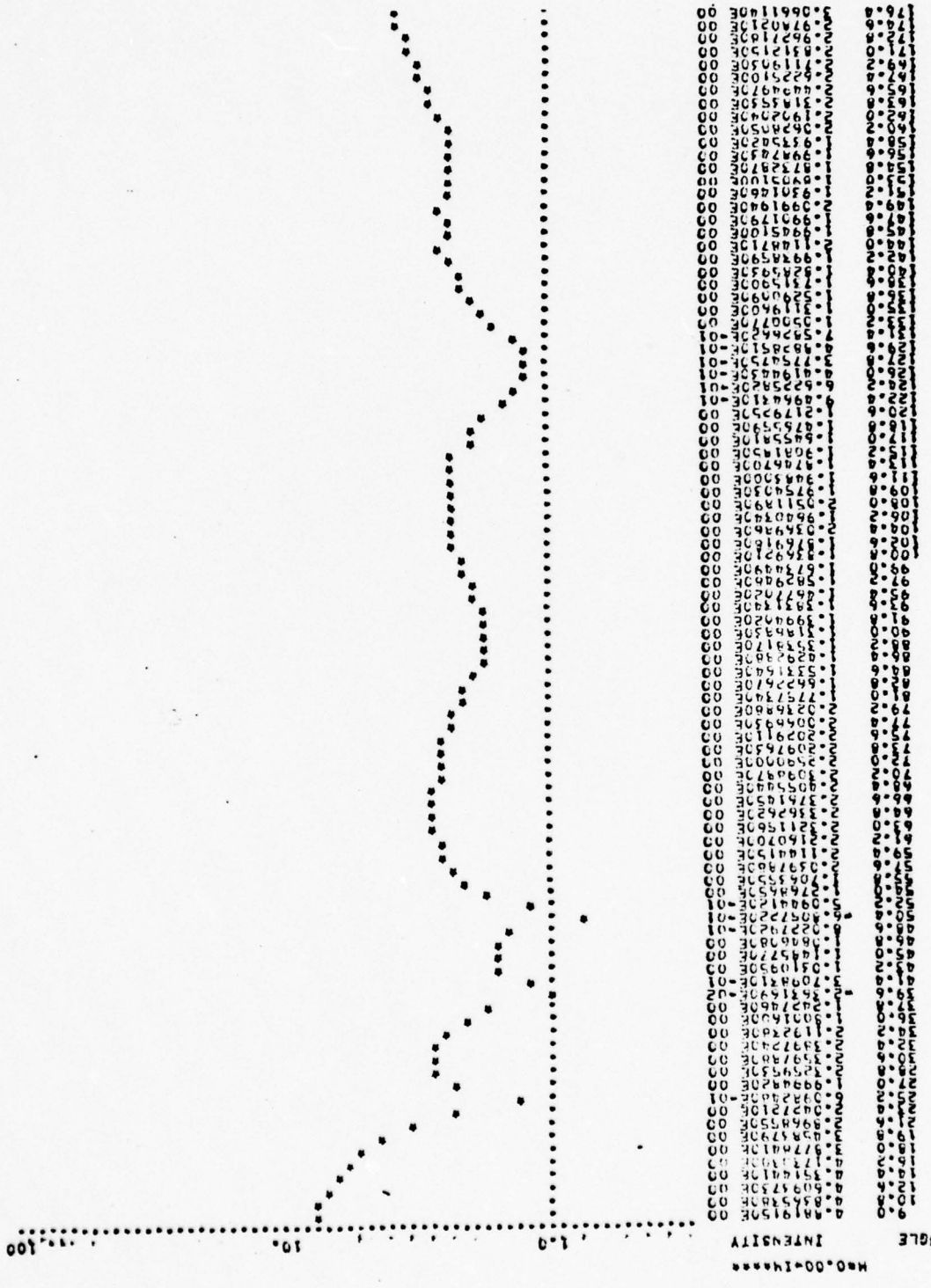

Fig. 27 Channel 2 latex data. Perpendicular polarized incident light.

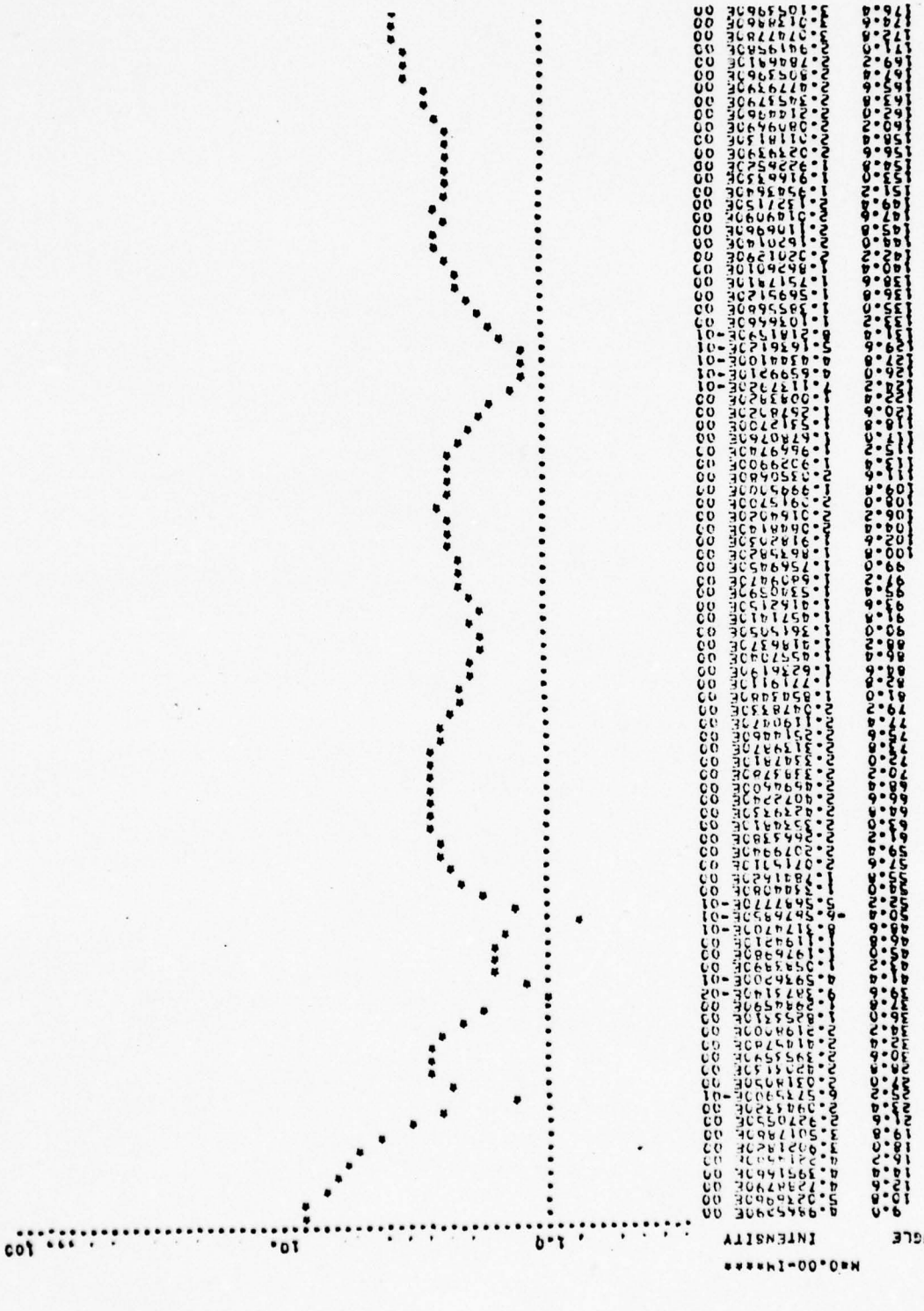

Fig. 28 Data of Fig. 27 before subtracting the background.

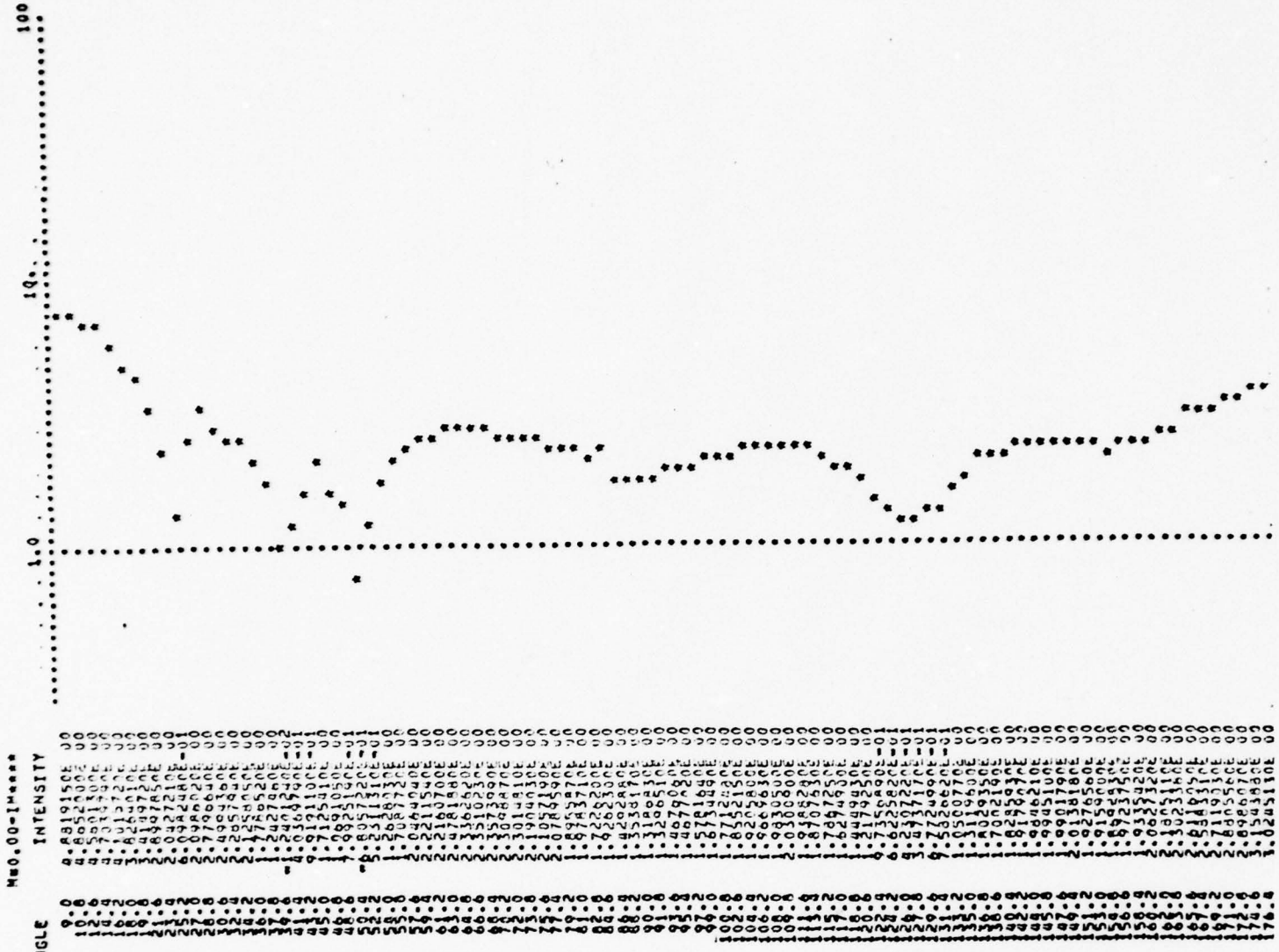

Fig. 29 Channel 2 latex data. Incident light plane polarized parallel to the plane of scattering.

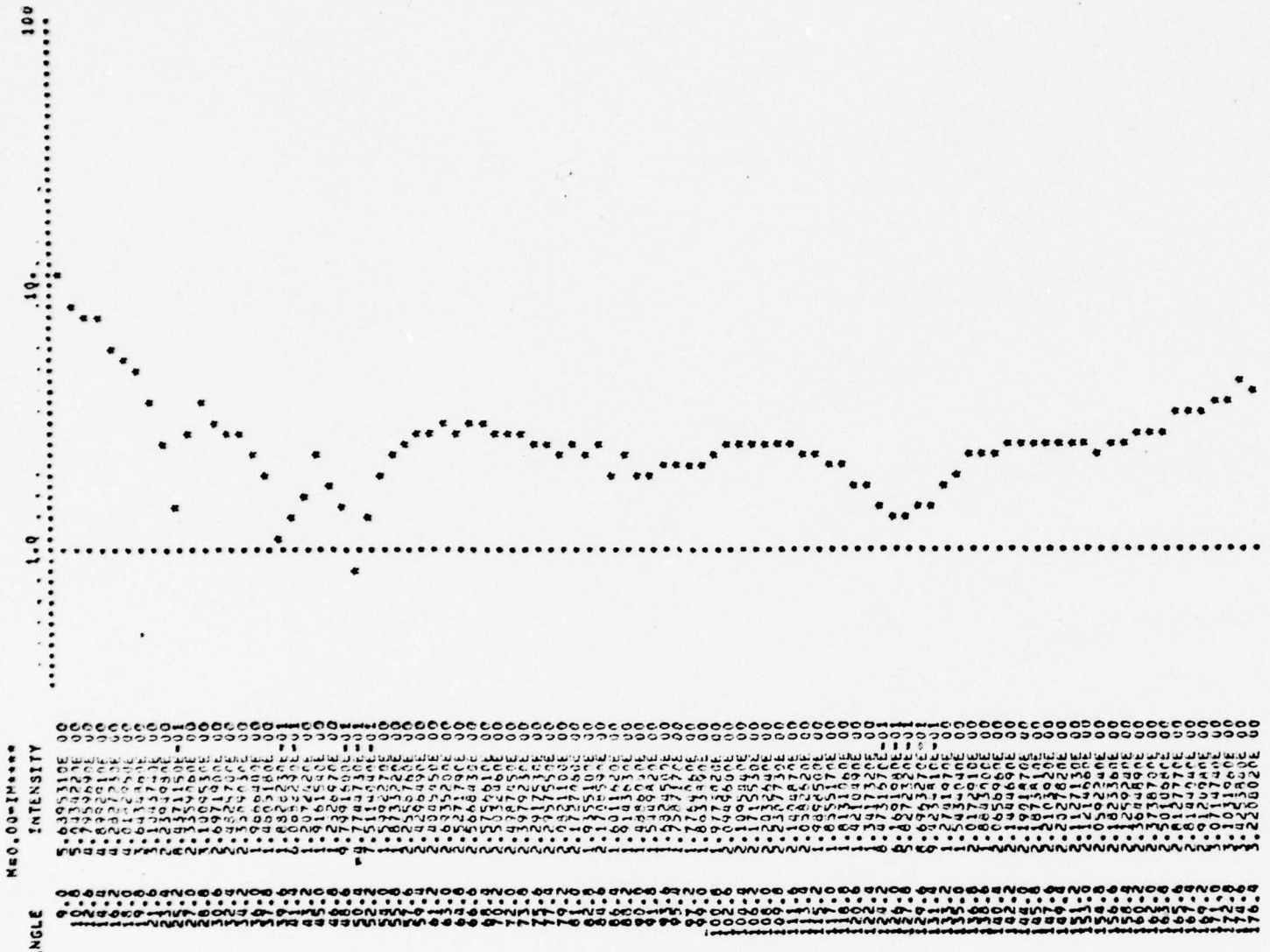

Fig. 30 Same as Fig. 29 with the background.

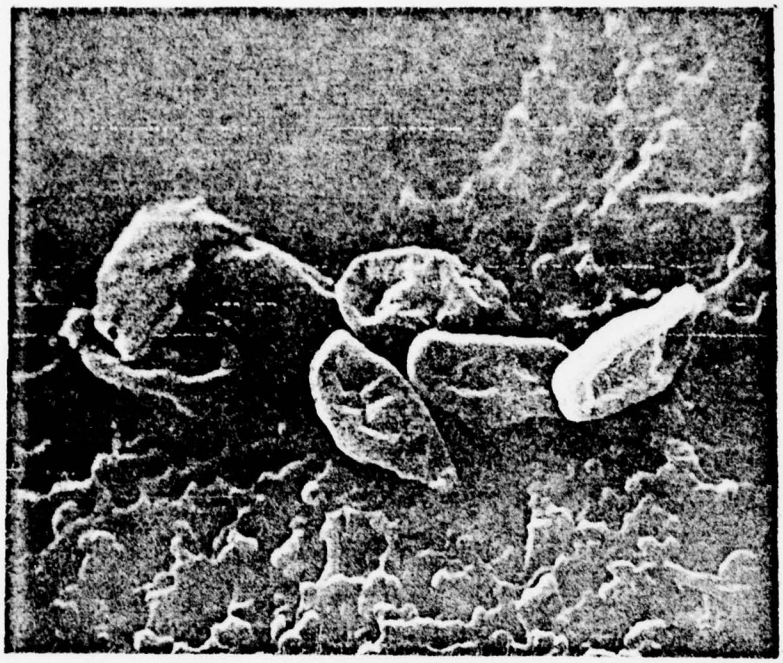

Fig. 31a Electron microscope picture of cladosporium spores. Magnification is 8200. The spores were not prepared for electron microscopy; so they shrunk during the coating process.

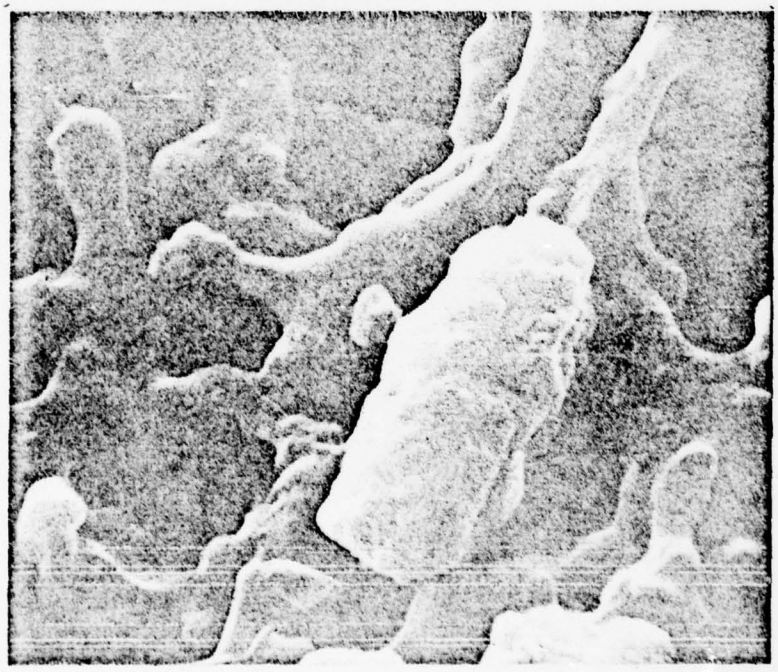

Fig. 31b Same as 31a with magnification 33000.

Fig. 32. Theoretical Mie results for channel 1, x=12.1, R=1.12.

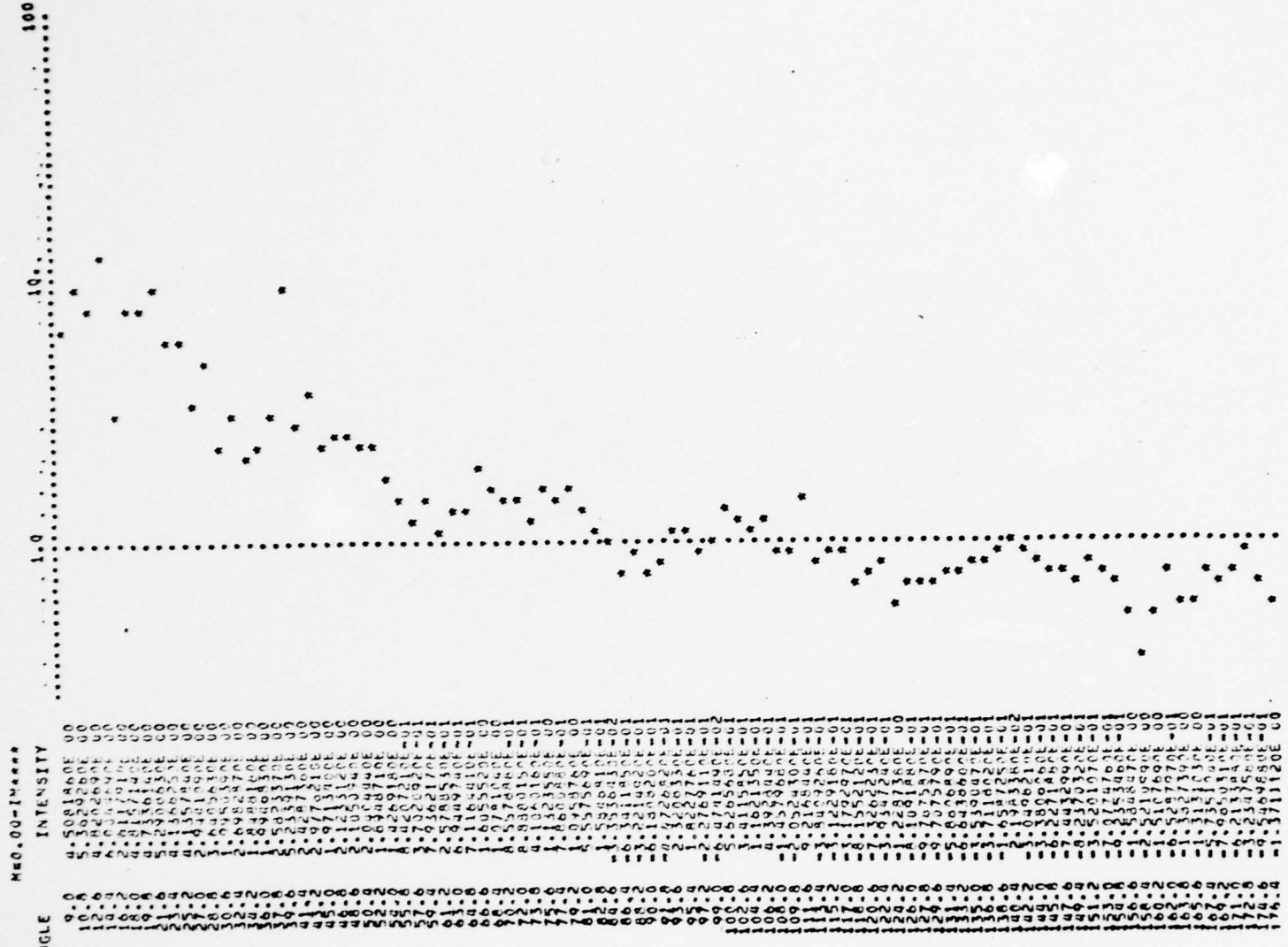

Fig. 33 Channel 1 cladosporum data. Incident light parallel polarized.

Fig. 34 Data of Fig. 33 before subtracting the background.

Fig. 35 Channel 1 cladosporium data. Incident light perpendicular polarized.

Fig. 36 Data of Fig. 35 before subtracting the background.

M=1.12-I*.0

ANGLE	INTENSITY
0.0	8.32075115E+00
1.8	8.26359065E+00
3.6	8.14582564E+00
5.4	7.96468715E+00
7.2	7.71526165E+00
9.0	7.39958[illegible]E+00
10.8	6.97523315E+00
12.6	6.45223105E+00
14.4	5.79369165E+00
16.2	4.98723185E+00
18.0	4.06605745E+00
19.8	3.71122965E+00
21.6	3.95035265E+00
23.4	4.14237125E+00
25.2	4.12155745E+00
27.0	3.90014945E+00
28.8	3.45454315E+00
30.6	2.77975615E+00
32.4	1.91872085E+00
34.2	-4.25359955E-01
36.0	4.90243705E-01
37.8	1.62574595E+00
39.6	1.96631475E+00
41.4	1.90106495E+00
43.2	1.63017335E+00
45.0	5.76449045E-01
46.8	1.50043075E-02
48.6	7.00101075E-01
50.4	5.51775405E-01
52.2	-2.59742085E-01
54.0	-9.64019605E-01
55.8	-2.27840105E-01
57.6	-6.74903485E-01
59.4	-1.16059035E+00
61.2	4.15283705E-02
63.0	3.75091405E-01
64.8	4.10013565E-01
66.6	2.38894745E-01
68.4	-1.07472425E-01
70.2	-5.69465745E-01
72.0	-8.91364615E-01
73.8	-7.49923175E-01
75.6	-3.95064395E-01
77.4	-1.10989675E-01
79.2	4.77030105E-02
81.0	9.17829685E-02
82.8	4.59645945E-02
84.6	-5.57850255E-02
86.4	-1.84068505E-01
88.2	-2.78694215E-01
90.0	-3.12402965E-01
91.8	-2.93676685E-01
93.6	-2.57356405E-01
95.4	-2.37876155E-01
97.2	-2.33166165E-01
99.0	-2.44099075E-01
100.8	-2.40546745E-01
102.6	-1.98873555E-01
104.4	-1.08824545E-01
106.2	2.85525765E-03
108.0	1.03721095E-01
109.8	1.65350765E-01
111.6	1.67770215E-01
113.4	9.78019465E-02
115.2	-5.18356855E-02
117.0	-2.78377005E-01
118.8	-5.45620395E-01
120.6	-7.39945505E-01
122.4	-7.66350965E-01
124.2	-4.65740365E-01
126.0	-1.78325765E-01
127.8	5.56267765E-02
129.6	2.07577065E-01
131.4	2.75030715E-01
133.2	2.62031265E-01
135.0	1.79088045E-01
136.8	3.40427725E-02
138.6	-1.51764275E-01
140.4	-3.55986165E-01
142.2	-5.51368245E-01
144.0	-7.27684315E-01
145.8	-8.01937105E-01
147.6	-1.10883315E+00
149.4	-1.37225545E+00
151.2	-1.65290015E+00
153.0	-1.77327437E+00
154.8	-1.57450875E+00
156.6	-1.21091575E+00
158.4	-9.10123775E-01
160.2	-7.17809465E-01
162.0	-6.56527405E-01
163.8	-7.37757015E-01
165.6	-9.60108585E-01
167.4	-1.24152175E+00
169.2	-1.68021005E+00
171.0	-1.97116235E+00
172.8	-1.97268135E+00
174.6	-1.67781145E+00
176.4	-1.26045615E+00
178.2	-1.05773795E+00
180.0	-6.79437415E-02

Fig. 37 Theoretical Mie results for channel 2, x=12.1, R=1.12.

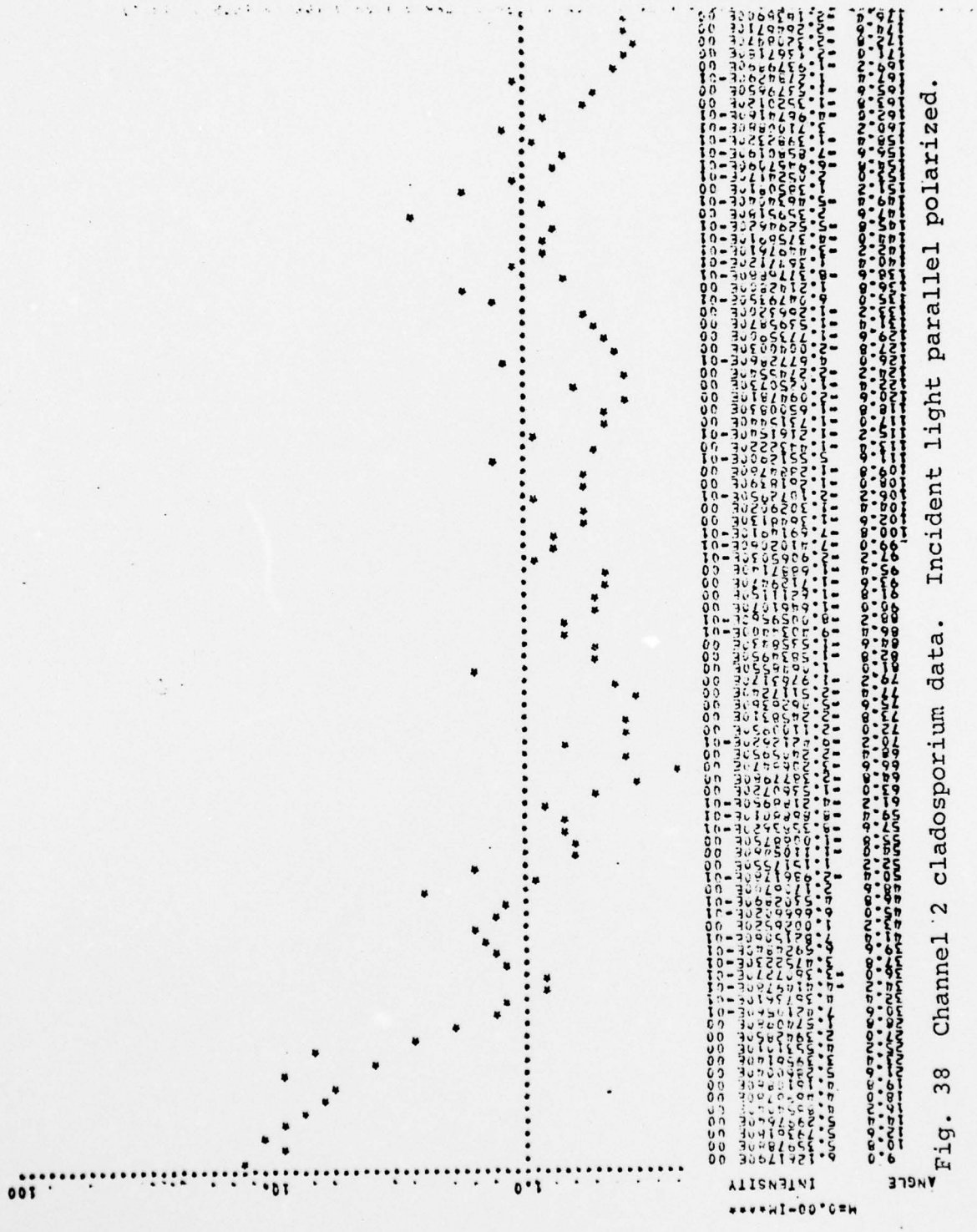

Fig. 38 Channel 2 cladosporium data. Incident light parallel polarized.

Fig. 39 Data of Fig. 38 before subtracting the background.

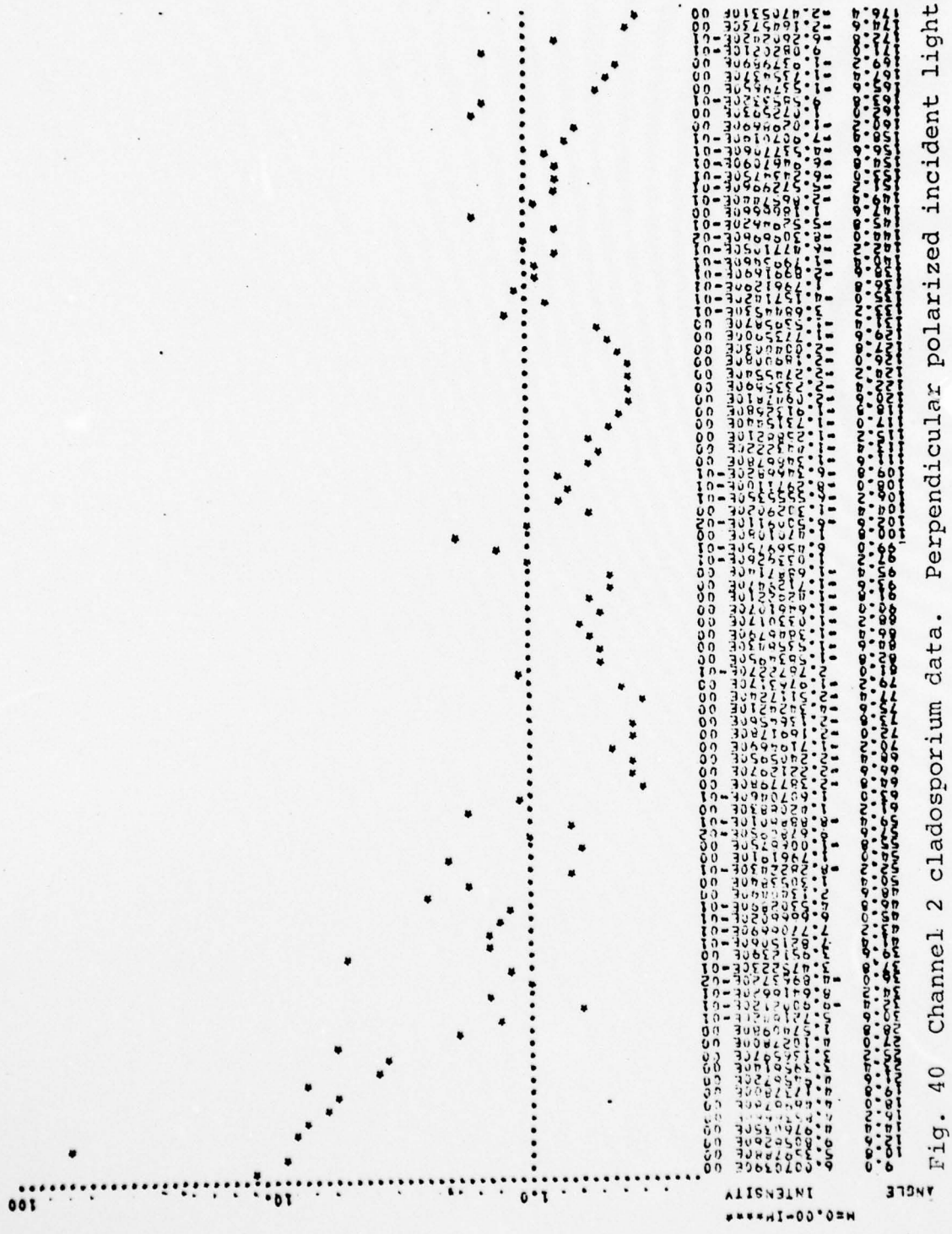

Fig. 40 Channel 2 cladosporium data. Perpendicular polarized incident light.

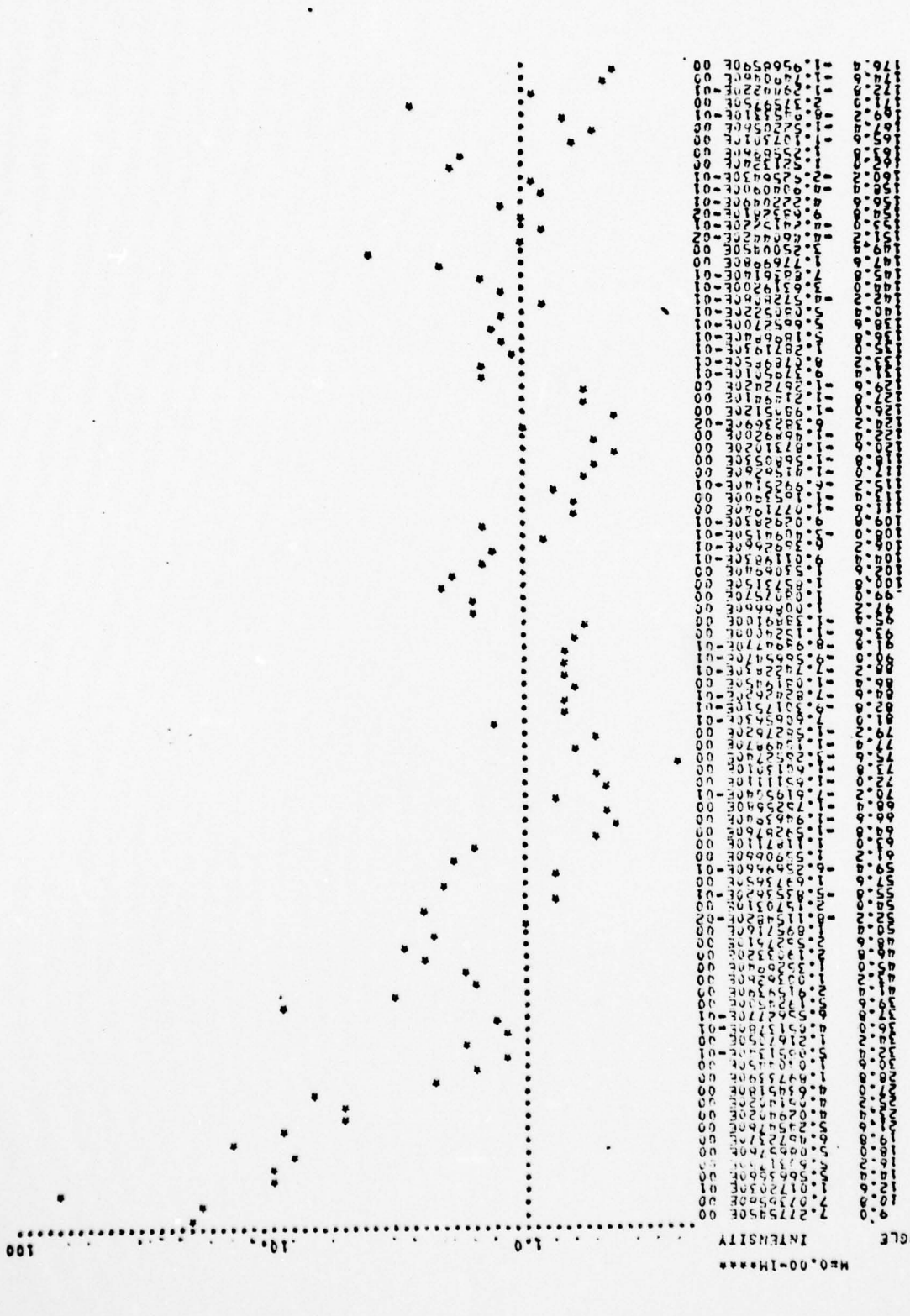

Fig. 41 Data of Fig. 40 before subtracting the background.

Fig. 42 Channel 1 cladosporium data. Incident beam is not polarized.

Fig. 43 Channel 2 cladosporium data. Incident light is not polarized.

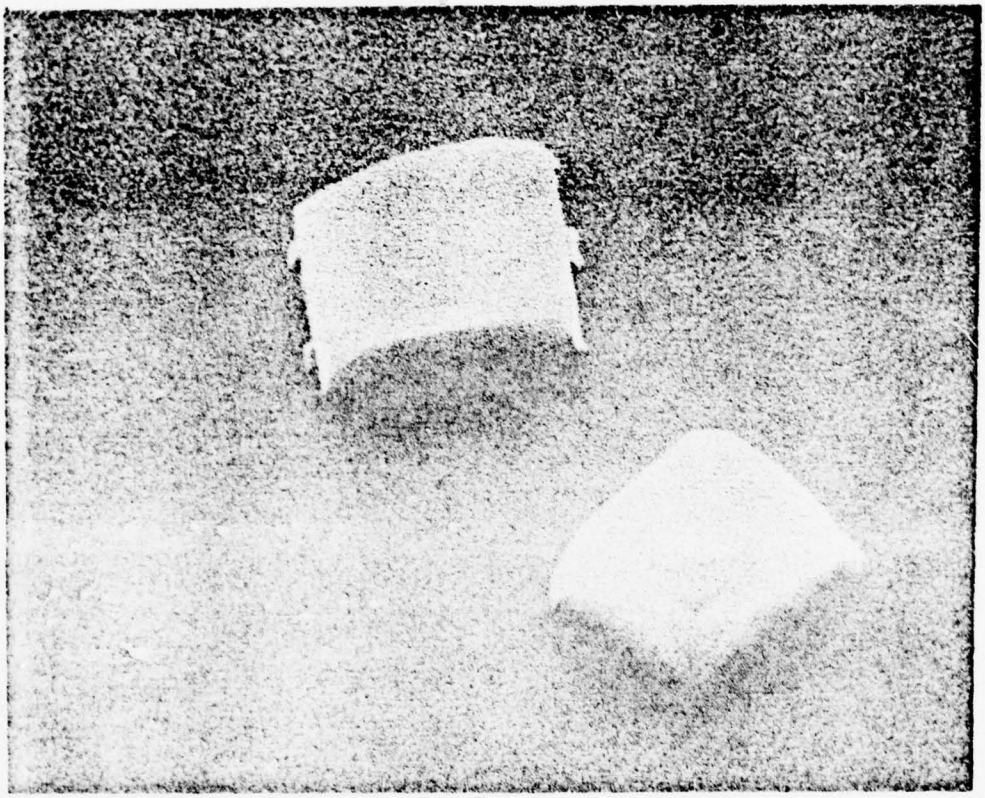

Fig. 44 SEM photograph of NaCl particles, collected on a glass slide. Magnification is 20000.

Fig. 45 Channel 1 theoretical Mie results, x=10.2, R=1.54.

AD-A055 835 FLORIDA UNIV GAINESVILLE DEPT OF ELECTRICAL ENGINEERING F/G 20/3
LIGHT SCATTERING FROM IRREGULAR DIELECTRIC PARTICLES.(U)
MAR 78 G WARD DAHC04-75-G-0100
UNCLASSIFIED ARO-12178.1-GS NL

2 OF 2
AD
A055 835

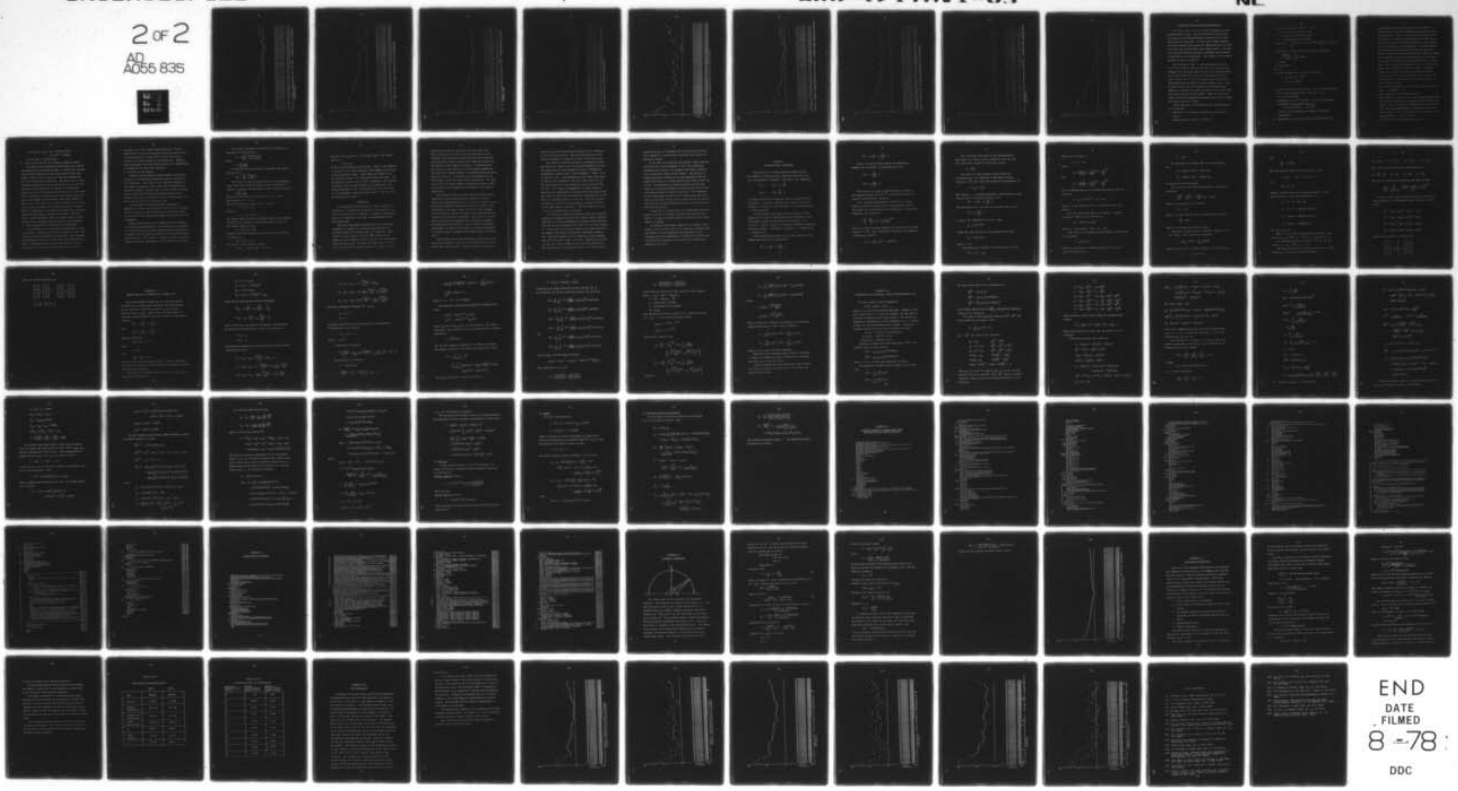

END
DATE FILMED
8-78
DDC

Fig. 46 Channel 1 experimental data for NaCl. Incident light at parallel polarization.

Fig. 47 Data of Fig. 46 before subtraction of the background.

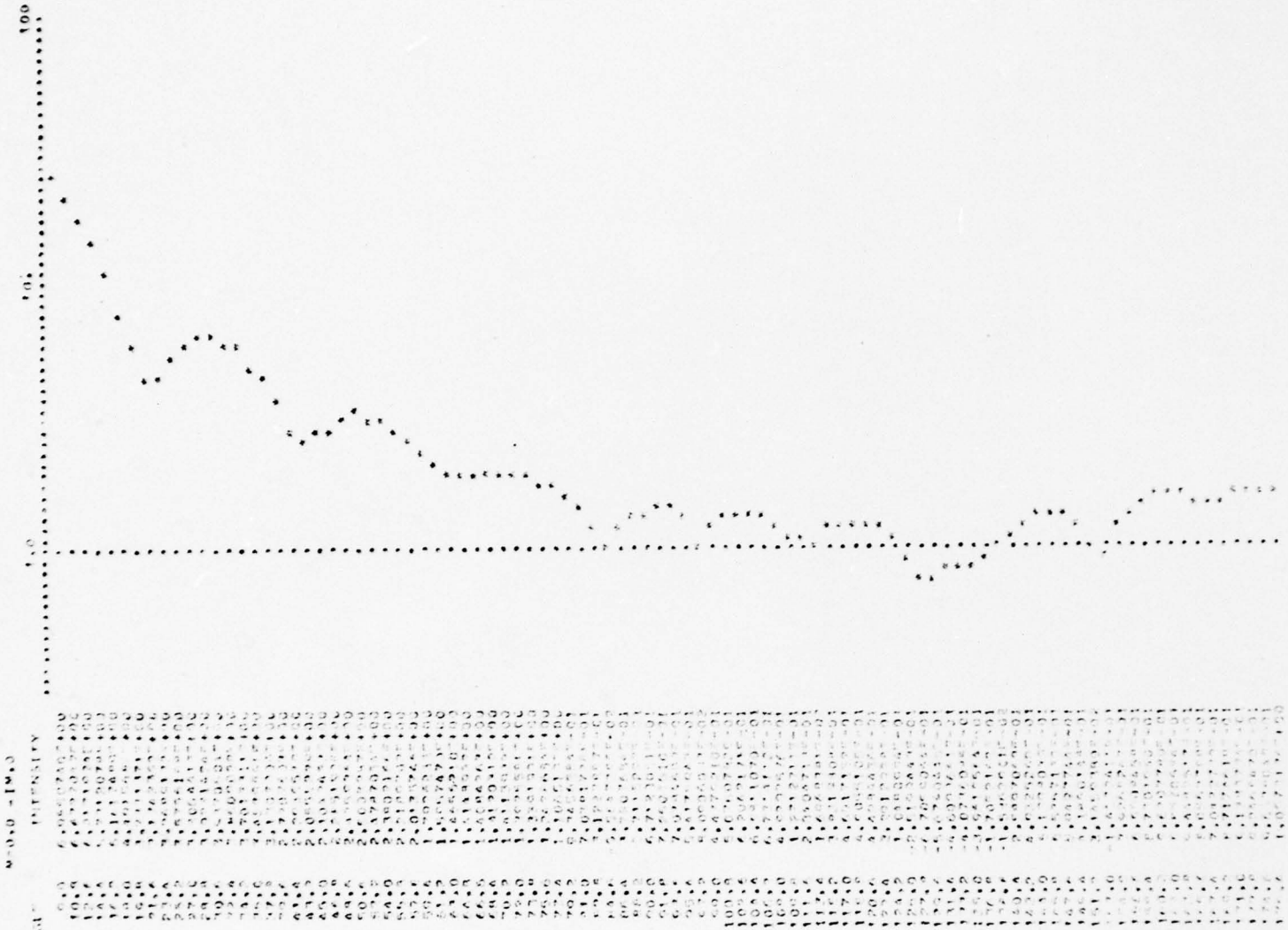

Fig. 48 Channel 1 experimental results for NaCl. Perpendicular polarized incident beam.

Fig. 49 Data of Fig. 48 with the background.

Fig. 50 Channel 2 theoretical Mie results, x=10.2, R=1.54.

Fig. 51 Channel 2 experimental data for NaCl. Incident light polarized parallel.

Fig. 52 Data of Fig. 51 before subtracting the background.

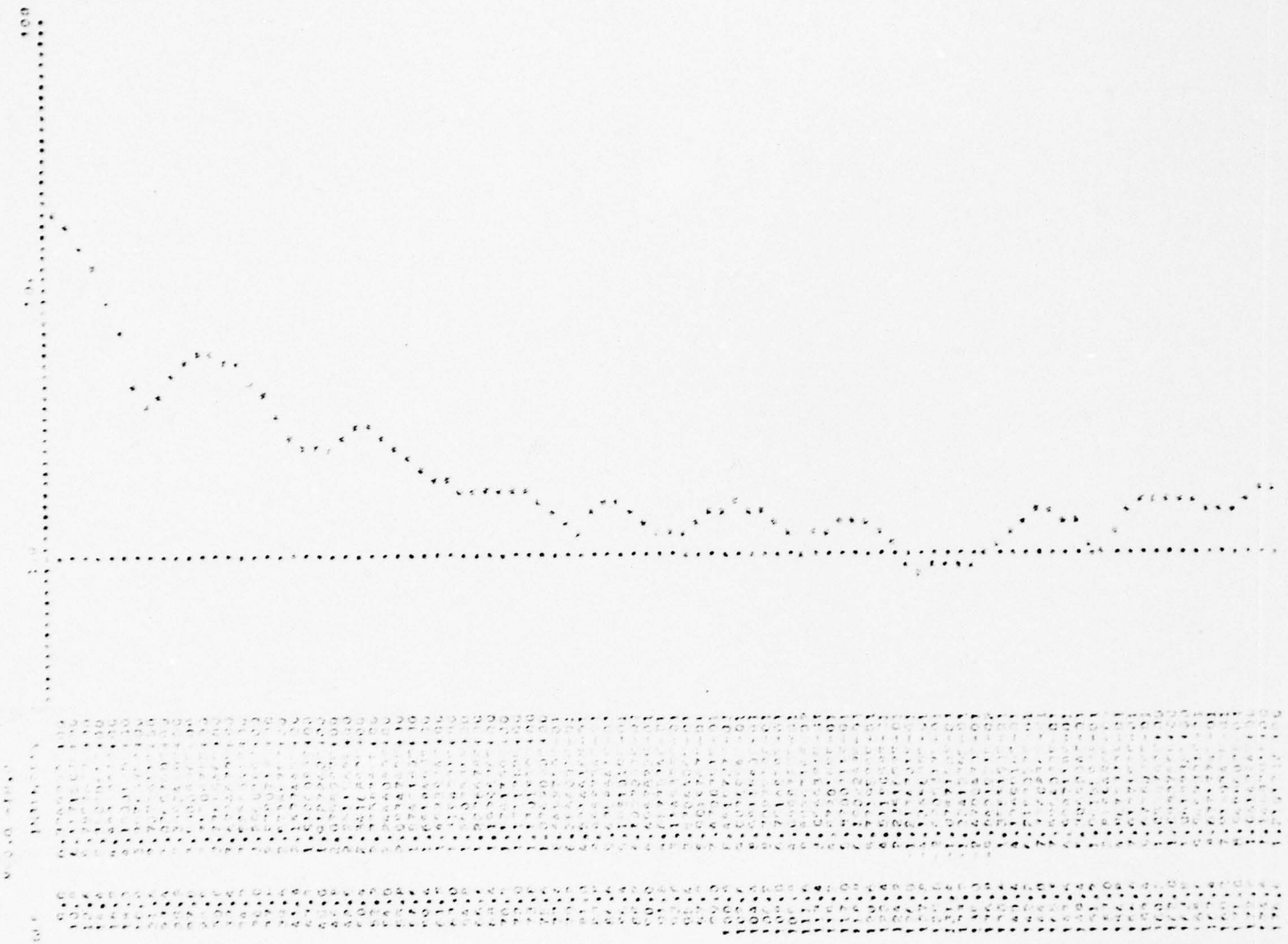

Fig. 53 Experimental data of channel 2 from NaCl. Incident light perpendicular polarized.

Fig. 54 Data of Fig. 53 with the background.

Analysis of Data and Error Calculations

The major source of error in the measurements is the photomultiplier tubes. The main problem we had was the variations in the photomultiplier characteristics after a long period of operation. In this case a short duration of high intensity light causes the photomultiplier to overload, and its recovery might take several weeks. The Channel 2 photomultiplier developed a permanent noise problem in the midst of our experiment. The results can be seen in Figures 38 through 41 and 43.

For instance in Fig. 3, the data points at 21.5^{o}, 37.7^{o}, 86.3^{o}, 95.3^{o}, 138.6^{o}, and $172,8^{o}$ are out of range. Although the scattering pattern seems to be somewhat similar to the theory (Fig. 37), the intensities at 27.0^{o}, 36.0^{o}, $43,2^{o}$, 48.6^{o}, 77.6^{o} and those closer to the back-scattering range are hard to explain without noise. Some of these points could be discarded as scattering from doublets or triplets but there is quite a lot of them that don't fall into the error bracket. These, we had to include in our data presentation because there was no reasonable way to get rid of them.

Other than this, the items for error considerations are as follows:

1. Probability of multiple scattering in interaction region:

   Assume particle density $3 \times 10^{6}/ ft^{3}$

particles main beam will hit = $\pi r^2 \ell n$

r - radius of scattering volume

ℓ - length of scattering volume

n - concentration of particles

particles = $3 \times 10^6 / \text{ft}^3 \times 3.53 \times 10^{-6} \frac{\text{ft}^3}{\text{cm}^3} \times 3.16 \times \frac{1}{9} \times 5$

= 16.7

particles in cone from point collision to mirror:

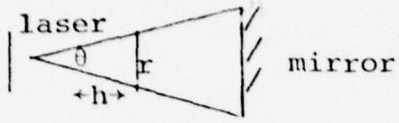

h = 2/3cm

θ = 1/36.6rad.

$2r = h\theta$

The conical volume from particle scattering:

$$v = \frac{1}{3} \pi r^2 h = \frac{1}{3} \frac{\pi}{4} h^3 \theta^2$$

$$v = 55.8 \times 10^{-6} \text{cm}^3$$

particles $55.8 \times 10^{-6} \times 10.59 = 591.48 \times 10^{-6}$ particles

Due to the irregularities, taking h = 1 cm

$v = 8.3 \times 10^{-4}$ cm^3

particles $8.3 \times 10^{-4} \times 10.59 = 8.7 \times 10^{-3}$ particles

Probability of Multiple scattering =

$= 8.7 \times 10^{-3} / 16.7 \simeq .5 \times 10^{-3}$

There is .05% probability of double or multiple scattering.

2. Probability of scattering from coagulated particles:

Approximately 10% coagulation of latex and 20% of cladosporium and NaCl was detected from electron microscope pictures. This is not taken into account in the calculations. Actually a 10% coagulation might cause one or two orders of magnitude increase in the intensities at a specific scattering angle. But this problem is avoided by putting an error bracket to the data points. This means the intensities that might be caused by coagulation of two or more particles are rejected. The values for rejection are determined by Mie calculation. The averaging is done for 5 runs at a time and there are at least 50 of these averages. Assuming there are at least 15 particles in the interaction region at one time, one data point is the average over 3750 particles. By rejecting one point out of 5, we make an error of 20%;

The overall probability of error for one data point is then .2 x 100/50 = .4%

3. False count rate due to Gamma Source:

There might be a false count in the photomultiplier due to the Kr.86 source used to neutralize the aerosol particles. This is given as 10^3 photons/cm^2 sec at 1 meter. The unshielded portion of photomultipliers are approximately 1 cm^2. Therefore false count rate is 10^3 photons/cm^2 sec x 1 cm^2 = 1/msec

Gate width of photomultipliers = 20 nsec

$\therefore$ False count rate = $20 \times 10^{-9}\text{sec}/10^{-3}\text{sec}$

$= 20 \times 10^{-6} = 1/50000$

1 false count in 50,000 shots

4. False count rate due to electronic command signals:

The digital data acquisition electronics have several discrepancies in recording the data. A high error rate has been detected especially in the first and the last data points. This is due to the start and stop commands fed into the system during operation. The error rate is experimentally determined to be as high as 80% at the first and last data points which are 9^{o} and 176.4^{o} respectively. Within the rest of the 92 data points there is a 20% chance of the occurence of a false count. This happens when the paper tape punches an undetermined code which might be a line less, a line more or a noniterated value as the count. In this case that point is regarded as an "out of range", which is indicated in the graphs by setting the scattering angle off with respect to the rest of them. This data point is then discarded. This, of course causes an error in the overall averaged value because of less averaging.

5. Error encountered in subtraction of background:

In obtaining the final values the background at each set of runs is subtracted from the averaged raw data. The accuracy of this procedure is questionable since sometimes the background values are higher than the experimental results. Background values are checked against Raleigh scattering, but even in the cases where there is poor

agreement, the final values remain unchanged. This is possibly due to the dust particles floating around in the scattering chamber or those that rise from the velvet lining on the walls because of the turbulance. Nevertheless we presented the data before and after the subtraction of background, to avoid this confusion.

6. Accuracy of the values:

Accuracy of the detected values depend on the sensitivity of the experimental apparatus and the variables of the experiment. Sensitivity of the apparatus depends on the angular resolution, noise level and threshold of the electronic system. Values below .2 volts cannot be detected due to the A/D threshold and photomultiplier noise. Angular resolution is limited to 1^{o} by an eyepiece slit at the receiving end of the analyser prism.

The volumetric scattering element explained in Appendix VI causes the experimental values to be an average of the intensities from an interval of scattering angles. As a result of this any two preceeding data points are not independent.

Using the mechanics of the system the error involved at each data point because of the geometry can be calculated as the ratio of the volume element from one particle to the mirror and the volume covered by the interaction region and the mirror. The latter is a function of the scattering angle; but we will approximate it by taking the mean value.

The angular dependence of the effective distance is expressed as: (Appendix VI)

$$D = L \frac{\cos\theta}{\sin\theta} \frac{R\cos\theta + L/2}{R + L/2\cos\theta}$$

Then,

$$D = \frac{L^2}{2R} \frac{\cos\theta}{\sin\theta}$$

To take the average we have to integrate this over an interval of 2π

$$D_{av} = \frac{L^2}{4\pi R} \int_0^{2\pi} \frac{\cos\theta}{\sin\theta} d\theta$$

The result of this integral gives us an indeterminate form; so we take $2 (L^2/4\pi R)\ 1/\tan\theta$ as the correction to length L; therefore the tolerance on the effective length is

$$\pm \frac{L^2}{2\pi R} \frac{1}{\tan\theta}$$

The correction gives us an average of 2.6, L = 5cm.

This gives us $L = 5 + 2.6$

The area considered is 2rl; and r = 1/3 cm

$$\therefore A = \frac{2}{3} (5 \pm 2.6)$$

which is

$$A = 3.33 \pm 1.74$$

The volume covered by the interaction region is the volume created by the effective area and the mirror facing it.

The volume comes up to be:

$$V_i = 36.6\ (2 \pm .86)$$

Volume of the cone covered by a particle and received by the mirror is:

$$V_c = 36.6 \times .17$$

The ratio of these volumes is then:

$$V_c/V_i = .17/(2 \pm .86) = .10 \pm .05$$

Therefore the accuracy of a data point due to the volume effect is

$$\pm (10 \pm 5)\%$$

We will take the mean of this as 10%. There is an additional 5% error due to the variation in the number of particles in the scattering volume. Since these are additive, on the average we have + 15% accuracy at each data point. As we mentioned earlier this is also a function of the scattering angle, and this can be taken as an additional + 5%, which diminishes at 90°. This means there is a 10% error in the forwardmost scattering angles and a + 20% error in the backward most angles.

Conclusion

The formulation and modelling of light scattering properties of nonspherical particles is of particular interest in work with the atmosphere. Accurate experimental data is of importance to be able to successfully accomplish this task.

The polar nephelometer designed for this particular experiment is capable of digitizing the intensity of scattered light at 94 angles with 1.8° intervals. This covers an angle range of 167.4°, whose limits can be chosen to start anywhere from 0° to 12.6° from the forward scattering direction. We chose the limits to be 9.0° to 176.4° because of the minor difraction of light from the

entrance slit and the reflection from the light trap. These could not be avoided since the divergence of the incident light beam was considerably high and to decrease this would have caused a noise level above detectable signal because of the angular resolution. Considering the fact that the last data point is not reliable because of the electronic command signals, we achieved taking accurate data up to 174.6°. To the best of our knowledge this is the furthest scattering angle range achieved yet. In addition to this the large number of data points taken in this range allows better comparison with theory on an angle to angle basis.

The vibrating orifice aerosol generator used in this experiment generates monodisperse aerosols of various shapes from approximately 0.5 μm to 50 μm in diameter, with an average geometrical standard deviation of 1.014. The wavelength of the light source can be varied from approximately 400 nm to 800 nm according to the type and the concentration of the dye to be pumped. This gives us a wide range of particle size parameters to measure and compare the scattering patterns with. Due to certain unavoidable limitations, we only had the chance to use one wavelength of incident light to examine three known shapes of one size each.

The disadvantage of the experimental apparatus is, the time that it takes to scan the entire angle range (23 sec). During this time there is a certain change in the number of

particles and their orientations because of the turbulance in the scattering region. This has been partially overcome by averaging a large sum of runs at each data point.

The angular scattering patterns of polystyrene latex particles were found to be in very good agreement with the Mie theory for the size parameter of 5.01, although the experimental results were a little smoother. (Figs. 13 to 17 and 22 to 26). The smoothness of the curves can either be due to the bandwidth of the laser light (Fig. 11), or the irregularities on the surface of the particles (Figs. 12 a,b). The effects of tumbling of a larger number of particles was significant at forward scattering angles when the incident light plane was polarized perpendicular to the plane of scattering (Figs. 18 and 19). This was detected at Channel 2 which is the perpendicular channel relative to the body frame of reference. This convinced us to use a lesser concentration of scatterers.

We found that angular scattering properties of prolate spheroidal cladosporium spores and cubical sodium chloride crystals are not very dependent on incident light polarization for the size parameters 12.1 and 10.2 that were examined. Since there are no exact theories for these particles, we compared them with Mie theory for equivalent spheres. The scattering pattern for the spheroid is much smoother than the Mie results (Figs. 32 to 43), although the figures are not very clear because of the noise that appeared in the system prior to these sets of runs. By following the

general pattern, we concluded that the backscatter pattern for a spheroid is significantly different than that of an equivalent sphere.

In the case of scattering from cubical sodium chloride particles for a size parameter of 10.2, the scattering properties were found to be smoother than those predicted for an equivalent sphere by Mie theory. The patterns at forward scattering angles are in good agreement, but the nonforward angles are overestimated by Mie theory (Figs. 45 to 54). The difference in backscattering patterns with respect to equivalent spheres are much greater for the prolate spheroid than the cubical particles. The smoothness of the experimental results can be explained by the variations in the laser output and the concentration of scatterers since the forward scattering patterns are in good agreement with the theory.

In general, we conclude that the backscatter from nonspherical particles differs significantly from that for spheres, so that a tumbled irregular particle is not equivalent to a sphere.

We refrain from further comment on the subject since theory is not our task, but it is necessary to mention that the results of this experiment are important for the interpretation of measurements of atmospheric aerosols and for successful modelling of scattering from tumbled nonspherical particles.

APPENDIX I

ELECTROMAGNETIC SCATTERING

The discussion of light scattering theory starts with Maxwell's equations [22], which form the basis for all electromagnetic phenomena. The set of four equations,

$$\nabla \cdot \underline{D} = \rho \qquad \nabla \times \underline{H} = \underline{J} + \frac{\partial \underline{D}}{\partial t}$$

$$\nabla \cdot \underline{B} = 0 \qquad \nabla \times \underline{E} + \frac{\partial \underline{B}}{\partial t} = 0$$

are known as Maxwell's equations, where $\underline{D}$ = dielectric displacement; $\underline{B}$ = magnetic induction; $\underline{H}$ = magnetic field intensity; $\underline{E}$ = electric field intensity; $\underline{J}$ = current density; $\underline{\rho}$ = charge density.

For macroscopic media the dynamical response of the aggregates of atoms is described by the constitutive relations which connect $\underline{D}$ and $\underline{J}$ with $\underline{E}$ and $\underline{H}$ with $\underline{B}$, e.g., $D = \varepsilon \underline{E}$, $\underline{J} = \sigma \underline{E}$, $\underline{B} = \mu \underline{H}$ for an isotropic, permeable conducting dielectric where ε = dielectric constant; σ = conductivity; μ = permeability.

The nonhomogeneous equations for each component of the damped wave motion then become [20],

$$\nabla^2 \underline{E} - \sigma\mu \frac{\partial \underline{E}}{\partial t} - \varepsilon\mu \frac{\partial^2 \underline{E}}{\partial t^2} = 0$$

$$\nabla^2 \underline{H} - \sigma\mu \frac{\partial \underline{H}}{\partial t} - \varepsilon\mu \frac{\partial^2 \underline{H}}{\partial t^2} = 0$$

However in nondissipative media the homogeneous undamped wave equations are expressed as (σ=0),

$$\nabla^2 \underline{E} - \varepsilon\mu \frac{\partial^2 \underline{E}}{\partial t^2} = 0$$

$$\nabla^2 \underline{H} - \varepsilon\mu \frac{\partial^2 \underline{H}}{\partial t^2} = 0$$

The velocity of light in various media is given by corresponding values of $(\varepsilon\mu)^{-1/2}$, since light itself is a form of electromagnetic radiation.

For a harmonic monochromatic light wave in a homogeneous medium the vectors $\underline{E}$ and $\underline{H}$ are perpendicular to each other and to the direction of propagation. The scalar components are related by

$$\frac{E_x}{H_y} = \frac{-E_y}{H_x} = Z_o = \left(\frac{\mu}{\varepsilon - i\sigma/\omega}\right)^{1/2}$$

where Z_o is the intrinsic impedance of the medium for plane waves; i is $\sqrt{-1}$. The associated electrostatic and magnetic energies are given by

$$U + T = \frac{1}{2} \int_V (\varepsilon |\underline{E}|^2 + \mu |\underline{H}|^2) dV$$

For a periodic field such as the electromagnetic wave there is a flux of energy crossing a unit area per unit time which is given by Poynting's vector,

$$\underline{S} = \underline{E}x\underline{H}$$

By taking the time average of this vector and utilizing E_x/H_y, the intensity or the flow of energy crossing a unit area along the direction of propagation is

$$I = (2Z_o)^{-1} \ |\underline{E}|^2$$

The function u satisfying equations; nonhomogeneous scalar wave equation in dissipative media ($\sigma>0$):

$$\nabla^2 u - \sigma\mu \frac{\partial u}{\partial t} - \varepsilon\mu \frac{\partial^2 u}{\partial t^2} = 0$$

and homogeneous wave equation in dielectric media ($\sigma=0$):

$$\nabla^2 u - \varepsilon\mu \frac{\partial^2 u}{\partial t^2} = 0$$

is one of the components of E or H. Then,

$$E_x = Ae^{i(\omega t - kz)}$$

Taking only the real part of the exponential we have

$$E_x = A\cos(\omega t - kz)$$

where $\omega = 2\pi\gamma$.

The propagation constant k is given by the relation

$$k^2 = \mu\varepsilon\omega^2 - i\mu\sigma\omega$$

which can be written as

$$k = \alpha_1 - i\beta_1$$

where

$$\alpha_1 = \omega\left\{\frac{\mu\varepsilon}{2}\left[\left(1 + \frac{\sigma^2}{\varepsilon^2\omega^2}\right)^{1/2} + 1\right]\right\}^{1/2}$$

and

$$\beta_1 = \omega\left\{\frac{\mu\varepsilon}{2}\left[\left(1 + \frac{\sigma^2}{\varepsilon^2\omega^2}\right)^{1/2} - 1\right]\right\}^{1/2}$$

For an undamped wave in a nonconducting medium ($\sigma=0$) k is real and

$$k = \alpha_1 = \omega(\mu\varepsilon)^{1/2} = \omega/v = 2\pi/\lambda$$

where v is the velocity and λ is the wavelength in the medium.

For the general case when k is complex, a complex refractive index m can be defined by

$$E_x = A\exp[i(\omega t - k_o m z)]$$

where $k_o = 2\pi/\lambda_o$ and $m = k/k_o = m_r - im_i$.

When there is an absorption, the absorption coefficient is defined by

$$I = I_o\exp[-a'z]$$

where the intensity of radiation decreases from I_o to I over the path length z,

$$a' = km_i$$

The components of E where there is no attenuation are,

$$E_x = A\exp[i(\tau+\delta_1)] = A\cos(\tau+\delta_1)$$

$$E_y = B\exp[i(\tau+\delta_2)] = A\cos(\tau+\delta_2)$$

by taking only the real parts.

The locus of E is found by eliminating τ from these equations,

$$\left(\frac{E_x}{A}\right)^2 + \left(\frac{E_g}{B}\right)^2 - 2\,\frac{E_x E_y}{AB}\cos\delta = \sin^2\delta$$

which is the equation of an ellipse,

$$B/A = \tan\alpha$$

where α is the semiside of the circumscribing rectangle,

$$I\,\frac{B_1}{A_1} = \tan\chi$$

where χ is the semiaxis of the ellipse.

The state of polarization is defined either by α and δ or χ and ψ. The intensity is given by,

$$I = \frac{1}{2Z_o}\,(A^2+B^2) = \frac{1}{2Z_o}\,(A_1^2+B_1^2)$$

When the polarization ellipse reduces to a straight line

$$\delta = j\pi \qquad (j = 0,\pm1,\pm2)$$

and

$$\frac{E_y}{E_x} = (-1)^m \frac{B}{A}$$

When the ellipse reduces to a circle, i.e., A=B,

$$\delta = \frac{1}{2} m\pi \qquad (m = \pm 1, \pm 3, \pm 5, \ldots)$$

and

$$E_x^2 + E_y^2 = A^2$$

Another representation of the polarized light is introduced by Stokes. The Stokes parameters are,

$$s_o = A^2 + B^2 = A_1^2 + B_1^2$$

$$s_1 = A^2 - B^2 = (A_1^2 + B_1^2)\cos 2\psi \cos 2\chi$$

$$s_2 = 2AB\cos\delta = (A_1^2 + B_1^2)\sin 2\psi \cos 2\chi$$

$$s_3 = 2AB\sin\delta = (A_1^2 + B_1^2)\sin 2\chi$$

$s_o^2 = s_1^2 + s_2^2 + s_3^2$.

When $\delta = 0°$ or $180°$ the radiation is linearly polarized, so $s_o = A^2+B^2$, $s_1 = A^2-B^2$, $s_2 = \pm 2AB$ and $s_3 = 0$.

For circularly polarized light $\delta = 90°$ or $270°$ and A=B so, $s_o = \pm s_3 = 2A^2$; $s_1 = s_2 = 0$.

One important property of Stokes' parameters is their additivity for incoherent polarized beams,

$$s_o = \sum_i s_{oi} \qquad s_1 = \sum_i s_{1i} \qquad s_2 = \sum_i s_{2i} \qquad s_3 = \sum_i s_{3i}$$

The polarized and natural parts are expressed as

$$s_o = s_o^p + s_o^n \qquad s_1 = s_1^p \qquad s_2 = s_2^p \qquad s_3 = s_3^p$$

The ratio of polarized intensity to the total is then

$$\frac{I_{pol}}{I_{tot}} = \frac{s_o^p}{s_o^p + s_o^n} = \frac{\left[(s_1^p)^2 + (s_2^p)^2 + (s_3^p)^2\right]^{1/2}}{s_o}$$

Using a matrix notation Stokes' parameters of the outgoing beam must be a homogeneous linear function of those of the

$$s_o' = a_{11}s_o + a_{12}s_1 + a_{13}s_2 + a_{14}s_3$$

$$s_1' = a_{21}s_o + a_{22}s_1 + a_{23}s_2 + a_{24}s_3$$

$$s_2' = a_{31}s_o + a_{32}s_1 + a_{33}s_2 + a_{34}s_3$$

$$s_3' = a_{41}s_o + a_{42}s_1 + a_{43}s_2 + a_{44}s_3$$

which can be applied to scattering as

$$\begin{bmatrix} I_s \\ Q_s \\ U_s \\ V_s \end{bmatrix} = \frac{1}{k^2} \begin{bmatrix} \\ S_{ij} \\ \\ \end{bmatrix} \begin{bmatrix} I_o \\ Q_o \\ U_o \\ V_o \end{bmatrix}$$

where the notation changes are:

$$\begin{bmatrix} s'_o \\ s'_1 \\ s'_2 \\ s'_3 \end{bmatrix} \Rightarrow \begin{bmatrix} I_s \\ Q_s \\ U_s \\ V_s \end{bmatrix} ; \qquad \begin{bmatrix} s_o \\ s_1 \\ s_2 \\ s_3 \end{bmatrix} \Rightarrow \begin{bmatrix} I_o \\ Q_o \\ U_o \\ V_o \end{bmatrix}$$

$$\begin{bmatrix} a_{ij} \end{bmatrix} = \frac{1}{k^2} \begin{bmatrix} S_{ij} \end{bmatrix}$$

APPENDIX II

GENERAL THEORY OF SCATTERING BY A SPHERE [23]

The electromagnetic properties of a particle may be defined by the incident wave, which has the field vectors $\underline{E}_i$, $\underline{H}_i$; the wave inside the particle, $\underline{E}_r$, $\underline{H}_r$ and the scattered wave, $\underline{E}_s$, $\underline{H}_s$. These vectors satisfy Maxwell's equations and the boundary conditions which are respectively given as,

$$\nabla^2 \underline{E} - \sigma\mu \frac{\partial \underline{E}}{\partial t} - \varepsilon\mu \frac{\partial^2 \underline{E}}{\partial t^2} = 0$$

and

$$\nabla^2 \underline{H} - \sigma\mu \frac{\partial \underline{H}}{\partial t} - \varepsilon\mu \frac{\partial^2 \underline{H}}{\partial t^2} = 0$$

boundary conditions:

$$(\underline{B}_2 - \underline{B}_1) \cdot \underline{n} = 0$$

where

$$\underline{B} = \mu \underline{H}$$

and

$$(\underline{H}_2 - \underline{H}_1) \cdot \underline{n} = \underline{L}$$

where L is the surface current density. Once the solutions for these are obtained, all electromagnetic phenomena related to the object are known.

The electric and magnetic Hertz vectors $\underline{\pi}_1$, and $\underline{\pi}_2$, are defined by the relations

$$B_1 = \mu\varepsilon\nabla \times \partial\pi_1/\partial t$$

$$\underline{E}_1 = \nabla\nabla\cdot\underline{\pi}_1 - \mu\varepsilon\partial^2\underline{\pi}_1/\partial t^2$$

$$\underline{D}_2 = -\mu\varepsilon\nabla \times \partial\underline{\pi}_2/\partial t$$

$$\underline{H}_2 = \nabla\nabla\cdot\underline{\pi}_2 - \mu\varepsilon\partial^2\underline{\pi}_2/\partial t^2 - \sigma\mu\underline{\pi}_2$$

These vectors also satisfy the wave equations,

$$\nabla^2\underline{\pi}_1 - \sigma\mu\frac{\partial\underline{\pi}_1}{\partial t} - \varepsilon_o\mu\frac{\partial^2\underline{\pi}_1}{\partial t_2} = -\frac{\underline{P}}{\varepsilon_o}$$

$$\nabla^2\underline{\pi}_2 - \sigma\mu_o\frac{\partial\underline{\pi}_2}{\partial t} - \varepsilon\mu_o\frac{\partial^2\underline{\pi}_2}{\partial t^2} = -\underline{M}$$

where P and M are the electric and magnetic polarizations. The scalar Hertz potentials π_1 and π_2 are derived as,

$$-\nabla\cdot\underline{\pi}_1 = \pi_1$$

$$-\nabla\cdot\underline{\pi}_2 = \pi_2$$

The spherical components of field vectors in terms of these potentials are then,

$$E_r = E_{1r} + E_{2r} = \frac{\partial^2(r\pi_1)}{\partial r^2} + k^2 r\pi_1 + 0$$

$$E_\theta = E_{1\theta} + E_{2\theta} = \frac{1}{r}\cdot\frac{\partial^2(r\pi_1)}{\partial r\partial\theta} + k_2\frac{1}{r\sin\theta}\frac{\partial(r\pi_2)}{\partial\phi}$$

$$E_\phi = E_{1\phi} + E_{2\phi} = \frac{1}{r\sin\theta}\frac{\partial^2(r\pi_1)}{\partial r\partial\phi} - k_2\frac{1}{r}\frac{\partial(r\pi_2)}{\partial\theta}$$

$$H_r = H_{1r} + H_{2r} = 0 + \frac{\partial^2(r\pi_2)}{\partial r^2} + k^2 r\pi_2$$

$$H_\theta = H_{1\theta} + H_{2\theta} = -k_1 \frac{1}{r\sin\theta} \frac{\partial(r\pi_1)}{\partial\phi} + \frac{1}{r} \frac{\partial^2(r\pi_2)}{\partial r\partial\theta}$$

$$H_\phi = H_{1\phi} + H_{2\phi} = k_1 \frac{1}{r} \frac{\partial(r\pi_1)}{\partial\theta} + \frac{1}{r\sin\theta} \frac{\partial^2(r^2\pi_2)}{\partial r\partial\phi}$$

where the propagation constant $k^2 = -k_1 k_2$

$$k_1 = i\omega\varepsilon + \sigma$$

$$k_2 = i\omega$$

The Debye potentials are the solutions of the homogeneous time-dependent wave equation,

$$\nabla^2\mu' + k^2\mu' = 0$$

where $\mu = \mu' e^{i\omega t}$.

In spherical coordinates,

$$\frac{1}{r}\left[\frac{\partial^2 r\Pi}{\partial r^2}\right] + \frac{1}{r^2\sin\theta} \frac{\theta}{2\theta} \left[\frac{\sin\theta\partial\Pi}{\partial\theta}\right] + \frac{1}{r^2\sin^2\theta} \frac{\partial^2\Pi}{\partial\phi} + k^2\Pi = 0$$

By separation of variables,

$$\Pi = k(r)\Theta(\theta)\Phi(\phi)$$

$$\frac{d^2 rR(r)}{dr^2} + \left[k^2 - \frac{n(n+1)}{r^2} \right] + R(r) = 0$$

$$\frac{1}{\sin\theta}\frac{d}{d\theta}\left[\frac{\sin\theta d\theta(\theta)}{d\theta}\right] + \left[n(n+1) - \frac{m^2}{\sin^2\theta}\right]\theta(\theta) = 0$$

$$\frac{d^2(\phi)}{d\phi^2} + m^2\phi(\phi) = 0$$

where m = -n,...0,...+n n-integer

The solutions for the first equation are Bessel functions

$$\psi_n(kr) = (\pi k_r/2)^{1/2} J_{n+\frac{1}{2}}(kr)$$

$$\chi_n(kr) = -(\pi k_r/2)^{1/2} N_{n+\frac{1}{2}}(kr)$$

where $J_{n+\frac{1}{2}}(kr)$ and $N_{n+\frac{1}{2}}(kr)$ are half-integral order Bessel functions. The solutions to the second equation are Legendre polynomials

$$\theta = P_n^{(m)}(\cos\theta)$$

For the third equation solutions are $\sin(m\phi)$ and $\cos(m\phi)$. The general solution of the scalar wave equation is then,

$$r\Pi = r \sum_{n=0}^{\infty} \sum_{m=-n}^{n} \pi_n^{(m)}$$

$$= \sum_{n=0}^{\infty} \sum_{m=-n}^{n} \left\{C_n\psi_n(kr) + d_n\psi_n(kr)\right\}\left\{P_n^{(m)}(\cos\theta)\right\}$$
$$\left\{a_m\cos(m\phi) + b_m\sin(m\phi)\right\}$$

The relative refractive index is defined as

$$m = k_1/k_2 = mk_o/m_2k_o = m_1/m_2$$

Considering the Debye potentials as the incident π_1^i, π_2^i the scattered π_1^s, π_2^s and inside the particle π_1^r, π_2^r we get

$$r\pi_1^i = \frac{1}{k^2} \sum_{n=1}^{\infty} i^{n-1} \frac{2n+1}{n(n+1)} \psi_n(k_2 r) P_n^{(1)}(\cos\theta)\cos\phi$$

$$r\pi_2^i = \frac{1}{k^2} \sum_{n=1}^{\infty} i^{n-1} \frac{2n+1}{n(n+1)} \psi_n(k_2 r) P_n^{(1)}(\cos\theta)\sin\phi$$

$$r\pi_1^s = -\frac{1}{k^2} \sum_{n=1}^{\infty} i^{n-1} \frac{2n+1}{n(n+1)} a_n \xi_n(k_2 r) P_n^{(1)}(\cos\theta)\cos\phi$$

$$r\pi_2^s = -\frac{1}{k^2} \sum_{n=1}^{\infty} i^{n-1} \frac{2n+1}{n(n+1)} b_n \xi_n(k_2 r) P_n^{(1)}(\cos\theta)\sin\phi$$

and

$$r\pi_1^r = \frac{1}{k_1^2} \sum_{n=1}^{\infty} i^{n-1} \frac{2n+1}{n(n+1)} C_n \psi_n(k_1 r) P_n^{(1)}(\cos\theta)\cos\phi$$

$$r\pi_2^r = \frac{1}{k_1^2} \sum_{n=1}^{\infty} i^{n-1} \frac{2n+1}{n(n+1)} d_n \psi_n(k_1 r) P_n^{(1)}(\cos\theta)\sin\phi$$

where $\xi_n(k_2 r)$ are the Hankel functions

$$\xi_n(kr) = \psi_n(kr) + i\chi_n(kr) = (\pi kr/2)^{1/2} H_{n+\frac{1}{2}}^{(2)}(kr)$$

The coefficients a_n, b_n are

$$a_n = \frac{\psi_n(\alpha)\psi_n'(\beta) - m\psi_n(\beta)\psi_n'(\alpha)}{\zeta_n(\alpha)\psi_n'(\beta) - m\psi_n(\beta)\zeta_n'(\alpha)}$$

$$b_n = \frac{m\psi_n(\alpha)\psi_n'(\beta) - \psi_n(\beta)\psi_n'(\alpha)}{m\zeta_n(\alpha)\psi_n'(\beta) - \psi_n(\beta)\zeta_n'(\alpha)}$$

(prime indicates derivative with respect to the argument.)

where $\alpha = k_2 a = 2\Pi a/\lambda = 2\Pi m_2 a/\lambda_o$

$\beta = k_1 a = 2\Pi m_1 a/\lambda_o = m\alpha$

λ_o = wavelength in vacuum

λ = wavelength in the medium

$m = m_1/m_2$

When the measured scattered field is far from the particle, i.e., $k_2 r >> n$, the solutions become easier,

$$\xi_n'(k_2 r) = i^{(n+1)} e^{-ik_2 r}$$

$$\xi_n'(k_2 r) = i^n e^{-ik_2 r}$$

With further simplification

$$E_\phi = \frac{H\theta}{m_2} = \frac{-ie^{-ik_2 r}}{k_2 r} \sin\phi \sum_{n=1}^{\infty} \frac{2n+1}{n(n+1)} \left\{ a_n \frac{P_n^{(1)}(\cos\theta)}{\sin\theta} + b_n \frac{dP_n^{(1)}(\cos\theta)}{d\theta} \right\}$$

$$E_\theta = -\frac{H\theta}{m_2} = \frac{ie^{-ik_2 r}}{k_2 r} \cos\phi \sum_{n=1}^{\infty} \frac{2n+1}{n(n+1)} \left\{ a_n \frac{dP_n^{(1)}(\cos\theta)}{d\theta} + b_n \frac{P_n^{(1)}(\cos\theta)}{\sin\theta} \right\}$$

Denoting

$$S_1 = \sum_{n=1}^{\infty} \frac{2n+1}{n(n+1)} \left\{ a_n \pi_n(\cos\theta) + b_n \tau_n(\cos\theta) \right\}$$

$$S_2 = \sum_{n=1}^{\infty} \frac{2n+1}{n(n+1)} \left\{ a_n \tau_n(\cos\theta) + b_n \pi_n(\cos\theta) \right\}$$

where

$$\pi_n(\cos\theta) = \frac{P_n^{(1)}(\cos\theta)}{\sin\theta}$$

$$\tau_n(\cos\theta) = \frac{dP_n^{(1)}(\cos\theta)}{d\theta}$$

Then, by Poynting's theorem, the intensity of scattered radiation polarized in the θ and ϕ azimuths is,

$$I_\phi = \frac{\lambda^2}{4\Pi^2 r^2} |S_1|^2 \sin^2\phi = \frac{\lambda^2}{4\Pi^2 r^2} i_1 \sin^2\phi$$

$$I_\theta = \frac{\lambda^2}{4\Pi^2 r^2} |S_2|^2 \cos^2\phi = \frac{\lambda^2}{4\Pi^2 r^2} i_2 \cos^2\phi$$

where i_1 and i_2 are intensity functions.

While the exact solutions give a means of standard to check the experimental work, solutions for irregular particles are not yet well know.

Further studies have been made on the subject which will not be explained in detail since it is beyond the scope of this thesis.

APPENDIX III

SCATTERING BY AN ELLIPSOID (A THIRD APPROXIMATION) [24]

Let the equation of the ellipsoid be

$$x^2/a^2 + y^2/b^2 + z^2/c^2 = 1$$

where a, b, c are the principal semi-axes. Suppose in the first place that a, b, c are all unequal, but this restriction can be removed in the final results. The dielectric constant and permeability of the ellipsoid are ε, μ, respectively, the external medium being a vacuum. Define the incident wave by the three sets of direction cosines,

(ℓ,m,n): direction of propagation,

(ℓ_1,m_1,n_1): electric vector,

(ℓ_2,m_2,n_2): magnetic vector.

Consider a steady state with time factor $e^{-i\omega t}$. The incident field is then given by

$$E^{(0)} = (\ell_1,m_1,n_1)e^{ik(\ell x+my+nz)}$$

$$H^{(0)} = (\ell_2,m_2,n_2)e^{ik(\ell x+my+nz)}$$

where $k = 2\pi/\lambda$, λ being the wavelength in vacuum.

We expand the incident field in powers of ik in the form

$$E^{(0)} = \sum_{p=0}^{\infty} E_p^{(0)}(ik)^p$$

$$H^{(0)} = \sum_{p=0}^{\infty} H_p^{(0)}(ik)^p$$

The first three terms in the expansions are

$$\underline{E}_0^{(0)} = (\ell_1, m_1, n_1)$$

$$\underline{E}_1^{(0)} = (\ell_1, m_1, n_1)(\ell x+my+nz)$$

$$\underline{E}_2^{(0)} = \tfrac{1}{2}(\ell_1, m_1, n_1)(\ell x+my+nz)^2$$

with similar expressions for $\underline{H}_{0,1,2}^{(0)}$ obtained by replacing (ℓ_1, m_1, n_1) by (ℓ_2, m_2, n_2).

Let $(\underline{E}, \underline{H})$ be the scattered field and $(\underline{E}^{(i)}, \underline{H}^{(i)})$ the field inside the ellipsoid. Then

$$\underline{E} = \sum_{p=0}^{\infty} \underline{E}_p (ik)^p, \text{ etc.}$$

$\underline{E}_0, \ldots, \underline{E}_2^{(i)}$ are given by the equations

$$\underline{E}_0 = \nabla V_0 \qquad \underline{E}_0^{(i)} = \nabla V_0^{(i)}$$

$$\underline{H}_1 = \underline{G}_1 + \nabla U_1 \qquad \underline{H}_1^{(i)} = \underline{G}_1^{(i)} + \nabla U_1^{(i)}$$

$$\underline{E}_2 = \underline{F}_2 + \nabla V_2 \qquad \underline{E}_2^{(i)} = \underline{F}_2^{(i)} + \nabla V_2^{(i)}$$

$$\text{curl}\underline{G}_1 = -\underline{E}_0 \qquad \text{curl}\underline{G}_1^{(i)} = -\varepsilon \underline{E}_0^{(i)}$$

$$\text{curl}\underline{F}_2 = \underline{H}_1 \qquad \text{curl}\underline{F}_2^{(i)} = \mu \underline{H}_1^{(i)}$$

$$\text{div}\underline{G}_1 = \text{div}\underline{G}_1^{(i)} = \text{div}\underline{F}_2 = \text{div}\underline{F}_2^{(i)} = 0$$

where $\underline{G}_1$, $\underline{F}_2$ vanish at infinity, V_0, U_1, V_2 are external harmonic functions, and $V_0^{(i)}$, $U_1^{(i)}$, $V_2^{(i)}$ internal harmonic functions, which satisfy the boundary conditions on the ellipsoid,

$$\underline{n} \times \nabla(V_0 - V_0^{(i)}) = -\underline{n} \times \underline{E}_0^{(0)}$$

$$\underline{n} \cdot \nabla(V_0 - \varepsilon V_0^{(i)} = -\underline{n} \cdot \underline{E}_0^{(0)}$$

$$\underline{n} \times \nabla(U_1 - U_1^{(i)} = -\underline{n} \times (\underline{G}_1 - \underline{G}_1^{(i)} + \underline{H}_1^{(0)})$$

$$\underline{n} \cdot \nabla(U_1 - \mu U_1^{(i)} = -\underline{n} \cdot (\underline{G}_1 - \mu\underline{G}_1^{(i)} + \underline{H}_1^{(0)})$$

$$\underline{n} \times \nabla(V_2 - V_2^{(i)} = -\underline{n} \times (\underline{F}_2 - \underline{F}_2^{(i)} + \underline{E}_2^{(0)})$$

$$\underline{n} \cdot \nabla(V_2 - \varepsilon V_2^{(i)} = -\underline{n} \cdot (\underline{F}_2 - \varepsilon\underline{F}_2^{(i)} + \underline{E}_2^{(0)})$$

where $\underline{n}$ denotes a unit vector along the outward normal. Further

$$\int \underline{n} \cdot \underline{E}_0 dS = \int \underline{n} \cdot \underline{H}_1 dS = \int \underline{n} \cdot \underline{E}_2 dS = 0$$

where the integrals are taken over the surface of the ellipsoid.

From these we obtain the results as

$$V_0 = A_1 x I_a(\xi) + A_2 y I_b(\xi) + A_3 z I_c(\xi)$$

$$V_0^{(i)} = A_1^{(i)} x + A_2^{(i)} y + A_3^{(i)} z$$

$$(\underline{G}_1)_x = A_2 z I_c(\xi) - A_3 y I_b(\xi)$$

$$(\underline{G}_1^{(i)})_x = \frac{\varepsilon}{2}(A_3^{(i)} y - A_2^{(i)} z)$$

$$U_1 = B X_\nu T_\nu(\xi) + B' X_\nu, T_\nu,(\xi) + B_1 yz I_{bc}(\xi)$$
$$+ B_2 zx I_{ca}(\xi) + B_3 xy I_{ab}(\xi)$$

$$U_1^{(i)} = B^{(i)} X_\nu + B'^{(i)} X_\nu, + B_1^{(i)} yz + B_2^{(i)} zx + B_3^{(i)} xy$$

$$\underline{F}_2 = \underline{F}_2' + \nabla V_2''$$

$$(\underline{F}_2')_x = -\frac{1}{2} A_1\left[x^2 I_a(\xi) + y^2 I_b(\xi) + z^2 I_c(\xi) - I(\xi)\right]$$
$$- \frac{1}{2} B_1\left[x^2 I_{ac}(\xi) + y^2 I_{bc}(\xi) + 3z^2 I_{cc}(\xi) - I_c(\xi)\right]$$
$$+ B_2 xy I_{ab}(\xi) + C_1 yz I_{bc}(\xi)$$

$$V_2'' = A_1\phi_x + A_2\phi_y + A_3\phi_z$$

$$\phi_x = \frac{1}{10}(x^2+y^2+z^2) x I_a(\xi) - \frac{1}{5} x I(\xi) - \frac{1}{50}(3a^2+b^2+c^2) x I_a(\xi)$$

$$(\underline{F}_2^{(i)})_x = \frac{\varepsilon\xi}{4} A_1^{(i)}(y^2+z^2) - \frac{\mu}{2} B_1^{(i)}(y^2-z^2) + C_1^{(i)} y z$$

$$V_2 = D_1 x I_a(\xi) + D_2 y I_b(\xi) + D_3 z I_c(\xi)$$

The y and z components are given by cyclic permutations of x, y, z, a, b, c and of the suffixes 1, 2, 3 in the constants A_1, A_2, A_3, etc.

The notation is as follows: ξ is one of the ellipsoidal coordinates of the point (x,y,z), defined as the greatest root of the equation

$$\Theta(\xi) \equiv \frac{x^2}{a^2+\xi} + \frac{y^2}{b^2+\xi} + \frac{z^2}{c^2+\xi} - 1 = 0$$

Further

$$X_\nu = (a^2+\nu)(b^2+\nu)(c^2+\nu)\Theta(\nu)$$

ν,ν' = roots of equation

$$\frac{1}{a^2+\nu} + \frac{1}{b^2+\nu} + \frac{1}{c^2+\nu} = 0$$

$$I(\xi) = \int_{\xi}^{\infty} \frac{du}{R(u)}$$

$$R(u) = \left[(a^2+u)(b^2+u)(c^2+u)\right]^{1/2}$$

$$I_a(\xi) = \int_{\xi}^{\infty} \frac{du}{(a^2+u)R(u)}$$

$$I_{ab}(\xi) = \frac{du}{(a^2+u)(b^2+u)R(u)}, \text{ etc.}$$

$$T_\nu(\xi) = \int_{\xi}^{\infty} \frac{du}{(u-\nu)^2 R(u)}$$

$$I = \int_0^{\infty} \frac{du}{R(u)}$$

$$I_a = \int_0^{\infty} \frac{du}{(a^2+u)R(u)}$$

$$I_{ab} = \int_0^{\infty} \frac{du}{(a^2+u)(b^2+u)R(u)}, \text{ etc.}$$

$$T_\nu = T_\nu(0)$$

$$A_1 = -(\varepsilon-1) f_1(\varepsilon) \ell_1$$

$$A_1^{(i)} = (2/abc) f_1(\varepsilon) \ell_1$$

$$f_1(\varepsilon) = \left[(\varepsilon-1) I_a + \frac{2}{abc}\right]^{-1}$$

$$B = \frac{\mu-1}{(\mu-1)T_\nu - (1/\nu abc)} \frac{1}{6(\nu-\nu')} \left\{\frac{\ell\ell_2}{a^2+\nu} + \frac{mm_2}{b^2+\nu} + \frac{nn_2}{c^2+\nu}\right\}$$

B' = same as B with ν, ν' interchanged,

$$B_1 = g_1(\mu)\left\{-\frac{\mu}{2}(b^2+c^2)(m_2n+n_2m) + m_2nc^2 + n_2mb^2 + \left[b^2I_b - c^2I_c - \frac{\mu}{2}(b^2+c^2)(I_b-I_c)\right]A_1 + \frac{\varepsilon\mu}{2}(b^2-c^2)A_1^{(i)}\right\}$$

$$g_1(\mu) = \left[(\mu-1)(b^2+c^2)I_{bc} + \frac{2}{abc}\right]^{-1}$$

$$B^{(i)} = \frac{B}{(\mu-1)\nu abc}, \qquad B'^{(i)} = \frac{B'}{(\mu-1)\nu' abc}$$

$$B_1^{(i)} = g_1(\mu)\left\{\frac{m_2n+n_2m}{abc} - \frac{b^2-c^2}{2}I_{bc}\ell_1 + \left[\frac{I_b-I_c}{abc} + \frac{b^2-c^2}{2}(I_b+I_c)I_{bc}\right]A_1 + \frac{\varepsilon\mu}{2}(b^2-c^2)I_{bc}A_1^{(i)}\right\}$$

$$C_1 = (b^2-c^2)[(a^2+\nu)B + (a^2+\nu')B']$$

$$C_1^{(i)} = -(2/3)\mu(b^2-c^2)[(a^2+\nu)B^{(i)} + (a^2+\nu')B'^{(i)}]$$

$$D_1 = (1/10)f_1(\varepsilon)\left\{(1-\varepsilon)\ell_1(a^2\ell^2+b^2m^2+c^2n^2) + \varepsilon(b^2mn_2-c^2nm_2) + [(2-\varepsilon)I - \varepsilon a^2I_a + 4a/bc]A_1 + (\varepsilon I_a+2I_c)B_1 + (1/2)\varepsilon^2\mu(b^2+c^2)A_1^{(i)} - \varepsilon\mu(b^2-c^2)B_1^{(i)}\right\}$$

Various relations connect the elliptic integrals (and T_ν, $T_{\nu'}$), of which we mention the following,

$$I_a + I_b + I_c = 2/abc$$

$$a^2 I_a + b^2 I_b + c^2 I_c = I$$

$$I_{ab} = (I_a - I_b)/(b^2 - a^2)$$

$$3I_{aa} + I_{ab} + I_{ac} = 2/a^3 bc$$

$$3a^2 I_{aa} + b^2 I_{ab} + c^2 I_{ac} = 3I_a$$

$$T_\nu = \frac{1}{2}\left(\frac{I_a}{a^2+\nu} + \frac{I_b}{b^2+\nu} + \frac{I_c}{c^2+\nu}\right) - \frac{1}{\nu abc}$$

To find the first three terms in the wave zone expansion, we require the coefficients of $1/R^3$, $1/R^4$ in E_{0R}, E_{1R}, and the coefficient of $1/R^3$ in E_{2R}. This necessitates expanding the integrals $I(\xi)$, etc., in powers of $1/R$.

$$\alpha = x/R, \quad \beta = y/R, \quad \gamma = z/R$$

so that (α,β,γ) are the direction cosines of the radius vector to the field point. Then

$$\xi = R^2 - (a^2\alpha^2 + b^2\beta^2 + c^2\gamma^2) + 0(1/R^2)$$

Hence, expanding the integrals $I(\xi)$, etc., in inverse powers of ξ, we find

$$I(\xi) = 2/R + (1/R^3\left[-\frac{1}{3}(a^2+b^2+c^2)\right.$$
$$\left. + a^2\alpha^2 + b^2\beta^2 + c^2\gamma^2\right] + 0(1/R^5)$$

$$I_a(\xi) = 2/3R^3 + (1/R^5)\left[-(1/5)(3a^2+b^2+c^2)\right.$$
$$\left. + a^2\alpha^2 + b^2\beta^2 + c^2\gamma^2\right] + 0(1/R^7)$$

$$I_{ab}(\xi) = 2/5R^5 + 0(1/R^7)$$

$$I_\alpha(\xi) = 2/5R^5 + 0(1/R^7)$$

For the remaining coefficients, when expressed in terms of surface harmonics, we find,

$$S_1^{(0,3)} = -(4/3)(A_1\alpha+A_2\beta+A_3\gamma)$$

$$S_2^{(1,4)} = p_1\alpha^2 + p_2\beta^2 + p_3\gamma^2 + q_1\beta\gamma + q_2\gamma\alpha + q_3\alpha\beta$$

$$S_1^{(2,3)} = r_1\alpha + r_2\beta + r_3\gamma$$

$$S_3^{(2,3)} = (\tfrac{2}{5})A_1\alpha\left[a^2\alpha^2+b^2\beta^2+c^2\gamma^2-(\tfrac{1}{5})(3a^2+b^2+c^2)\right]$$
$$+ (\tfrac{2}{5})A_2\beta\left[a^2\alpha^2+b^2\beta^2+c^2\gamma^2-(\tfrac{1}{5})(3b^2+c^2+a^2)\right]$$
$$+ (\tfrac{2}{5})A_3\gamma\left[a^2\alpha^2+b^2\beta^2+c^2\gamma^2-(\tfrac{1}{5})(3c^2+a^2+b^2)\right]$$

where

$$p_1 = (6/5)\left[(b^2+\nu)(c^2+\nu)\bar{B} + (b^2+\nu')(c^2+\nu')\bar{B}'\right]$$

$$q_1 = (2/5)\left[(b^2-c^2)\bar{A}_1 + 3\bar{B}_1\right]$$

$$r_1 = (2/75)\left[(9a^2-2b^2-2c^2)A_1 + 5B_1 - 50D_1\right]$$

$$P = k^2\left[\tfrac{1}{2}\,S_1^{(0,3)}\right] + k^4\left[-\tfrac{1}{2}\,S_1^{(2,3)} + \tfrac{1}{18}\,S_2^{(1,4)}\right.$$
$$\left. + \tfrac{1}{18}\,S_3^{(2,3)}\right]$$

For the wave zone field we have

$$E_\theta = H_\phi = \left(\frac{\partial P}{\partial \theta} + \frac{1}{\sin\theta}\frac{\partial \bar{P}}{\partial \phi}\right)\frac{e^{ikR}}{R}$$

$$E_\phi = -H_\theta = \left(\frac{1}{\sin\theta}\frac{\partial P}{\partial \phi}\frac{\partial \bar{P}}{\partial \theta}\right)\frac{e^{ikR}}{R}$$

where, as far as the term in k^4,

$$P = k^2(K_1\alpha + K_2\beta + K_3\gamma) + k^4\big[L_1\alpha + L_2\beta + L_3\gamma + M_1\alpha^2 + M_2\beta^2 + M_3\gamma^2 + N_1\beta\gamma + N_2\gamma\alpha + N_3\alpha\beta - (1/30)(K_1\alpha + K_2\beta + K_3\gamma)(a^2\alpha^2+b^2\beta^2+c^2\gamma^2)\big]$$

Here (R,θ,ϕ) are polar coordinates of the field point, while (α,β,γ) are direction cosines of the radius vector to the field point, and are therefore functions of θ,ϕ which depend on the choice of the polar axis. The constants $K_1, L_1, \ldots$ are defined as follows,

$$K_1 = \left(\frac{2}{3}\right)(\varepsilon-1) f_1(\varepsilon)\, \ell_1$$

$$15L_1 = f_1(\varepsilon)\Big\{(\varepsilon-1)\ell_1\Big[\left(\tfrac{1}{3}\right)(6a^2-b^2-c^2) - (a^2\ell^2+b^2m^2+c^2n^2)\Big] + \varepsilon(b^2mn_2-c^2nm_2)\Big\} + [f_1(\varepsilon)]^2\ell_1\Big\{(\varepsilon-1)[(\varepsilon-2)I + \varepsilon a^2 I_a - 4a/(bc)] + \varepsilon^2\mu(b^2+c^2)/(abc)\Big\} + f_1(\varepsilon)g_1(\mu)\Big\{(I_b-I_c) \times [(\mu/2)(b^2+c^2)(mn_2+nm_2) - mn_2b^2 - nm_2c^2]$$

$$-\varepsilon\mu(b^2-c^2)(mn_2+nm_2)/(abc)\Big\} + [f_1(\varepsilon)]^2$$

$$\times g_1(\mu)(I_b-I_c)\ell_1\left[(\varepsilon-1)k_1(\mu)\right.$$

$$\left.+ \varepsilon\mu(\varepsilon\mu-2)(b^2-c^2)/(abc)\right]$$

$$M_1 = \frac{\varepsilon-1}{45Q}\left[(\varepsilon-1)(I_{ab}nn_1+I_{ac}mm_1-2I_{b1}\ell\ell_1)\right.$$

$$\left.+ \frac{2\varepsilon}{abc(\sum a^2b^2)}(2a^2\ell\ell_1-b^2mm_1-c^2nn_1)\right]$$

$$15N_1 = -\left(\tfrac{1}{3}\right)(\mu-1)f_1(\mu)(b^2-c^2)\ell_2 + g_1(\varepsilon)$$

$$\times\left[(\varepsilon/2)(b^2+c^2)(mn_1+nm_1) - b^2mn_1 - c^2nm_1\right]$$

$$+ f_1(\mu)g_1(\varepsilon)\ell_2[\varepsilon\mu(b^2-c^2)/(abc) - (\mu-1)k_1(\varepsilon)]$$

where

$$k_1(\varepsilon) = b^2I_b - c^2I_c - (\varepsilon/2)(b^2+c^2)(I_b-I_c)$$

$$Q = (\varepsilon-1)^2(I_{ab}I_{bc}+I_{bc}I_{ca}+I_{ca}I_{ab})$$

$$- \frac{4\varepsilon(\varepsilon-1)}{abc}\left(J + \frac{\sum a^2}{\sum a^2b^2}J'\right) + \frac{4\varepsilon^2}{a^2b^2c^2(\sum a^2b^2)}$$

$$J = \int_0^\infty \frac{du}{[R(u)]^3} = (I_{ab}-I_{ac})/(c^2-b^2)$$

$$J' = \int_0^\infty \frac{udu}{[R(u)]^3} = I_{ab} - c^2J, \text{ etc.}$$

$$\sum a^2 = a^2 + b^2 + c^2$$

$$\sum a^2b^2 = a^2b^2 + b^2c^2 + c^2a^2$$

I, I_a, etc. are elliptic integrals.

The scattering coefficient s (ratio of energy scattered by ellipsoid to energy incident on ellipsoid) is found to be

$$s = (\ell^2 b^2 c^2 + m^2 c^2 a^2 + n^2 a^2 b^2)^{-1/2}$$
$$\times \left\{ (8/3)k^4 \sum_{j=1}^{3} (|K_j|^2 + |\bar{K}_j|^2) + (16/3)k^6 \right.$$
$$\times \left[\mathrm{Re} \sum_{j=1}^{3} (K_j L_j^* + \bar{K}_j \bar{L}_j^*) - (1/150) \right.$$
$$\times \left((3a^2+b^2+c^2)(|K_1|^2 + |\bar{K}_1|^2) \right.$$
$$+ (3b^2+c^2+a^2)(|K_2|^2 + |\bar{K}_2|^2)$$
$$\left.\left.\left. + (3c^2+a^2+b^2)(|K_3|^2 + |\bar{K}_3|^2) \right) \right] \right\} + 0(k^7)$$

(1) Spheroid

If two of the principal axes of the ellipsoid are equal, the elliptic integrals become elementary integrals. We find for the

prolate spheroid (a=b<c):

$$I = (c^2-a^2)^{-1/2} \log \frac{c + (c^2-a^2)^{1/2}}{c - (c^2-a^2)^{1/2}}$$

while for the

oblate spheroid (a=b>c):

$$I = 2(a^2-c^2)^{-1/2} \cos^{-1}(c/a)$$

Exact solutions for spheroids have been found by Asano and Yamamoto [25].

(2) Sphere

If a=b=c, we find easily

$$I = 2/a,\ I_a = 2/(3a^3),\ I_{aa} = 2/(5a^5)$$

$$J = 2/(7a^7),\ J' = 4/(35a^5)$$

There is further no loss of generality in taking the z axis as the direction of propagation and the x axis as the direction of the electric vector, so that

$$n = \ell_1 = m_2 = 1$$

the other direction cosines vanishing. We then find

$$E_\theta = H_\phi = \left\{k^2a^3\left[\frac{\varepsilon-1}{\varepsilon+2}\cos\theta + \frac{\mu-1}{\mu+2}\right] + k^4a^5 \right.$$
$$\times \left[F(\varepsilon,\mu)\cos\theta + F(\mu,\varepsilon) + \frac{\varepsilon-1}{6(2\varepsilon+3)}\cos 2\theta \right.$$
$$\left.\left. + \frac{\mu-1}{6(2\mu+3)}\cos\theta\right]\right\}\cos\phi\ \frac{e^{ikR}}{R}$$

$$E_\phi = -H_\theta = -\left\{k^2a^3\left[\frac{\varepsilon-1}{\varepsilon+2} + \frac{\mu-1}{\mu+2}\cos\theta\right] + k^4a^5 \right.$$
$$\times \left[F(\varepsilon,\mu) + F(\mu,\varepsilon)\cos\theta + \frac{\varepsilon-1}{6(2\varepsilon+3)}\cos\theta \right.$$
$$\left.\left. + \frac{\mu-1}{6(2\mu+3)}\cos 2\theta\right]\right\}\sin\phi\ \frac{e^{ikR}}{R}$$

where

$$F(\varepsilon,\mu) = (3/10)(\varepsilon+2)^{-2}(\varepsilon^2-6\varepsilon+4+\varepsilon^2\mu)$$

(3) Perfectly Conducting Ellipsoid

We can deduce this case by putting $\mu=0$ and making $|\varepsilon|\to\infty$ in our general results. Thus

$$K_1 = (2/3I_a)\,\ell_1$$

$$L_1 = (1/15I_a)\left\{\ell_1\left[\left(\tfrac{1}{3}\right)(6a^2-b^2-c^2) = (a^2\ell^2+b^2m^2+c^2n^2)\right]\right.$$
$$\left. + b^2mn_2 - c^2nm_2\right\} + (\ell_1/15I_a^2)(I+a^2I_a)$$

$$M_1 = \frac{1}{45Q'}\left[I_{ab}nn_1 + I_{ac}mm_1 - 2I_{bc}\ell\ell_1\right.$$
$$\left. + \frac{2}{abc(\sum a^2b^2)}(2a^2\ell\ell_1-b^2mm_1-c^2nn_1)\right]$$

$$Q' = I_{ab}I_{bc} + I_{bc}I_{ca} + I_{ca}I_{ab}$$
$$- \frac{4}{abc}\left(J + \frac{\sum a^2}{\sum a^2b^2}J'\right) + \frac{4}{a^2b^2c^2(\sum a^2b^2}$$

$$N_1 = \frac{1}{18}\frac{b^2-c^2}{I_b+I_c}\ell_2 + \frac{1}{15I_{bc}}(mn_1+nm_1)$$

$$\bar{K}_1 = -\frac{2}{3}\frac{2}{I_b+I_c}$$

$$\bar{L}_1 = \frac{\ell_2}{15(I_b+I_c)}\left[a^2\ell^2 + b^2m^2 + c^2n^2 - \tfrac{1}{3}(6a^2-b^2-c^2)\right]$$
$$+ \frac{2\ell_2}{15(I_b+I_c)^2}\left[I + \frac{2a}{bc} + \tfrac{1}{4}(b^2-c^2)^2I_{bc}\right]$$
$$+ \frac{b^2-c^2}{30(I_b+I_c)}(mn_1+nm_1)$$

$$\bar{M}_1 = \frac{1}{45} \frac{I_{ab}nn_2+I_{ac}mm_2-2I_{bc}\ell\ell_2}{I_{ab}I_{bc}+I_{bc}I_{ca}+I_{ca}I_{ab}}$$

$$\bar{N}_1 = \frac{b^2-c^2}{45I_a}\ell_1 + \frac{1/15}{(b^2+c^2)I_{bc}-2/(abc)}$$

$$\times [b^2mn_2+c^2nm_2-(\ell_1/I_a)(b^2I_b-c^2I_c)]$$

The remaining constants $K_2, K_3, \ldots$ are obtained by cyclic permutation as before.

APPENDIX IV

COMPUTER PROGRAM TO DECODE PAPER TAPE AND AVERAGE OVER STATISTICAL DATA

```
      DIMENSION AV1(94), AV2(94)
      DIMENSION Y1(94),Y2(94),ANG(94),ANG1(94)
      DIMENSION HEADER (20,80)
      DIMENSION MEAN1(94),MEAN2(94),VAR1(94),VAR2(94),OFF1(94),OFF2(94)
      DIMENSION DUM1(94),DUM2(94)
      DIMENSION STAT(5,2,94),IGPS(21),INOB(5)
      DIMENSION AB1(94),AB2(94)
      DIMENSION W(94),YF1(94),YF2(94),YD1(94),YD2(94),YA1(94),YA2(94)
      DIMENSION G(16,94),A(16),AA(16)
      DIMENSION ISKP(20), VALUE(2,94)
      DIMENSION AAN(94),ARE(94)
      REAL MEAN1,MEAN2
      REAL K
      DATA RFR,RFI,K/3*0.0/
      OFF=0.
      YMAX1=11.
      YMAX2=11.
      AC=7.2/57.3
      AP=7.2
      NOR=20
      ISK=1
      NF=16
      IG=1
      ITOT=1
      IND=1
      IOC=1
      I=1
      N=94
      FACT=1.8
      FACT1=1.8/57.3
      DO 50 I=1,N
      W(I)=1.
      G(1,I)=1.
      DO 51 J=2,NF
      G(J,I)=FLOAT(I)**(J-1)
51    CONTINUE
      ANG(I)=FACT*FLOAT(I)+AP
      ANG1(I)=FACT1*FLOAT(I)+AO
      OFF1(I)=OFF
      OFF2(I)=OFF
      DUM1(I)=0.
      DUM2(I)=0.
   50 CONTINUE
C   DATA INPUT:
C   FIRST DATA CARD READS IN THE # RUNS IN A GROUP THAT WILL BE AVERAGED
C SECOND CARD SPECIFIES THE NUMBER BACKGROUND RUNS START RESPECTIVELY
C THIRD ONE IS THE # RUN TO BE SKIPPED. FIRST 2 CARDS SKIPPS ARE N.T INCLUDED
      READ(5,1000) IGPS
1000  FORMAT(11,2012)
      READ(5,1001) INOB
1001  FORMAT(12,4I3)
      READ(5,1000) ISKP
      DO 13 I=1,NOR
```

```
      READ (5,20) (HEADER(I,J),J=1,80)
   20 FORMAT(80A1)
   13 CONTINUE
      I=1
12    CONTINUE
      WRITE(6,21) (HEADER(I,J),J=1,80)
   21 FORMAT('1',80A1)
4049  CONTINUE
      IF(ISK.GT.20) GO TO 4050
      IF(ISKP(ISK).EQ.ITOT) GO TO 9050
4050  CONTINUE
      IMX=IGPS(IOD)
      IF(IMX.EQ.0) CALL EXIT
      IF(INOD(IND).EQ.1) GO TO 5000
5050  CONTINUE
      CALL STATS(STAT,94,IMX,MEAN1,MEAN2,VAR1,VAR2,OFF1,OFF2,0)
 5052 CONTINUE
      CALL MGLLS(N,NF,MEAN1,G,W,A,Y1,YD1,CSQ,RECSQ,RECI,IER1)
      CALL MGLLS(N,NF,MEAN2,G,W,AA,Y2,YD2,CSQ,RECSQ,RECI,IER2)
      READ(5,1771) DIS,LEN,RAD
 1771 FORMAT(3F10.6)
      READ(5,1772) CAL1,CAL2,PART
 1772 FORMAT(2F10.6,E16.7)
      DO 55 J=1,N
      PI=3.1415
      AAN(J)=ANG(J)*PI/180.
      ARE(J)=(4.*DIS-LEN*COS(AAN(J)))*LEN*(COS(AAN(J))**2.)/(PI*RAD*SIN(
     1AAN(J)))
   55 CONTINUE
      DO 90 J=1,N
      WRITE(6,100) ANG(J),Y1(J),Y2(J),MEAN1(J),MEAN2(J),VAR1(J),VAR2(J)
     1,(STAT(L,1,J),STAT(L,2,J),L=1,IMX)
100   FORMAT(' ',17F7.1)
      AB1(J)=COM(VAR1(J))
      AB2(J)=COM(VAR2(J))
      Y1(J)=COM(Y1(J))
      Y2(J)=COM(Y2(J))
      AV1(J)=COM(MEAN1(J))*(ARE(J)+CAL1)
      AV2(J)=COM(MEAN2(J))*(ARE(J)+CAL2)
   90 CONTINUE
      IF(IER1.GT.0) GO TO 91
      CALL GRAPH1(ANG,Y1,N,YMAX1,RER,REI,K)
91    CONTINUE
      IF(IER2.GT.0) GO TO 92
      CALL GRAPH1(ANG,Y2,N,YMAX2,RER,REI,K)
92    CONTINUE
 1111 CONTINUE
C     CALL GRAPH1(ANG,AB1,N,YMAX1,RER,REI,K)
C     CALL GRAPH1(ANG,AB2,N,YMAX2,RER,REI,K)
      CALL GRAPH1(ANG,AV1,N,YMAX1,RER,REI,K)
      CALL GRAPH1(ANG,AV2,N,YMAX2,RER,REI,K)
      IF(IOK.EQ.1) GO TO 5051
      CALL STATS(STAT,94,IMX,MEAN1,MEAN2,VAR1,VAR2,DUM1,DUM2,1)
      IF(IG.GE.2) GO TO 5051
      IG=IG+1
      GO TO 5052
 5051 CONTINUE
      IG=1
      I=I+IMX
      ICO=ICO+1
      ITOT=IOD
      IOK=0
      GO TO 12
5000  CONTINUE
      CALL STATS(STAT,94,IMX,MEAN1,MEAN2,VAR1,VAR2,DUM1,DUM2,0)
      DO 9091 J=1,N
      OFF1(J)=MEAN1(J)
      OFF2(J)=MEAN2(J)
      AB1(J)=COM(VAR1(J))
      AB2(J)=COM(VAR2(J))
      AV1(J)=COM(MEAN1(J))
      AV2(J)=COM(MEAN2(J))
      WRITE(6,100) ANG(J),MEAN1(J),MEAN2(J),VAR1(J),VAR2(J),(STAT(L,1,J)
     1,STAT(L,2,J),L=1,IMX)
9091  CONTINUE
      IND=IND+1
      IMX=1
      GO TO 1111
9050  CONTINUE
      CALL PAPER(VALUE)
      ITOT=ITOT+1
      ISK=ISK+1
      GO TO 4049
      END
```

```
      FUNCTION COM(A)
      COM=A*10./(4096.)
      RETURN
      END

      SUBROUTINE PAPER(VALUE)
      DIMENSION LOK2(64)
      DIMENSION VALUE (2,94)
      INTEGER*2 LOOKUP (156), IBUF(100)
      INTEGER R1,R2
      COMMON /BUF/IBUF
      DATA IF/1/
      DATA IFST/0/
      NC=94
      NUM=90
      DO 1313 I=1,NU
      VALUE(1,I)=0.
      VALUE(2,I)=0.
1313  CONTINUE
      IF(IFST.NE.0) GO TO 600
      DO 13 I=1,156
   13 LOOKUP(I)=999
C INITIALIZE IBUF
      DO 12 I=1,100
   12 IBUF(I)=0
      DO 1010 II=1,100
      I=II-1
      IA=MOD(I,10)
      IB=I/10
      IND=(IB*16)+IA
C       IND=(IA*16)+IB
 1010 LOOKUP(IND+1)=I
C BUILD A/D LOOKUP TABLE
      DO 5050 III=1,2
      I1=III-1
      DO 5050 II2=1,2
      I2=II2-1
      DO 5050 II3=1,2
      I3=II3-1
      DO 5050 II4=1,2
      I4=II4-1
      DO 5050 II5=1,2
      I5=II5-1
      DO 5050 II6=1,2
      I6=II6-1
      INDX=I1*32+I2*16+I3*8+I4*4+I5*2+I6+1
      IVUE=I6*32+I5*16+I4*8+I3*4+I2*2+I1
      LOK2(INDX)=IVUE
 5050 CONTINUE
      IFST=1
600   CONTINUE
      INDEX=0
C FIND DELETES
      CALL FIND(IF)
   11 INDEX=INDEX+1
C GET THE STEP #
      IF(IGET(IF).GT.156) GO TO 6096
      INDEP=LOOKUP(IGET(IF)+1)
      IF(INDEP.EQ.INDEX) GO TO 20
C BUG SECTION
C CHECK TO SEE IF THE STEP # IS BEFORE THIS POINT
C     IF(IF.EQ.1) GO TO  70
C     DO 50 IZ=1,4
C     ITEST=IF-IZ
C     IDEP=LOOKUP(IGET(ITEST)+1)
C     IF(INDEP.NE.INDEX) GO TO 50
C     IF(LOOKUP(IGET(ITEST+5)+1).EQ.INDEX+1) GO TO 60
C  50 CONTINUE
C     GO TO 70
C  60 CONTINUE
C RESYNC
C     IF(IZ.LT.2) GO TO 71
C     VALUE(1,INDEX-1)=99999
C     IF=IF-2
C  71 VALUE (2,INDEX-1)=99999
C     IF=IF-2
C  72 GO TO 20
C CHECK TO SEE IF THE STEP # IS AFTER THIS POINT
   70 CONTINUE
C     DO 80 IZ=1,10
      DO 80 IZ=1,100
      ITEST=IF+IZ
      IF(IGET(ITEST).GT.156) GO TO 6094
      INDEP=LOOKUP(IGET(ITEST)+1)
```

```
      IF(INDEP.LT.INDEX.OR.INDEP.GT.INDEX+2) GO TO 85
      IF(IGLT(ITEST+5).GT.15)) GO TO 6094
      IF(LOOKUP(IGLT(ITEST+5)+1).EQ.INDEP+1) GO TO 90
   85 CONTINUE
   90 CONTINUE
      PRINT 91
   91 FORMAT (' I AM IN TROUBLE')
 6094 IF=ITEST
      GO TO 6096
   80 CONTINUE
C RESYNC
      INDEPP=INDEP-1
      IF(INDEPP.LE.0) GO TO 2020
      DO 91 IZ=INDEX,INDEPP
      VALUE(1,IZ)=99999
   91 VALUE(2,IZ)=99999
      INDEX=INDEP
 2020 CONTINUE
      IF=ITEST
   20 CONTINUE
C BUILD THE NUMBERS
      DO 100 I=1,2
      IF=IF+1
      IF(IGET(IF).GT.156) GO TO 6096
      IR1=MOD(IGET(IF),64)+1
      R1=LOK2(IR1)
      IF=IF+1
      IF(IGET(IF).GT.156) GO TO 6096
      IR2=MOD(IGET(IF),64)+1
      R2=LOK2(IR2)
  100 VALUE (I,INDEX)=R1*64+R2
      IF=IF+1
      IF(INDEX.NE.NO) GO TO 11
 6095 CONTINUE
      CALL FIND(IF)
      RETURN
 6096 CONTINUE
      IF(INDEX.GE.NO-2) GO TO 6095
      INDEX=0
      CALL FIND(IF)
      GO TO 11
      END

      SUBROUTINE FIND(IFF)
      IF=IFF
 9080 CONTINUE
      IF(IGET(IF).NE.255) GO TO 9090
      IF(IGET(IF+1).NE.255) GO TO 9091
 9090 CONTINUE
      IF=IF+1
      GO TO 9080
 9091 CONTINUE
      IF=IF+1
      IFF=IF
      RETURN
      END

      FUNCTION IG(I)
      INTEGER*2 IBUF(100)
      LOGICAL*1 IB(200)
      EQUIVALENCE (IBUF(1),IB(1))
      COMMON/BUF/IBUF
      DATA ISVE/0/
      NUM=90
      NUM2=NUM*2
      J=MOD(I,NUM)
      IF(J.EQ.0) J=NUM
      IF(J.NE.1) GO TO 20
      IF(I.EQ.ISVE) GO TO 20
      READ(5,10) (IB(II),II=2,NUM2,2)
   10 FORMAT(80A1)
      WRITE(6,1010) IBUF
 1010 FORMAT(2016)
   20 IG=IBUF(J)
      ISVE=I
      RETURN
      END

      SUBROUTINE GRAPH1(K,Y,N,YMAX,RFR,RFI,X)
      DIMENSION K(N),Y(N),LINE(101)
      REAL LINE,K
      DATA DOT,STAR,BLANK/'.','*',' '/
      DO 1 J=1,101
1     LINE(J)=DOT
```

```
      WRITE(6,10) REF,REFX
   10 FORMAT('1',10X,'M=',F4.2,'-IM',F4.3,5X,'K=',F4.1)
      WRITE(6,11)
   11 FORMAT('0',2X,'ANGLE',7X,'INTENSITY',5X,'.01',22X,'0.1',22X,'1.0',
     122X,'10.',22X,'100')
      WRITE (6,2) LINE
    6 FORMAT(F10.1,1PE16.7,4X,101A1)
    2 FORMAT(30X,101A1)
      DO 5 I=1,N
      IF (ABS(Y(I)) .GT. YMAX) GO TO 4
      DO 3 J=1,101
    3 LINE(J)=BLANK
      LINE(51)=DOT
      J=50.0*(Y(I)/YMAX+1.0)+1.5
      LINE(J)=STAR
      WRITE (6,6) K(I),Y(I),LINE
      GO TO 5
    4 WRITE(6,7) K(I),Y(I)
    7 FORMAT (F10.5,E16.7,5X,'OUT OF RANGE')
    5 CONTINUE
      RETURN
      END

      FUNCTION IGET(I)
      DIMENSION IBEF(10)
      DATA ISVE/0/
      DATA ILST/0/
      DATA IMAX/10/
      IF(ISVE.EQ.0) GO TO 90
      IF(I.GT.ISVE) GO TO 50
      IDP=(I-ISVE)+ILST
      IF(IDP.LT.1) GO TO 9090
      IGET=IBEF(IDP)
      ILST=IDP
      ISVE=I
      GO TO 999
   50 CONTINUE
      IDP=(I-ISVE)
      IK=ILST+IDP
      IF(IK.LE.IMAX) GO TO 60
      IDIFF=IK-IMAX
      IMUK=IMAX-IDIFF
      DO 51 J=1,IMUK
      JJ=J+IDIFF
      IBEF(J)=IBEF(JJ)
   51 CONTINUE
      DO 52 J=1,IDIFF
      JJ=J+IMUK
      IF=IF+1
      IBEF(JJ)=IG(IF)
   52 CONTINUE
      ILST=ILST+IDP-IDIFF
      IGET=IBEF(ILST)
      ISVE=I
      GO TO 999
   60 CONTINUE
      IGET=IBEF(IK)
      ILST=IK
      ISVE=I
      GO TO 999
   90 CONTINUE
      DO 99 J=1,IMAX
      IST=I-1+J
   99 IBEF(J)=IG(IST)
      IGET=IBEF(1)
      ISVE=I
      ILST=1
      IF=10
  999 CONTINUE
 1099 FORMAT(6I5)
      RETURN
 9090 CONTINUE
      WRITE(6,1099) IGET,I,ILST,IK,IMUK,ISVE
      WRITE(6,120)
  120 FORMAT(' WHAT ARE YOU DOING? I AM BOMBING MYSELF OUT ')
      CALL EXIT
      END
ING** END STATEMENT NOT PRECEDED BY A TRANSFER

      SUBROUTINE STATS(STAT,N,IMX,MEAN1,MEAN2,VAR1,VAR2,OFF1,OFF2,ISK)
      DIMENSION STAT(5,2,94),MEAN1(94),MEAN2(94),VAR1(94),VAR2(94)
      DIMENSION OFF1(94),OFF2(94)
      DIMENSION VALUE(2,94)
      REAL MEAN1,MEAN2
```

```
      IF(ISK.EQ.1) GO TO 50
      DO 90 K=1,IMX
      CALL PAPER(VALUE)
      DO 91 J=1,N
      STAT(K,1,J)=VALUE(1,J)
      STAT(K,2,J)=VALUE(2,J)
91    CONTINUE
90    CONTINUE
50    CONTINUE
      DO 92 J=1,N
      MEAN1(J)=0.
      MEAN2(J)=0.
      VAR1(J)=0.
      VAR2(J)=0.
      DO 93 K=1,IMX
      MEAN1(J)=MEAN1(J)+STAT(K,1,J)
      MEAN2(J)=MEAN2(J)+STAT(K,2,J)
93    CONTINUE
      MEAN1(J)=MEAN1(J)/FLOAT(IMX)
      MEAN2(J)=MEAN2(J)/FLOAT(IMX)
      DO 94 K=1,IMX
      VAR1(J)=(MEAN1(J)-STAT(K,1,J))**2+VAR1(J)
      VAR2(J)=(MEAN2(J)-STAT(K,2,J))**2+VAR2(J)
94    CONTINUE
      VAR1(J)=VAR1(J)/FLOAT(IMX)
      VAR2(J)=VAR2(J)/FLOAT(IMX)
      MEAN1(J)=MEAN1(J)-OFF1(J)
      MEAN2(J)=MEAN2(J)-OFF2(J)
      IF(MEAN1(J).LT.0.) MEAN1(J)=0.
      IF(MEAN2(J).LT.0.) MEAN2(J)=0.
92    CONTINUE
      RETURN
      END

      SUBROUTINE MGLLS (N,M,Y,G,W,A,YFIT,DIF,CHISQR,REDCSQ,REDCHI,IER)
C
C   MGLLS IS A GENERAL LEAST-SQUARE FIT ROUTINE WHICH DETERMINES THE
C   COEFFICIENTS A1, A2, ... , AM IN THE FUNCTION
C
C      YFIT=A1*G1(X) + A2*G2(X) + ... + AM*GM(X)
C
C   FIT TO THE INPUT ARRAY Y AT N DATA POINTS.
C
C   MGLLS PERFORMS THE SAME CALCULATION AS SUBROUTINE GLLS, WITH THE
C   FOLLOWING ADDITIONS:
C      1. WEIGHTS ARE ALLOWED AND ARE COMPULSORY.  THE ARRAY W IS USED
C         TO WEIGHT THE DATA.  FOR AN UNWEIGHTED FIT, W MUST CONSIST
C         OF ALL ONES.
C      2. THE FUNCTIONS YFIT,DIF,CHISQR,REDCSQ,REDCHI ARE CALCULATED AS
C         DESCRIBED BELOW.
C
C   G IS AN INPUT ARRAY GIVEN BY  G(J,K)=GJ(X(K)); I.E. G(J,K) IS
C   THE JTH FUNCTION GJ IN THE ABOVE EXPRESSION FOR YFIT, EVALUATED AT
C   THE KTH GRID POINT X(K).  (NOTE THAT X ITSELF IS NOT NEEDED AS
C   AN INPUT.)
C
      REAL Y(N),G(M,N),W(N),A(M),YFIT(N),DIF(N),FD(625)
C
C   INPUTS--
C     N: NUMBER OF DATA POINTS TO BE FIT.
C     M: NUMBER OF COEFFICIENTS TO BE DETERMINED (M.LE.N; M.LE.25)
C     Y: N-ELEMENT ARRAY CONTAINING Y-VALUES OF THE DATA TO BE FIT.
C     G: (M,N)-ELEMENT ARRAY OF FITTING FUNCTIONS, DESCRIBED ABOVE.
C     W: N-ELEMENT ARRAY OF INPUT WIEGHTS.  THIS ROUTINE MINIMIZES
C        THE FUNCTION:  SUM(W*(F-Y)**2).
C
C   OUTPUTS--
C     A: M-ELEMENT ARRAY OF COEFFICIENTS
C     YFIT: N-ELEMENT ARRAY CONTAINING THE VALUES OF THE FUNCTION
C       YFIT=SUM(A*G)
C     DIF:  N-ELEMENT ARRAY WITH ERROR VALUES, Y-YFIT.
C     CHISQR: CHI SQUARE -- SUM(W*(YFIT-Y)**2)
C     REDCSQ: REDUCED CHI SQUARE -- CHISQR/(N-M)
C     REDCHI: REDUCED CHI -- SQRT(REDCSQ)
C     IER: ERROR INDICATOR--
C       IER=0: NORMAL TERMINATION.
C       IER=1: SINGULAR MATRIX RETURNED FROM SIMQ.  PROBABLE CAUSE:
C         FUNCTIONS G1, G2, ... , GM USED TO GENERATE G ARE NOT
C         LINEARLY INDEPENDENT.
C       IER=2: M TOO BIG
C
C   SUBPROGRAMS CALLED:
C     SIMQ: IBM SCIENTIFIC SUBROUTINE
```

```
      IF (P.GT.25) GO TO 999
      DO 10 K=1,N
      A(K)=0.
      DO 10 J=1,N
10    A(K)=A(K)+W(J)*Y(J)*G(K,J)
      DO 30 I=1,N
      DO 30 J=1,P
      SUM=0.
      DO 20 K=1,N
20    SUM=SUM+W(K)*G(I,K)*G(J,K)
30    FD((I-1)*M+J)=SUM
      CALL SIMQ(FD,A,N,IER)
      IF (IER.NE.0) RETURN
      CHISQR=0.
      DO 50 I=1,N
      YFIT(I)=0.
      DO 40 J=1,N
40    YFIT(I)=YFIT(I)+A(J)*G(J,I)
      DIF(I)=Y(I)-YFIT(I)
50    CHISQR=CHISQR+W(I)*DIF(I)*DIF(I)
      IF (N.NE.M) REDCSQ=CHISQR/(N-M)
      IF (N.EQ.M) REDCSQ=1.
      REDCHI=SQRT(REDCSQ)
      RETURN
999   IER=2
      RETURN
      END
C                                                                     SIMQ  10
C     .................................................................SIMQ  20
C                                                                     SIMQ  30
C        SUBROUTINE SIMQ                                              SIMQ  40
C                                                                     SIMQ  50
C        PURPOSE                                                      SIMQ  60
C           OBTAIN SOLUTION OF A SET OF SIMULTANEOUS LINEAR EQUATIONS.SIMQ  70
C           AX=B                                                      SIMQ  80
C                                                                     SIMQ  90
C        USAGE                                                        SIMQ 100
C           CALL SIMQ(A,B,N,KS)                                       SIMQ 110
C                                                                     SIMQ 120
C        DESCRIPTION OF PARAMETERS                                    SIMQ 130
C           A - MATRIX OF COEFFICIENTS STORED COLUMNWISE.  THESE ARE   SIMQ 140
C               DESTROYED IN THE COMPUTATION.  THE SIZE OF MATRIX A IS SIMQ 150
C               N BY N.                                               SIMQ 160
C           B - VECTOR OF ORIGINAL CONSTANTS (LENGTH N). THESE ARE    SIMQ 170
C               REPLACED BY FINAL SOLUTION VALUES, VECTOR X.          SIMQ 180
C           N - NUMBER OF EQUATIONS AND VARIABLES. N MUST BE .GT. ONE.SIMQ 190
C           KS - OUTPUT DIGIT                                         SIMQ 200
C                0 FOR A NORMAL SOLUTION                              SIMQ 210
C                1 FOR A SINGULAR SET OF EQUATIONS                    SIMQ 220
C                                                                     SIMQ 230
C        REMARKS                                                      SIMQ 240
C           MATRIX A MUST BE GENERAL.                                 SIMQ 250
C           IF MATRIX IS SINGULAR , SOLUTION VALUES ARE MEANINGLESS.  SIMQ 260
C           AN ALTERNATIVE SOLUTION MAY BE OBTAINED BY USING MATRIX   SIMQ 270
C           INVERSION (MINV) AND MATRIX PRODUCT (GMPRD).              SIMQ 280
C                                                                     SIMQ 290
C        SUBROUTINES AND FUNCTION SUBPROGRAMS REQUIRED                SIMQ 300
C           NONE                                                      SIMQ 310
C                                                                     SIMQ 320
C                                                                     SIMQ 330
C        METHOD                                                       SIMQ 340
C           METHOD OF SOLUTION IS BY ELIMINATION USING LARGEST PIVOTAL SIMQ 350
C           DIVISOR. EACH STAGE OF ELIMINATION CONSISTS OF INTERCHANGINGSIMQ 360
C           ROWS WHEN NECESSARY TO AVOID DIVISION BY ZERO OR SMALL    SIMQ 370
C           ELEMENTS.                                                 SIMQ 380
C           THE FORWARD SOLUTION TO OBTAIN VARIABLE N IS DONE IN      SIMQ 390
C           N STAGES. THE BACK SOLUTION FOR THE OTHER VARIABLES IS    SIMQ 400
C           CALCULATED BY SUCCESSIVE SUBSTITUTIONS. FINAL SOLUTION    SIMQ 410
C           VALUES ARE DEVELOPED IN VECTOR B, WITH VARIABLE 1 IN B(1),SIMQ 420
C           VARIABLE 2 IN B(2),.....,VARIABLE N IN B(N).              SIMQ 430
C           IF NO PIVOT CAN BE FOUND EXCEEDING A TOLERANCE OF 0.0,    SIMQ 440
C           THE MATRIX IS CONSIDERED SINGULAR AND KS IS SET TO 1. THIS SIMQ 450
C           TOLERANCE CAN BE MODIFIED BY REPLACING THE FIRST STATEMENT.SIMQ 460
C                                                                     SIMQ 470
C     .................................................................SIMQ 480
C                                                                     SIMQ 490
      SUBROUTINE SIMQ(A,B,N,KS)                                       SIMQ 500
      DIMENSION A(1),B(1)                                             SIMQ 510
C                                                                     SIMQ 520
C        FORWARD SOLUTION                                             SIMQ 530
C                                                                     SIMQ 540
      TOL=0.0                                                         SIMQ 550
      KS=0                                                            SIMQ 560
      JJ=-N                                                           SIMQ 570
```

```
      DO 65 J=1,N                                                    SIMQ 570
      JY=J+1                                                         SIMQ 580
      JJ=JJ+N+1                                                      SIMQ 590
      BIGA=0                                                         SIMQ 600
      IT=JJ-J                                                        SIMQ 610
      DO 20 I=J,N                                                    SIMQ 620
C                                                                    SIMQ 630
C        SEARCH FOR MAXIMUM COEFFICIENT IN COLUMN                    SIMQ 640
C                                                                    SIMQ 650
      IJ=IT+I                                                        SIMQ 660
      IF(ABS(BIGA)-ABS(A(IJ))) 20,30,30                              SIMQ 670
   20 BIGA=A(IJ)                                                     SIMQ 680
      IMAX=I                                                         SIMQ 690
   30 CONTINUE                                                       SIMQ 700
C                                                                    SIMQ 710
C        TEST FOR PIVOT LESS THAN TOLERANCE (SINGULAR MATRIX)        SIMQ 720
C                                                                    SIMQ 730
      IF(ABS(BIGA)-TOL) 35,35,40                                     SIMQ 740
   35 KS=1                                                           SIMQ 750
      RETURN                                                         SIMQ 760
C                                                                    SIMQ 770
C        INTERCHANGE ROWS IF NECESSARY                               SIMQ 780
C                                                                    SIMQ 790
   40 I1=J+N*(J-2)                                                   SIMQ 800
      IT=IMAX-J                                                      SIMQ 810
      DO 50 K=J,N                                                    SIMQ 820
      I1=I1+N                                                        SIMQ 830
      I2=I1+IT                                                       SIMQ 840
      SAVE=A(I1)                                                     SIMQ 850
      A(I1)=A(I2)                                                    SIMQ 860
      A(I2)=SAVE                                                     SIMQ 870
C                                                                    SIMQ 880
C        DIVIDE EQUATION BY LEADING COEFFICIENT                      SIMQ 890
C                                                                    SIMQ 900
   50 A(I1)=A(I1)/BIGA                                               SIMQ 910
      SAVE=B(IMAX)                                                   SIMQ 920
      B(IMAX)=B(J)                                                   SIMQ 930
      B(J)=SAVE/BIGA                                                 SIMQ 940
C                                                                    SIMQ 950
C        ELIMINATE NEXT VARIABLE                                     SIMQ 960
C                                                                    SIMQ 970
      IF(J-N) 55,70,55                                               SIMQ 980
   55 IQS=N*(J-1)                                                    SIMQ 990
      DO 65 IX=JY,N                                                  SIMQ1000
      IXJ=IQS+IX                                                     SIMQ1010
      IT=J-IX                                                        SIMQ1020
      DO 60 JX=JY,N                                                  SIMQ1030
      IXJX=N*(JX-1)+IX                                               SIMQ1040
      JJX=IXJX+IT                                                    SIMQ1050
   60 A(IXJX)=A(IXJX)-(A(IXJ)*A(JJX))                                SIMQ1060
   65 B(IX)=B(IX)-(B(J)*A(IXJ))                                      SIMQ1070
C                                                                    SIMQ1080
C        BACK SOLUTION                                               SIMQ1090
C                                                                    SIMQ1100
   70 NY=N-1                                                         SIMQ1110
      IT=N*N                                                         SIMQ1120
      DO 80 J=1,NY                                                   SIMQ1130
      IA=IT-J                                                        SIMQ1140
      IB=N-J                                                         SIMQ1150
      IC=N                                                           SIMQ1160
      DO 80 K=1,J                                                    SIMQ1170
      B(IB)=B(IB)-A(IA)*B(IC)                                        SIMQ1180
      IA=IA-N                                                        SIMQ1190
   80 IC=IC-1                                                        SIMQ1200
      RETURN                                                         SIMQ1210
      END                                                            SIMQ1220

$ENTRY
```

APPENDIX V

THEORETICAL MIE PROGRAM

```
      DIMENSION STHETD(101),SELTRM(4,101),POL1(101),POL2(101),U(101)
      DIMENSION PINT1(101),PINT2(101)
      DIMENSION ELT1(101),ELT2(101),ELO1(101),ELO2(101)
      REAL*8 X,RFR,RFI,THETD(100),QEXT,QSCAT,CTBROS,ELTRMX(4,100,2)
      RFR=1.592
      RFI=0.000
      PI=3.14159265358979323846
      READ(5,200) PM,E,D
  200 FORMAT(3F10.6)
      DO 100 I=1,101
      ELO1(I)=0.
      ELO2(I)=0.
  100 CONTINUE
      DO 7 N=1,101
    7 STHETD(N)=-1.8+N*1.8
      DO 8 N=1,51
    8 THETD(N)=STHETD(N)
      DO 25 KK=1,17
      READ(5,250) P
  250 FORMAT(F10.6)
      Y=EXP(-((P-PM)/E)**2/2)
      X=PI*D/P
      CALL DBMIE (X,RFR,RFI,THETD,51,QEXT,QSCAT,CTBROS,ELTRMX)
      DO 9 J=1,51
      DO 9 I=1,4
    9 SELTRM(I,J)=ELTRMX(I,J,1)
      DO 10 J=1,50
      JJ=51-J
      DO 10 I=1,4
   10 SELTRM(I,51+J)=ELTRMX(I,JJ,2)
      DO 30 K=1,101
      ELT1(K)=Y*SELTRM(1,K)
      ELT2(K)=Y*SELTRM(2,K)
      ELO1(K)=ELO1(K)+ELT1(K)
      ELO2(K)=ELO2(K)+ELT2(K)
   30 CONTINUE
   25 CONTINUE
      DO 20 K=1,101
      U(K)=STHETD(K)*PI/180.
      POL1(K)=(ELO1(K)*COS(U(K))+ELO2(K)*SIN(U(K)))**2
      POL2(K)=(ELO2(K)*COS(U(K))-ELO1(K)*SIN(U(K)))**2
   20 CONTINUE
      DO 21 K=1,101
      PINT1(K)=ALOG10(POL1(K))
   21 PINT2(K)=ALOG10(POL2(K))
      CALL GRAPH1(STHETD,PINT1,101,10.0,RFR,RFI,X)
      CALL GRAPH1(STHETD,PINT2,101,10.0,RFR,RFI,X)
      STOP
      END
```

```
      SUBROUTINE DEMIE (X,RFR,RFI,THETD,JX,QEXT,QSCAT,CTBROS,ELTRMX)     DBMIE001
C     SUBROUTINE FOR COMPUTING THE PARAMETERS OF THE ELECTROMAGNETIC     DBMIE002
C     COMPUTATIONS IN DOUBLE PRECISION ARITHMETIC.                       DBMIE004
C     THIS SUBROUTINE COMPUTES THE CAPITAL A FUNCTION BY MAKING USE OF   DBMIE005
C     DOWNWARD RECURRENCE RELATIONSHIP.                                  DBMIE006
C     X : SIZE PARAMETER OF THE SPHERE,( 2 * PI * RADIUS OF THE SPHERE)/DBMIE007
C     WAVELENGTH OF THE INCIDENT RADIATION).                             DBMIE008
C     RF: REFRACTIVE INDEX OF THE MATERIAL OF THE SPHERE.COMPLEX         DBMIE009
C     QUANTITY..FORM: ( RFR  -  I * RFI )                                DBMIE010
C     THETD(J): ANGLE IN DEGREES BETWEEN THE DIRECTIONS OF THE INCIDENT  DBMIE011
C     AND THE SCATTERED RADIATION. THETD(J) IS < OR = 90.0               DBMIE012
C     IF THETD(J) SHOULD HAPPEN TO BE GREATER THAN 90.0, ENTER WITH      DBMIE013
C     SUPPLEMENTARY VALUE; SEE COMMENTS BELOW ON ELTRMX..                DBMIE014
C     JX: TOTAL NUMBER  OF THETD FOR WHICH THE COMPUTATIONS ARE          DBMIE015
C     REQUIRED. JX SHOULD NOT EXCEED 100 UNLESS THE DIMENSIONS           DBMIE016
C     STATEMENTS ARE APPROPRIATELY MODIFIED.                             DBMIE017
C     MAIN PROGRAM SHOULD ALSO HAVE REAL*8 THETD(100),ELTRMX(4,100,2).   DBMIE018
C     THE DEFINITIONS FOR THE FOLLOWING SYMBOLS CAN BE FOUND IN ' LIGHT  DBMIE019
C     SCATTERING BY SMALL PARTICLES.H.C. VAN DE HULST. JOHN WILEY & SONSDBMIE020
C     . INC.. NEW YORK. 1957 ' .                                         DBMIE021
C     QEXT: EFFIECIENCY FACTOR FOR EXTINCTION.VAN DE HULST.P.14 & 127.   DBMIE022
C     QSCAT: EFFIECIENCY FACTOR FOR SCATTERING.VAN DE HULST.P.14 & 127.  DBMIE023
C     CTBROS: AVERAGE(COSINE THETA) * QSCAT.VAN DE HULST.P.128.          DBMIE024
C     ELTRMX(I,J,K): ELEMENTS OF THE TRANSFORMATION MATRIX F.VAN DE HUL  DBMIE025
C     ST,P.34,45 & 125. I = 1: ELEMENT M SUB 2..I = 2: ELEMENT M SUB 1..DBMIE026
C     I = 3: ELEMENT S SUB 21.. I = 4: ELEMENT D SUB 21..                DBMIE027
C     ELTRMX(I,J,1) REPRESENTS THE ITH ELEMENT OF THE MATRIX FOR         DBMIE028
C     THE ANGLE THETD(J).. ELTRMX(I,J,2) REPRESENTS THE ITH ELEMENT      DBMIE029
C     OF THE MATRIX FOR THE ANGLE 180.0 - THETD(J) ..                    DBMIE030
    5 FORMAT(T10,' THE VALUE OF THE SCATTERING ANGLE IS GREATER THAN     DBMIE031
     1 90.0 DEGREES. IT IS ',D15.4)                                      DBMIE032
    6 FORMAT (//T10,' PLEASE READ COMMENTS.'//)                          DBMIE033
    7 FORMAT(//T10,'THE VALUE OF THE ARGUMENT JX IS GREATER THAN 100')   DBMIE034
    8 FORMAT(//T10,'THE UPPER LIMIT FOR ACAP IS NOT ENOUGH. SUGGEST GET  DBMIE035
     1DETAILED OUTPUT AND MODIFY SUBROUTINE'//)                          DBMIE036
      REAL*8 X,PX,RFR,RFI,QEXT,QSCAT,T(5),TA(4),TB(2),TC(2)              DBMIE037
      REAL*8 TD(2),TE(2),CTBROS                                          DBMIE038
      REAL*8 ELTRMX(4,100,2),PI(3,100),TAU(3,100),CSTHT(100),SI2THT(100)DBMIE039
     1,THETD(100)                                                        DBMIE040
      COMPLEX*16 RF,RRF,RRFX,WM1,FNA,FNB,TC1,TC2,WFN(2),ACAP(7000)       DBMIE041
      COMPLEX*16 FNAP,FNBP                                               DBMIE042
C     TA(1): REAL PART OF WFN(1).. TA(2): IMAGINARY PART OF WFN(1)..     DBMIE043
C     TA(3): REAL PART OF WFN(2)..TA(4): IMAGINARY PART OF WFN(2).       DBMIE044
C     TB(1): REAL PART OF FNA.. TB(2): IMAGINARY PART OF FNA..           DBMIE045
C     TC(1): REAL PART OF FNB.. TC(2): IMAGINATRY PART OF FNB..          DBMIE046
C     TD(1): REAL PART OF FNAP..TD(2) IMAGINARY PART OF FNAP.            DBMIE047
C     TE(1): REAL PART OF FNBP.. TE(2): IMAGINARY PART OF FNBP.          DBMIE048
C     FNAP & FNBP ARE THE PRECEDING VALUES OF FNA & FNB RESPECTIVELY.    DBMIE049
      EQUIVALENCE (WFN(1),TA(1)),(FNA,TB(1)),(FNB,TC(1))                 DBMIE050
      EQUIVALENCE(FNAP,TD(1)),(FNBP,TE(1))                               DBMIE051
      IF ( JX .LE. 100 ) GO TO 20                                        DBMIE052
      WRITE(6,7)                                                         DBMIE053
      WRITE(6,6)                                                         DBMIE054
      CALL EXIT                                                          DBMIE055
   20 RF  = DCMPLX(RFR,-RFI)                                             DBMIE056
      RRF = 1.0D0/RF                                                     DBMIE057
      PX = 1.0D0/X                                                       DBMIE059
      RRFX = RRF * PX                                                    DBMIE059
      T(1) = (X**2)*(RFR**2 + RFI**2)                                    DBMIE060
      T(1) = DSQRT(T(1))                                                 DBMIE061
      NMX = 1.10D0 * T(1)                                                DBMIE062
      IF ( NMX1 .LE. 6999 ) GO TO 21                                     DBMIE063
      WRITE(6,8)                                                         DBMIE064
      CALL EXIT                                                          DBMIE065
   21 NMX2 = T(1)                                                        DBMIE066
      IF ( NMX1  .GT. 150 ) GO TO 22                                     DBMIE067
      NMX1 = 150                                                         DBMIE068
```

```
      NMX2 = 135                                                        DBMIE069
   22 ACAP(NMX1 + 1 ) = ( 0.0D0, 0.0D0 )                                DBMIE070
      DO 23 N = 1,NMX1                                                  DBMIE071
      NN = NMX1 - N + 1                                                 DBMIE072
      ACAP(NN) = (NN+1) * RRFX - 1.0D0/((NN+1)*RRFX + ACAP(NN+1))       DBMIE073
   23 CONTINUE                                                          DBMIE074
      DO 30 J = 1,JX                                                    DBMIE075
      IF ( THETD(J) .LT. 0.0D0 ) THETD(J) = DABS(THETD(J))              DBMIE076
      IF ( THETD(J) .GT. 0.0D0 ) GO TO 24                               DBMIE077
      CSTHT(J) = 1.0D0                                                  DBMIE078
      SI2THT(J) = 0.0D0                                                 DBMIE079
      GO TO 30                                                          DBMIE080
   24 IF ( THETD(J) .GE. 90.0D0 ) GO TO 25                              DBMIE081
      T(1) = ( 3.1415926535897932 * THETD(J))/180.0D0                   DBMIE082
      CSTHT(J) = DCOS(T(1))                                             DBMIE083
      SI2THT(J) = 1.0D0 - CSTHT(J)**2                                   DBMIE084
      GO TO 30                                                          DBMIE085
   25 IF ( THETD(J) .GT. 90.0D0 ) GO TO 28                              DBMIE086
      CSTHT(J) = 0.0D0                                                  DBMIE087
      SI2THT(J) = 1.0D0                                                 DBMIE088
      GO TO 30                                                          DBMIE089
   28 WRITE(6,5) THETD(J)                                               DBMIE090
      WRITE(6,6)                                                        DBMIE091
      CALL EXIT                                                         DBMIE092
   30 CONTINUE                                                          DBMIE093
      DO 35 J = 1,JX                                                    DBMIE094
      PI(1,J) = 0.0D0                                                   DBMIE095
      PI(2,J) = 1.0D0                                                   DBMIE096
      TAU(1,J) = 0.0D0                                                  DBMIE097
      TAU(2,J) = CSTHT(J)                                               DBMIE098
   35 CONTINUE                                                          DBMIE099
      T(1) = DCOS(X)                                                    DBMIE100
      T(2) = DSIN(X)                                                    DBMIE101
      WM1 = DCMPLX( T(1),-T(2))                                         DBMIE102
      WFN(1) = DCMPLX(T(2),T(1))                                        DBMIE103
      WFN(2) = RX * WFN(1) - WM1                                        DBMIE104
      TC1 = ACAP(1) * RRF + RX                                          DBMIE105
      TC2 = ACAP(1) * RF + RX                                           DBMIE106
      FNA = (TC1*TA(3) - TA(1))/(TC1*WFN(2) - WFN(1))                   DBMIE107
      FNB = ( TC2*TA(3) - TA(1))/(TC2 * WFN(2) - WFN(1))                DBMIE109
      FNAP = FNA                                                        DBMIE109
      FNBP = FNB                                                        DBMIE110
      T(1) = 1.50D0                                                     DBMIE111
C     FROM HERE TO THE STATEMENT NUMBER 90, ELTRMX(I,J,K) HAS THE       DBMIE112
C     FOLLOWING MEANING:                                                DBMIE113
C     ELTRMX(1,J,K): REAL PART OF THE FIRST COMPLEX AMPLITUDE.          DBMIE114
C     ELTRMX(2,J,K): IMAGINARY PART  OF THE FIRST COMPLEX AMPLITUDE.    DBMIE115
C     ELTRMX(3,J,K): REAL PART OF THE SECOND COMPLEX AMPLITUDE.         DBMIE116
C     ELTRMX(4,J,K): IMAGINARY PART OF THE SECOND COMPLEX AMPLITUDE.    DBMIE117
C     K = 1 : FOR THETD(J) AND K = 2 : FOR 180.0 - THETD(J)             DBMIE118
C     DEFINITION OF THE COMPLEX AMPLITUDE: VAN DE HULST,P.125.          DBMIE119
      TB(1) = T(1) * TB(1)                                              DBMIE120
      TB(2) = T(1) * TB(2)                                              DBMIE121
      TC(1) = T(1) * TC(1)                                              DBMIE122
      TC(2) = T(1) * TC(2)                                              DBMIE123
      DO 60 J = 1,JX                                                    DBMIE124
      ELTRMX(1,J,1) = TB(1) * PI(2,J) + TC(1) * TAU(2,J)                DBMIE125
      ELTRMX(2,J,1) = TB(2) * PI(2,J) + TC(2) * TAU(2,J)                DBMIE126
      ELTRMX(3,J,1) = TC(1) * PI(2,J) + TB(1) * TAU(2,J)                DBMIE127
      ELTRMX(4,J,1) = TC(2) * PI(2,J) + TB(2) * TAU(2,J)                DBMIE128
      ELTRMX(1,J,2) = TB(1) * PI(2,J) - TC(1) * TAU(2,J)                DBMIE129
      ELTRMX(2,J,2) = TB(2) * PI(2,J) - TC(2) * TAU(2,J)                DBMIE130
      ELTRMX(3,J,2) = TC(1) * PI(2,J) - TB(1) * TAU(2,J)                DBMIE131
      ELTRMX(4,J,2) = TC(2) * PI(2,J) - TB(2) * TAU(2,J)                DBMIE132
   60 CONTINUE                                                          DBMIE133
      QEXT = 2.0D0 * ( TB(1) + TC(1))                                   DBMIE134
      QSCAT =(TB(1)**2 + TB(2)**2 + TC(1)**2 + TC(2)**2)/0.75D0         DBMIE135
      CTBRQS = 0.0D0                                                    DBMIE136
      N = 2                                                             DBMIE137
   65 T(1) = 2*N - 1                                                    DBMIE138
      T(2) = N - 1                                                      DBMIE139
      T(3) = 2 * N + 1                                                  DBMIE140
```

```
      DO 70 J = 1,JX                                                    DBMIE141
      PI(3,J) = (T(1)*PI(2,J)*CSTHT(J)-N*PI(1,J))/T(2)                  DBMIE142
      TAU(3,J) = CSTHT(J)*(PI(3,J)-PI(1,J))-T(1)*SI2THT(J)*PI(2,J)+     DBMIE143
     1 TAU(1,J)                                                         DBMIE144
   70 CONTINUE                                                          DBMIE145
      WM1 = WFN(1)                                                      DBMIE146
      WFN(1) = WFN(2)                                                   DBMIE147
      WFN(2) = T(1)*RX*WFN(1) - WM1                                     DBMIE148
      TC1 = ACAP(N)*RRF + N*RX                                          DBMIE149
      TC2 = ACAP(N)*RF + N*RX                                           DBMIE150
      FNA = (TC1*TA(3)-TA(1))/(TC1*WFN(2) - WFN(1))                     DBMIE151
      FNB = (TC2*TA(3)-TA(1))/(TC2*WFN(2) - WFN(1))                     DBMIE152
      T(5) = N                                                          DBMIE153
      T(4) = T(1)/(T(5)*T(2))                                           DBMIE154
      T(2) = (T(2)*(T(5) + 1.0D0))/T(5)                                 DBMIE155
      CTBRQS = CTBRQS + T(2)*(TD(1)*TB(1) + TD(2)*TB(2) + TE(1)*TC(1) + DBMIE156
     1 TE(2)*TC(2)) + T(4)*(TD(1)*TE(1) + TD(2)*TE(2))                  DBMIE157
      QEXT = QEXT + T(3)*(TB(1)+TC(1))                                  DBMIE158
      T(4) = TB(1)**2 + TB(2)**2 + TC(1)**2 + TC(2)**2                  DBMIE159
      QSCAT = QSCAT + T(3) *T(4)                                        DBMIE160
      T(2) = N*(N+1)                                                    DBMIE161
      T(1) = T(3)/T(2)                                                  DBMIE162
      K = (N/2)*2                                                       DBMIE163
      DO 80 J = 1,JX                                                    DBMIE164
      ELTRMX(1,J,1)=ELTRMX(1,J,1)+T(1)*(TB(1)*PI(3,J)+TC(1)*TAU(3,J))   DBMIE165
      ELTRMX(2,J,1)=ELTRMX(2,J,1)+T(1)*(TB(2)*PI(3,J)+TC(2)*TAU(3,J))   DBMIE166
      ELTRMX(3,J,1)=ELTRMX(3,J,1)+T(1)*(TC(1)*PI(3,J)+TB(1)*TAU(3,J))   DBMIE167
      ELTRMX(4,J,1)=ELTRMX(4,J,1)+T(1)*(TC(2)*PI(3,J)+TB(2)*TAU(3,J))   DBMIE168
      IF ( K .EQ. N ) GO TO 75                                          DBMIE169
      ELTRMX(1,J,2)=ELTRMX(1,J,2)+T(1)*(TB(1)*PI(3,J)-TC(1)*TAU(3,J))   DBMIE170
      ELTRMX(2,J,2)=ELTRMX(2,J,2)+T(1)*(TB(2)*PI(3,J)-TC(2)*TAU(3,J))   DBMIE171
      ELTRMX(3,J,2)=ELTRMX(3,J,2)+T(1)*(TC(1)*PI(3,J)-TB(1)*TAU(3,J))   DBMIE172
      ELTRMX(4,J,2)=ELTRMX(4,J,2)+T(1)*(TC(2)*PI(3,J)-TB(2)*TAU(3,J))   DBMIE173
      GO TO 80                                                          DBMIE174
   75 ELTRMX(1,J,2)=ELTRMX(1,J,2)+T(1)*(-TB(1)*PI(3,J)+TC(1)*TAU(3,J))  DBMIE175
      ELTRMX(2,J,2)=ELTRMX(2,J,2)+T(1)*(-TB(2)*PI(3,J)+TC(2)*TAU(3,J))  DBMIE176
      ELTRMX(3,J,2)=ELTRMX(3,J,2)+T(1)*(-TC(1)*PI(3,J)+TB(1)*TAU(3,J))  DBMIE177
      ELTRMX(4,J,2)=ELTRMX(4,J,2)+T(1)*(-TC(2)*PI(3,J)+TB(2)*TAU(3,J))  DBMIE178
   80 CONTINUE                                                          DBMIE179
      IF( T(4) .LT. 1.0D-14 ) GO TO 100                                 DBMIE180
      N = N + 1                                                         DBMIE181
      DO 90 J = 1,JX                                                    DBMIE182
      PI(1,J) = PI(2,J)                                                 DBMIE183
      PI(2,J) = PI(3,J)                                                 DBMIE184
      TAU(1,J) = TAU(2,J)                                               DBMIE185
      TAU(2,J) = TAU(3,J)                                               DBMIE186
   90 CONTINUE                                                          DBMIE187
      FNAP = FNA                                                        DBMIE188
      FNBP = FNB                                                        DBMIE189
      IF ( N .LE. NMX2 ) GO TO 65                                       DBMIE190
      WRITE(6,8 )                                                       DBMIE191
      CALL EXIT                                                         DBMIE192
  100 DO 120 J = 1, JX                                                  DBMIE193
      DO 120 K = 1,2                                                    DBMIE194
      DO 115 I = 1,4                                                    DBMIE195
      T(I) = ELTRMX(I,J,K)                                              DBMIE196
  115 CONTINUE                                                          DBMIE197
      ELTRMX(2,J,K) = T(1)**2 + T(2)**2                                 DBMIE198
      ELTRMX(1,J,K) = T(3)**2 + T(4)**2                                 DBMIE199
      ELTRMX(3,J,K) = T(1)*T(3) + T(2)*T(4)                             DBMIE200
      ELTRMX(4,J,K) = T(2)*T(3) - T(4)*T(1)                             DBMIE201
  120 CONTINUE                                                          DBMIE202
      T(1) = 2.0D0 * NMX**2                                             DBMIE203
      QEXT = QEXT * T(1)                                                DBMIE204
      QSCAT = QSCAT * T(1)                                              DBMIE205
      CTBRQS = 2.0D0 * CTBRQS * T(1)                                    DBMIE206
C     THE DETAILS ABOUT THIS SUBROUTINE CAN BE FOUND IN THE FOLLOWING   DBMIE207
C     REPORT: ' SUBROUTINES FOR COMPUTING THE PARAMETERS OF THE         DBMIE208
C     ELECTROMAGNETIC RADIATION SCATTERED BY A SPHERE ' J.V. DAVE.      DBMIE209
C     I B M SCIENTIFIC CENTER, PALO ALTO , CALIFORNIA.                  DBMIE210
C     REPORT NO. 320 - 3236 .. MAY 1968 ..                              DBMIE211
      RETURN                                                            DBMIE212
```

APPENDIX VI

VOLUMETRIC CORRECTION

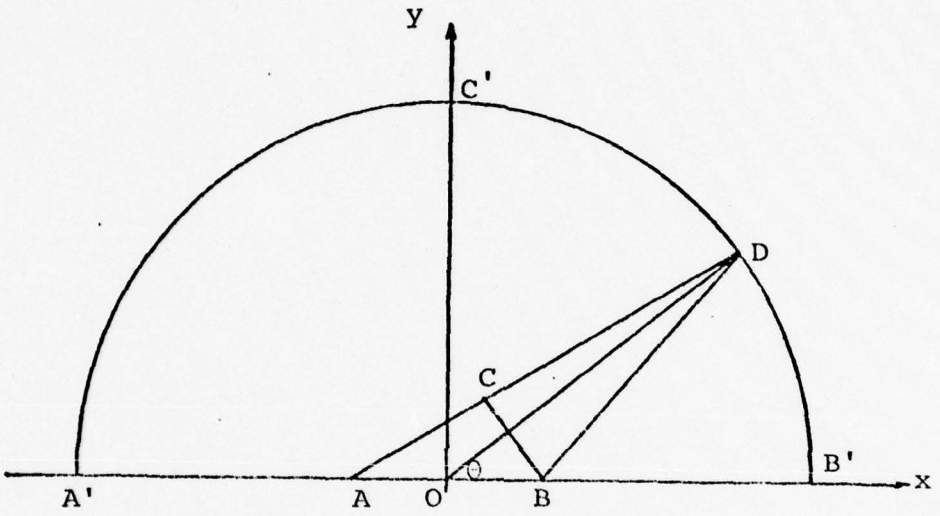

The figure given above represents the scattering geometry. The direction of incident laser light is + x, and the direction of flow of the aerosol particles is + y. Aerosols enter the chamber through a circular opening of diameter AB. They get hit by the laser beam in the interaction region AB. The scattered light is then collected by the semicircular arrangement of mirrors A'C'B'. The incident light is focused at the interaction region. The radius of the light beam is negligible compared to its length. Therefore the problem reduces to a cross sectional area rather than volume. The effective area observed by the

mirror at D is CB. In order to find this we find the equations for the line CB and AB, and intersect them to find the coordinates of C and B.

The length of AB = L

$\therefore$ AO = OB = L/2

OD = R

Angle DOB = θ

Equation of CB:

$$y = -\frac{1}{\tan\theta}\, x + \frac{L/2}{\tan\theta} \qquad (1)$$

Since its slope is $-1/\tan$ because CB is perpendicular to OD. Then, finding the slope for AD, we get:

$$m_{AD} = \frac{R\sin\theta}{R\cos\theta + L/2}$$

Equation of AD:

$$y = \frac{R\sin\theta}{R\cos\theta + L/2} + \frac{(L/2)R\sin\theta}{R\cos\theta + L/2} \qquad (2)$$

Intersecting 1 and 2, we get the coordinates of point C:

$$x_C = L/2\, \frac{(2R\sin^2\theta - R - (L/2)\cos\theta)}{R + (L/2)\cos\theta}$$

$$y_C = L\, \frac{\cos}{\sin}\, \frac{R\sin^2\theta - R - (L/2)\cos\theta}{R + (L/2)\cos\theta}$$

Equation of the line BD is

$$y = \frac{R\sin\theta}{R\cos\theta - L/2}\, x - \frac{L/2\ \sin\theta}{R\cos\theta - L/2}$$

Coordinates of point B is then:

$$x_B = L/2$$

$$y_B = 0$$

Using the distance formula

$$D = \sqrt{(x_B - x_C)^2 + (y_B - y_C)^2}$$

we get

$$D = L \frac{\cos\theta}{\sin\theta} \frac{R\cos\theta + L/2}{R + (L/2)\cos\theta}$$

At this point because of the relative gain factor to be used we can take the problem as a volumetric one, then the effective volume is

$$V_e = \pi r^2 D$$

r being the radius of laser beam.

Relative volume ratio is taken to be V_e/V_{max}

where $V_{max} = \pi r^2 L$

Therefore the volume ratio G(θ) is:

$$G_1(\theta) = \frac{\cos}{\sin} \frac{R\cos\theta + L/2}{R + (L/2)\cos\theta}$$

Assuming R >> L

$$G_1(\theta) = \frac{\cos^2\theta}{\sin\theta}$$

In addition to this, due to the charging of the particle and the cross sectional effects we have an arbitrary correction of N(θ) which is the number of light particles (photons) scattered into a unit area at angle θ [26]

$$N(\theta) = k/R^2 \sin^4(\theta/2)$$

K is an arbitrary constant which depends on the charge and the kinetic energy of the particle. Therefore our correction factor becomes:

$$G(\theta) = K \frac{\cos\theta}{\sin\theta} \frac{R\cos\theta + L/2}{R + (L/2)\cos\theta} / (R^2 \sin^4(\theta/2))$$

A graph of this function is given in Fig. A VI-1.

Fig. A VI-1 The log intensity versus scattering angle graph of the volumetric correction factor, treated as angular gain.

APPENDIX VII

SCATTERING EXPECTATIONS

There are a few variables that enable us to calculate the expected scattering values, and compare them with the real data points. They are actually the basic considerations of our experimental system design. Aside from several other factors that effect the measured values like the coagulation of particles, multiple scattering and variation of number of particles in the scattering region, an approximate estimation of the first order can be done by using the quantities listed below:

1 - laser output power and bandwidth,

2 - # particles in interaction region and their velocities,

3 - The angular resolution and the attenuation of light due to mirror reflections and the glan air prism,

4 - Photomultiplier gain,

5 - Digital conversion.

The power output of the dye laser is estimated by a comparitive measurement of the nitrogen and the dye laser outputs (Figs. 8 a,b).

The power output of the nitrogen laser is calculated

by the readings from a thermopile and the half width obtained from the oscilloscope picture through a fast photo diode.

We read an average of 86 μV output from the thermopile at 10 pps, counted by modulating a frequency counter. Calibrating this with a He-Ne laser of known output power which gave 24 μV at 2 mW we get:

$$\frac{86 \times 2}{24} = 7.17 \text{ mW average output power}$$

$$7.17 \text{ m J/sec} \quad 1/10 \text{ pulse/sec} = .717 \text{ m J/pulse}$$

Half width = 6 ns

$$\therefore P = \frac{.717 \text{ mJ/pulse}}{6 \times 10^{-9} \text{ sec/pulse}} = 120 \text{ kW}$$

Comparing the amplitudes:

$$\left[\frac{P_{N_2}}{P_{dye}}\right]^2 \simeq \frac{I_{N_2}}{I_{dye}}$$

Dye laser power output:

$$P = \left(\frac{70}{150}\right)^{\frac{1}{2}} \times 120 = 81.98 \text{ kW}$$

Assuming losses of 45% including 25% due to the Glan air prism that is used to polarize the incident beam and 20% due to the focusing lens

$$P = 50 \text{ kW approximately}$$

The measured half width for dye laser output is also 6 ns, therefore comparing with N_2 laser we have approximately .3 mJ/pulse

Energy of a photon = hC/λ

Assuming λ = 627 nm

$$E = \frac{6.62 \times 10^{-34} \text{ joule sec} \times 3 \times 10^{8} \text{ m/sec}}{1.6 \times 10^{-19} \frac{\text{joule}}{\text{sec}} \times 627 \times 10^{-9} \text{ m}} = 2\text{eV}$$

Number of photons per pulse is then

$$\frac{3 \times 10^{-4} \text{ joule/pulse}}{1.6 \times 10^{-19} \frac{\text{joule}}{\text{ev}} \times 2 \text{ ev/photon}} =$$

$$= 9.4 \times 10^{14} \text{ photon/pulse}$$

Assuming 1% of the beam is scattered equally in all directions and knowing the solid angle covered by the mirror:

$$\text{Solid angle} = \frac{\pi(.63)^2}{4\pi(36.6)^2} = 7.4 \times 10^{-5}$$

the number of photons detected per pulse is: (taking the number of photons per pulse as 5×10^{14} due to losses)

$$5 \times 10^{14} \times 8 \times 10^{-5} = 4 \times 10^{10} \text{ photons detected per pulse}$$

The photomultiplier specifications are given in table A VII-1. At 627 nm the radiant cathode sensitivity $E(\lambda)$ is

$$E(\lambda) = 30.4 \text{ mA/W}$$

with 4×10^{10} photons : we get 12.8×10^{-9} joules

$$4 \times 10^{10} \times 2 \frac{\text{ev}}{\text{photon}} \times 1.6 \times 10^{-19} \text{ joule/ev} =$$

$$= 12.8 \times 10^{-9}$$

Therefore the photocurrent from cathode at 10 ns will be

$$I_k = 30.4 \frac{\text{mA}}{\text{W}} \times \frac{12.8 \times 10^{-9} \text{ W}}{10 \times 10^{-9}} = 38.9 \text{ mA}$$

Taking into account the 25% attenuation due to the analyser prism we get approximately 30 mA output from the photomultipliers. This value is only an estimate but can

be used to determine the absolute quantities.

A better approximation can be calculated by knowing the number of particles in the interaction region, their sizes and shapes, and refractive indexies.

The number of particles in the interaction region depend on the concentration of the aerosols in their suspension or in the solvent, the liquid flow rate and the frequency of the sinusoidal voltage at which they are generated. These are the variables of the experiment. They are calculated at each run and the data is corrected accordingly.

The electronic data acquisition system has its errors in detecting voltages. These are given in Table A VII-2. The raw data is corrected due to the relative standard deviation of these functions.

TABLE A VII-1

Photomultiplier Characteristics

	PMT 1	PMT 2
Type	RCA7265	RCA7265
Serial #	P 57379	P 12542
Cathode Sensitivity	220 μA/l	255 μA/l
Cathode Red Sensitivity	1.05 μA	1.25 μA
Anode Sensitivity	15500 A/l	2700 A/l
@	2400 V	2400 V
Dark Current	.045 μA	.03 μA
@	193 OV	220 V

TABLE A VII-2

Calibration Data for Electronics

Regulated Applied voltage (volts)	Channel 1 Average voltage output (volts)	Channel 2 Average voltage output (volts)
0	.073	.068
1	1.040	1.060
2	2.130	2.140
3	3.100	3.030
4	4.120	4.150
5	5.080	5.060
6	6.100	6.090
7	7.140	7.090
8	8.190	8.050
9	9.160	9.080

APPENDIX VIII

DATA TABULATION

An example of two data sets, which are the average of 5 consecutive runs each, of latex particles, are given in Fig. A VIII-1 and A VIII-2. The former is Channel 1, and the latter is channel 2. The incident light in this case is polarized perpendicular to the plane of scattering. As can be observed from both of these graphs, the angle at 151.2 is set off, and the axis point is not typed. This data point is considered as "out of range". The appearance of the out of range point is because of the miscoding of the paper tape in one of the five runs that are averaged. In the overall averaging this point is discarded as well as some other points that might have occurred due to the scattering from coagulated particles. These are rejected if they are within the range of the error bracket set by Mie theory. The rejected values are the intensity at 156.6^{o} of Fig. A VIII-1, and the intensities at 28.8^{o}, 45.0^{o}, 66.6^{o}, 79.2^{o}, 86.4^{o}, 88.2^{o}, 97.2^{o}, 163.8^{o}, and 174.6^{o} of Fig. A VIII-2. The occurence of so many rejections in the second channel can be better understood by observing the graphs of the two channels before the subtraction of the background intensities, which are given in Figs. A VIII-3

and A VIII-4.

It is clearly seen that, while the first channel is giving a smooth output, the second channel is very inconsistent. This cannot be due to the coagulation of the latex particles since, the scattered light is detected by both channels at the same time, from the same orientation of particles. Therefore we conclude that it is a noise problem of the second channel photomultiplier, which is random. Nevertheless the data points corresponding to this effect are discarded.

The same kind of reasoning can be applied to the cladosporium and NaCl datas. An example of a set of cladosporium data is given in Figs. A VIII-5 and A VIII-6.

Most of these data points are either rejected or omitted within reasonable limits.

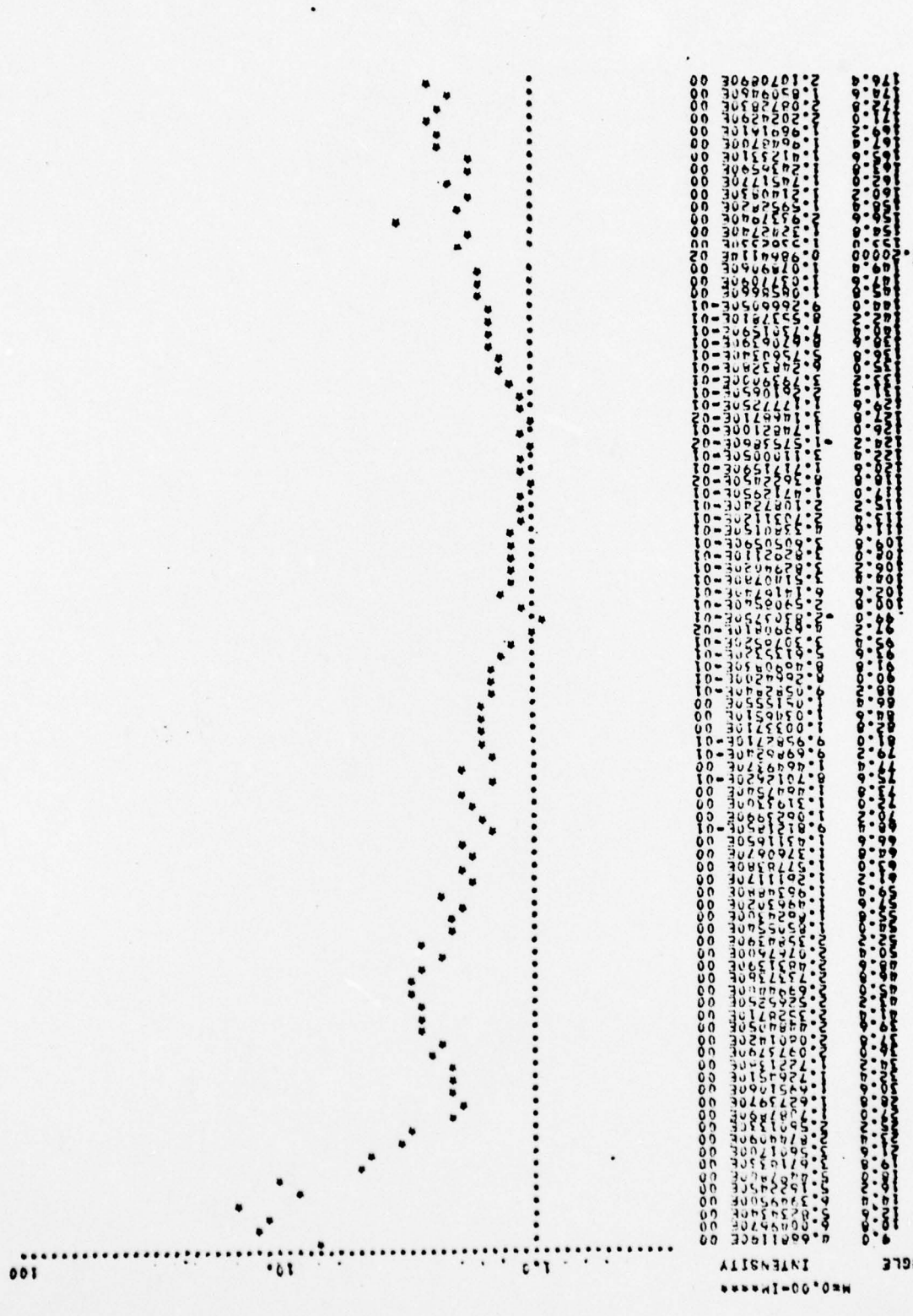

Fig. A VIII-1 Channel 1 experimental data of 5 averages.
Incident light polarized perpendicularly.

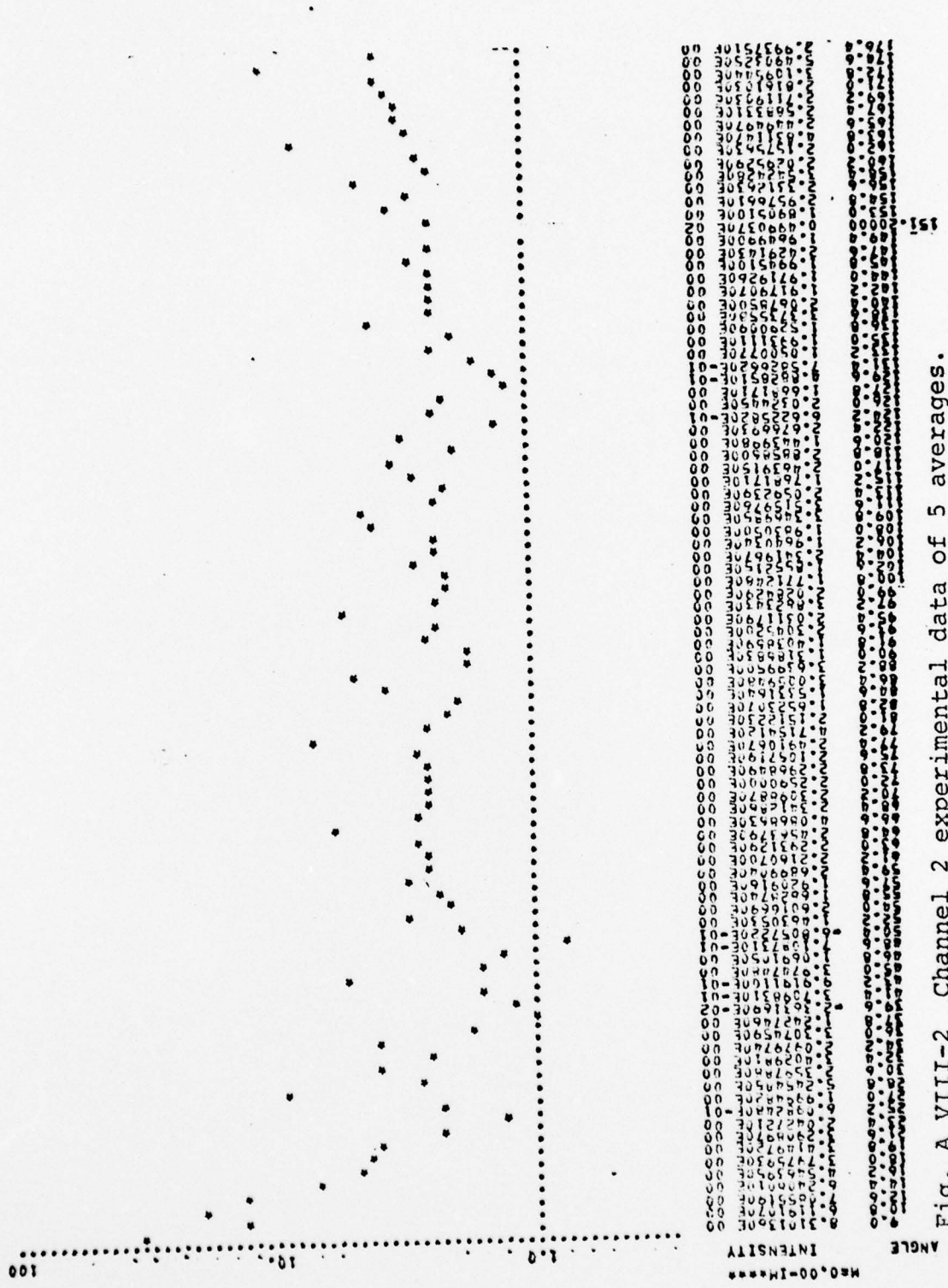

Fig. A VII-2 Channel 2 experimental data of 5 averages.
Incident light perpendicularly polarized.

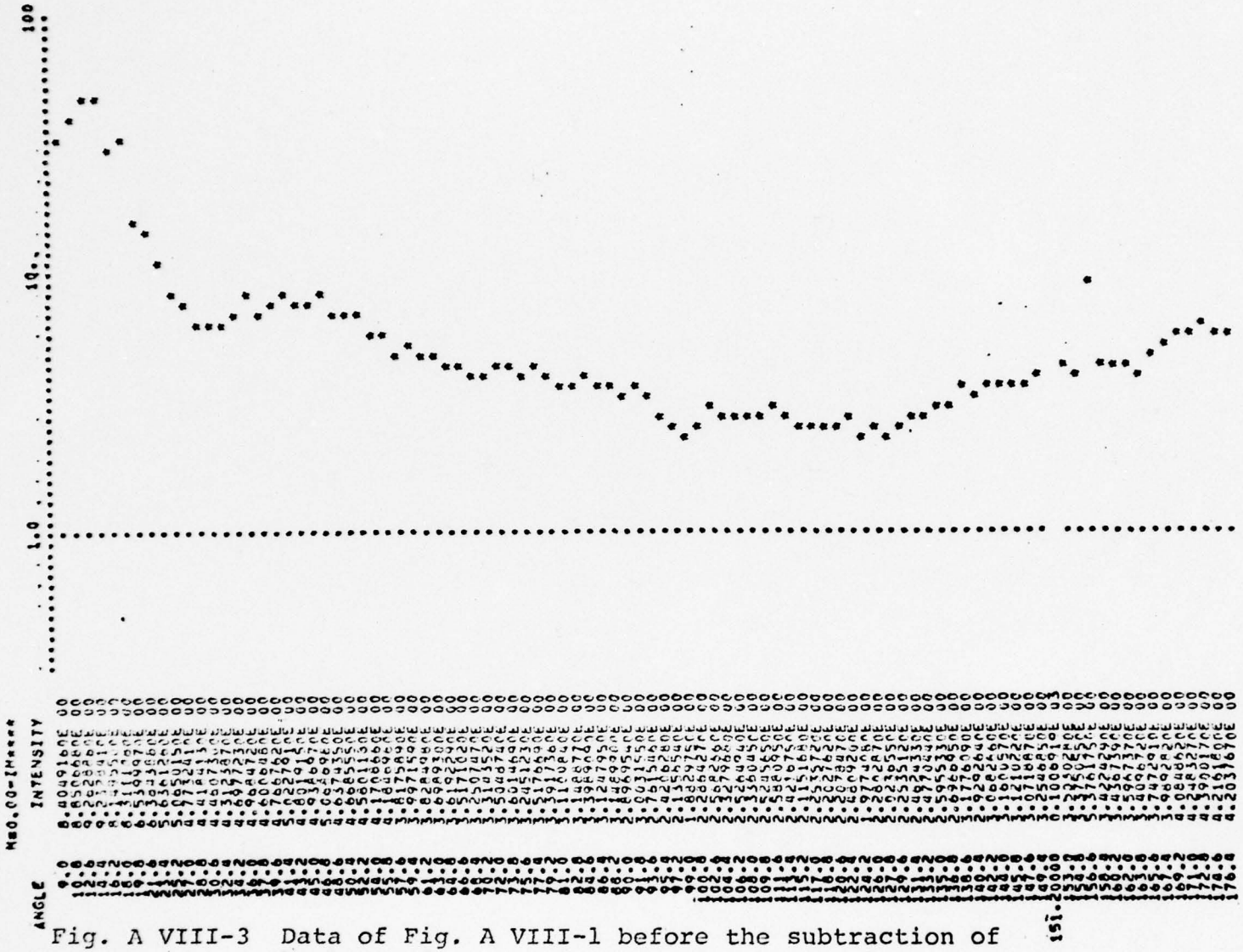

Fig. A VIII-3 Data of Fig. A VIII-1 before the subtraction of background.

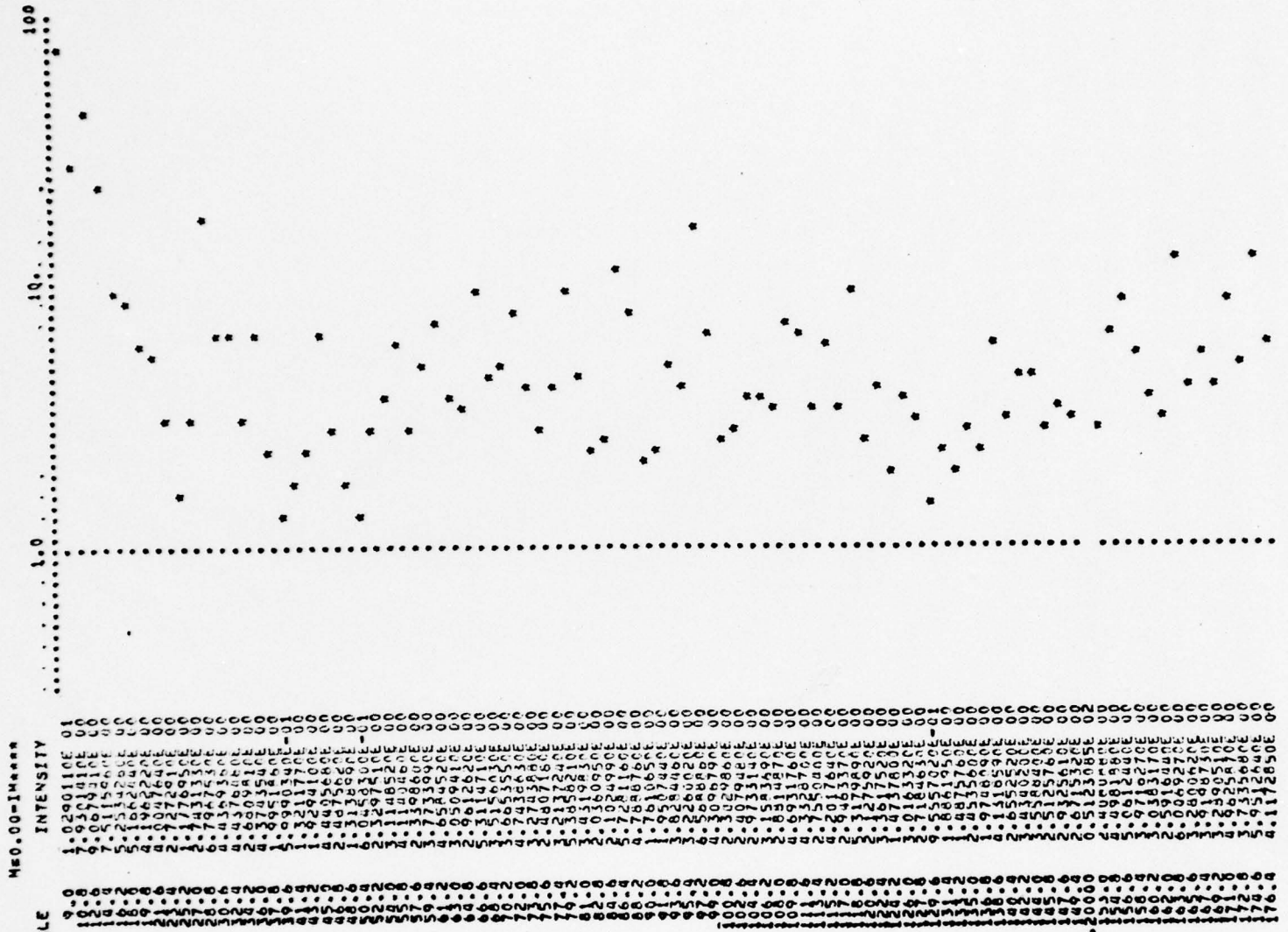

Fig. A VIII-4 Data of Fig. A VIII-2 before the subtraction of background.

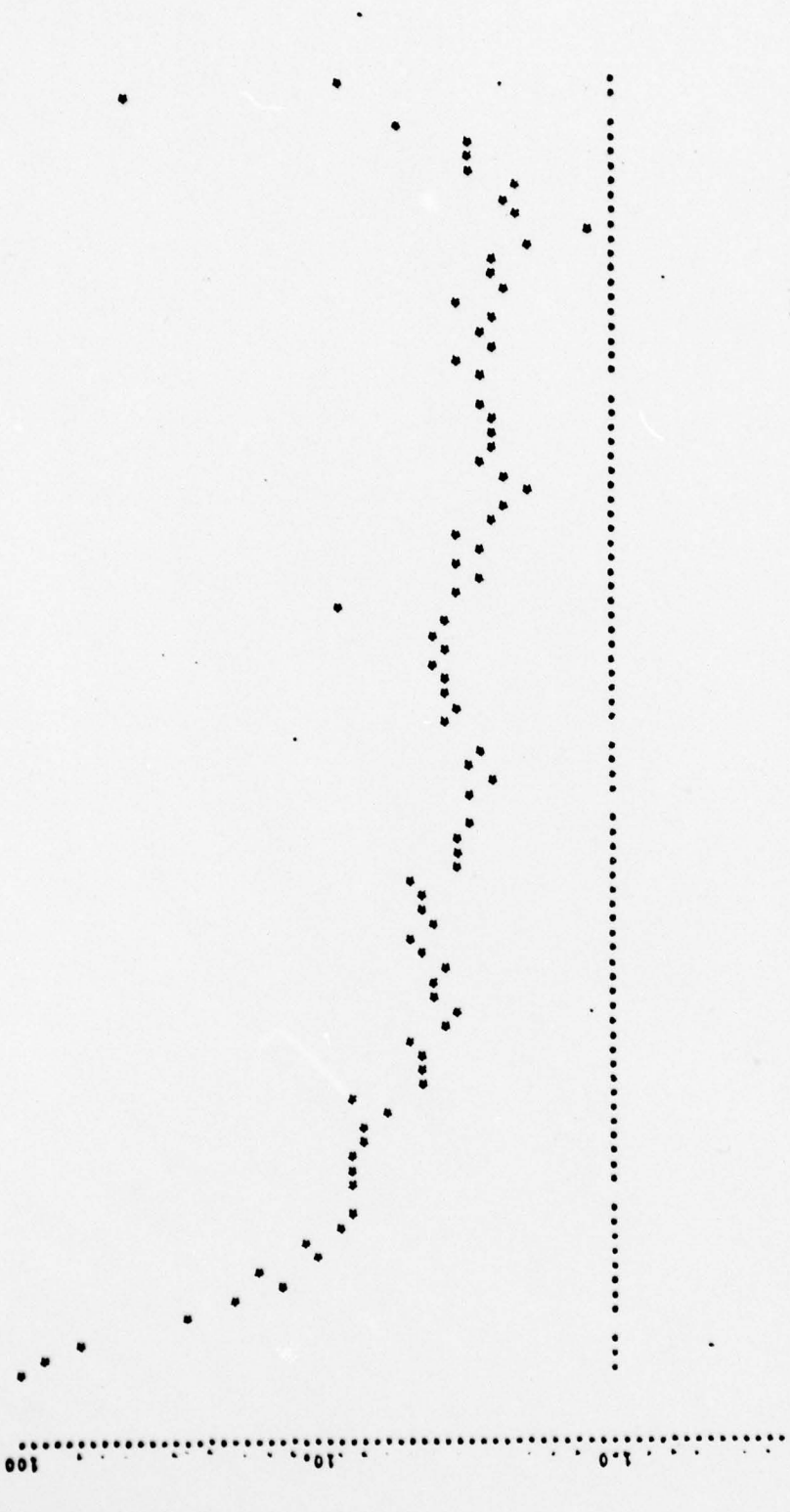

Fig. A VIII-5 Cladosporium data of channel 1. Incident light is perpendicularly polarized.

Fig. A VII-6 Cladosporium data of channel 2 when the incident light is perpendicularly polarized.

LIST OF REFERENCES

[1] Gray Ward, Proc. IEEE, Southeastcon 74, 160 (1974).

[2] C. Yeh, P. Barber, UCLA-ENG-7431 (1974).

[3] P.C. Waterman, Proc. IEEE, 53, 805 (1965).

[4] Reiner Eiden, Appl. Opt. 5, 569 (1966).

[5] Herschel Weil, C.M. Chu, Appl. Opt. 15, 1832 (1976).

[6] Gray Ward, 7th International Laser Radar Conference, 111A (1975).

[7] Charles Acquista, Appl. Opt. 15, 2932 (1976).

[8] K.S. Shifrin, "Scattering of Light in a Turbid Medium" (Moscow, 1951) (NASA Technical Translation TTF-477, 1968).

[9] R.G. Pinnick, D.E. Carroll, D.J. Hofmann, Appl. Opt. 15, 384 (1976).

[10] B.S. Pritchard, W.G. Elliott, J. Opt. Soc. Am. 50, 191 (1960).

[11] Kurt Bullrich, Advanced in Geophysics, Landsberg & Miegham ed. (AP, 1964).

[12] Reiner Eiden, Appl. Opt. 5, 569 (1966).

[13] A.C. Holland, G. Gagne, Appl. Opt. 9, 1113 (1970).

[14] Gerald W. Grams, "Airborne Laser Polar Nephalometer," Laser Radar Studies of the Atmosphere Conference, Williamsburg, Va., June 4-6 (1973).

[15] H.H. Blau, Jr., M.L. Cohen, L.B. Lapson, P. von Thüna, R.T. Ryan, D. Watson, Appl. Opt. 9, 1798 (1970).

[16] H.H. Blau, Jr., D.J. McCleese, D. Watson, Appl. Opt. 9, 2522 (1970).

[17] Frank T. Gucker, Jiri Tuma, Horny-Min Lin, Chao-Ming Huang, Stephen C. Ems, Thomas R. Marshall, Aerosol Science 4, 389 (1973).

[18] A.J. Hunt, O.R. Hoffman, Rev. Sci. Instrum. 44, 1753 (1973).

[19] R.G. Pinnick, D.E. Carroll, D.J. Hofmann, Appl. Opt. 15, 384 (1976).

[20] P. Schenck, H. Metcalf, Appl. Opt. 12, 183 (1973).

[21] R.N. Berglund, B.Y. Liu, Env. Sci. & Tech. 7, 147 (1973).

[22] J.D. Jackson, "Classical Electrodynamics," (Wiley, N.Y., 1962).

[23] Milton Kerker, "The Scattering of Light and Other Electromagnetic Radiation," p. 40 (Academic, N.Y., 1969).

[24] A.F. Stevenson, J. Appl. Phys. 24, 1143 (1953).

[25] S. Asano, G. Yamamoto, Appl. Opt. 14, 29 (1975).

[26] Atam P. Arya, "Elementary Modern Physics," p. 139, (Addison-Wesley, Reading, Mass., 1976).